NASA Contractor Report 198516
SLI-R-96-012

Study of Critical Heat Flux and Two-Phase Pressure Drop Under Reduced Gravity

Davood Abdollahian and Joseph Quintal
S. Levy Incorporated
Campbell, California

Fred Barez, Jennifer Zahm, and Victor Lohr
San Jose State University
San Jose, California

December 1996

Prepared for
Lewis Research Center
Under Contract NAS3–26550

National Aeronautics and
Space Administration

ABSTRACT

The design of the two-phase flow systems which are anticipated to be utilized in future spacecraft thermal management systems requires a knowledge of two-phase flow and heat transfer phenomena in reduced gravities. This program was funded by NASA headquarters in response to NRA-91-OSSA-17 and was managed by Lewis Research Center. The main objective of this program was to design and construct a two-phase test loop, and perform a series of normal gravity and aircraft trajectory experiments to study the effect of gravity on the Critical Heat Flux (CHF) and onset of instability. The test loop was packaged on two aircraft racks and was also instrumented to generate data for two-phase pressure drop. The normal gravity tests were performed with vertical up and downflow configurations to bound the effect of gravity on the test parameters. One set of aircraft trajectory tests was performed aboard the NASA DC-9 aircraft. These tests were mainly intended to evaluate the test loop and its operational performance under actual reduced gravity conditions, and to produce preliminary data for the test parameters.

The test results were used to demonstrate the applicability of the normal gravity models for prediction of the two-phase friction pressure drop. It was shown that the two-phase friction multipliers for vertical upflow and reduced gravity conditions can be successfully predicted by the appropriate normal gravity models. Limited critical heat flux data showed that the measured CHF under reduced gravities are of the same order of magnitude as the test results with vertical upflow configuration. A simplified correlation was only successful in predicting the measured CHF for low flow rates. Instability tests with vertical upflow showed that flow becomes unstable and critical heat flux occurs at smaller powers when a parallel flow path exists. However, downflow tests and a single reduced gravity instability experiment indicated that the system actually became more stable with a parallel single-phase flow path.

Several design modifications have been identified which will improve the system performance for generating reduced gravity data. The modified test loop can provide two-phase flow data for a range of operating conditions and can serve as a test bed for component evaluation.

TABLE OF CONTENTS

SLI-R-96-012

STUDY OF CRITICAL HEAT FLUX AND TWO-PHASE PRESSURE DROP UNDER REDUCED GRAVITY

Contract Number: NA53-26550

Final Report

October 1996

Prepared by:

Davood Abdollahian
Joseph Quintal
S. Levy Incorporated
3425 S. Bascom Avenue
Campbell, CA 95008

Fred Barez
Jennifer Zahm
Victor Lohr
San Jose State University

Prepared for:

National Aeronautics and Space Administration
Lewis Research Center
Cleveland, Ohio 44135

LIST OF FIGURES

LIST OF FIGURES

1.0 INTRODUCTION

Two-phase gas/liquid flow distribution is strongly affected by the gravity level. The flow regime maps developed for the normal gravity conditions are not valid in a microgravity environment. Variations in the flow distribution may affect pressure drop characteristics, heat transfer rates, and flow dynamics. In addition to two-phase flow parameters, several criteria including heat transfer boundaries and instability mechanisms, are expected to be strongly dependent on the acceleration levels and should be analyzed in detail.

Two-phase systems are generally designed for operation under nucleate boiling regime in order to utilize the high heat transfer characteristics of two-phase flow. Operation of these systems beyond the critical heat flux may lead to a sudden jump in the surface temperature due to reduction in the heat transfer coefficient (film boiling regime). This temperature is usually above the melting point of many materials; therefore, this maximum surface heat flux is also called the limit of stable burnout. In many practical situations, two-phase components fail at heat fluxes well below the limit of stable burnout. This is due to hydrodynamic instabilities which result in sudden reductions in flow and burnout at smaller heat fluxes. Knowledge of stable burnout and the onset of hydrodynamic instability are crucial for operation of any two-phase loop.

Current information on two-phase flow and heat transfer is mainly derived from terrestrial experiments. Unlike pool boiling which has been studied extensively under high and low accelerations, very little work has been done on understanding and modeling two-phase flow. The majority of low gravity fluid mechanics and heat transfer experiments have been performed in drop towers or under simulated reduced gravity conditions. Several recent efforts have provided limited useful data from aircraft trajectory tests.

The parameters and criteria of immediate importance for design of two-phase systems are:

- Two-phase friction multiplier
- Forced convective heat transfer coefficient
- Two-phase heat transfer boundaries
- Flow regime map
- Void-quality relationship
- Hydrodynamic instability

Among the above parameters, the hydrodynamic instability which is usually of secondary importance for the conventional two-phase systems operating at normal gravity, is believed to be quite significant for spacecraft applications. This is due to the expected variations in the gravity level and use of parallel components with two-phase flow.

The recent and ongoing efforts have mainly concentrated on generating the data and developing models for two-phase pressure drop, flow regime transition, and two-phase heat transfer coefficients. At this stage, it is generally concluded that considerably more data, preferably under

long duration steady-state conditions, is needed to complete and confirm the design approaches for application to reduced gravities.

1.1 Background

As mentioned earlier, hydrodynamic instabilities may lead to system failures at heat fluxes well below the limit of stable burnout. There are a number of mechanisms which lead to hydrodynamic instability. Some of these mechanisms are not important for the systems designed for operation at normal gravity, but are believed to be very important under reduced gravity operation.

Excursive or Ledinegg instability is the simplest form of hydrodynamic instability in forced convective systems. It occurs under operating conditions which result in an increase in two-phase pressure drop with decreasing flow rate. For an imposed pressure under such conditions, operation at more than one flow rate is possible. Small disturbances may lead to a shift from one flow rate to another (usually lower) in a non-recurring manner and burnout may occur.

Pressure drop-flow rate characteristics of two-phase channels occasionally follow an "S" shaped behavior as shown in Figure 1.1. Operation in the negative slope part of this system may lead to excursive instability. If a dynamic feedback mechanism exists, it can also lead to oscillatory behavior. In the absence of such feedback mechanism, static equations can be used for a simple analytical treatment. Physical interpretation of the results of such an analysis is that, if the slope of the pressure drop-flow rate characteristic is more negative than the imposed external supply system, an oscillation will occur. For example, in a constant head supply system (zero slope) as shown in Figure 1.1, operation at points 1 and 3 would be stable while operation at point 2 would be unstable (slope of the system characteristic is more negative than supply slope). Physically, if the flow rate at point 2 is slightly decreased along (A), the external system is supplying less pressure drop than that which is required to maintain the flow. The flow rate will be decreased until point 3 is reached. The new operating point may be so low that burnout could occur. With a nearly constant flow delivery system (slope of - ∞) no excursion is possible. Most external supply systems fall in between the two extremes mentioned above and have a characteristic as shown by (C). With such a system, point 9 is stable while operation at point 8 is unstable. It should be noted that a positive displacement pump will provide a nearly constant flow rate for a good portion of the expected pressure drop.

Oscillatory instability may result if an energy storage mechanism exists in a two-phase forced convective loop that provides feedback. The simplest form of such an energy storage is a compressible volume just upstream or within the heated length.

It is believed that excursion and oscillatory instabilities which result from the characteristics of the two-phase systems are particularly important at reduced gravities. In addition, these instabilities may severely affect the operation of boiling a system at high accelerations if the flow is in the direction of the acceleration.

For a given heat flux, the maximum and minimum of the pressure drop-flow rate characteristic depend on the particular system. A boiling channel with vertical upward flow can operate into the negative slope region before becoming unstable. However, the same channel with downward

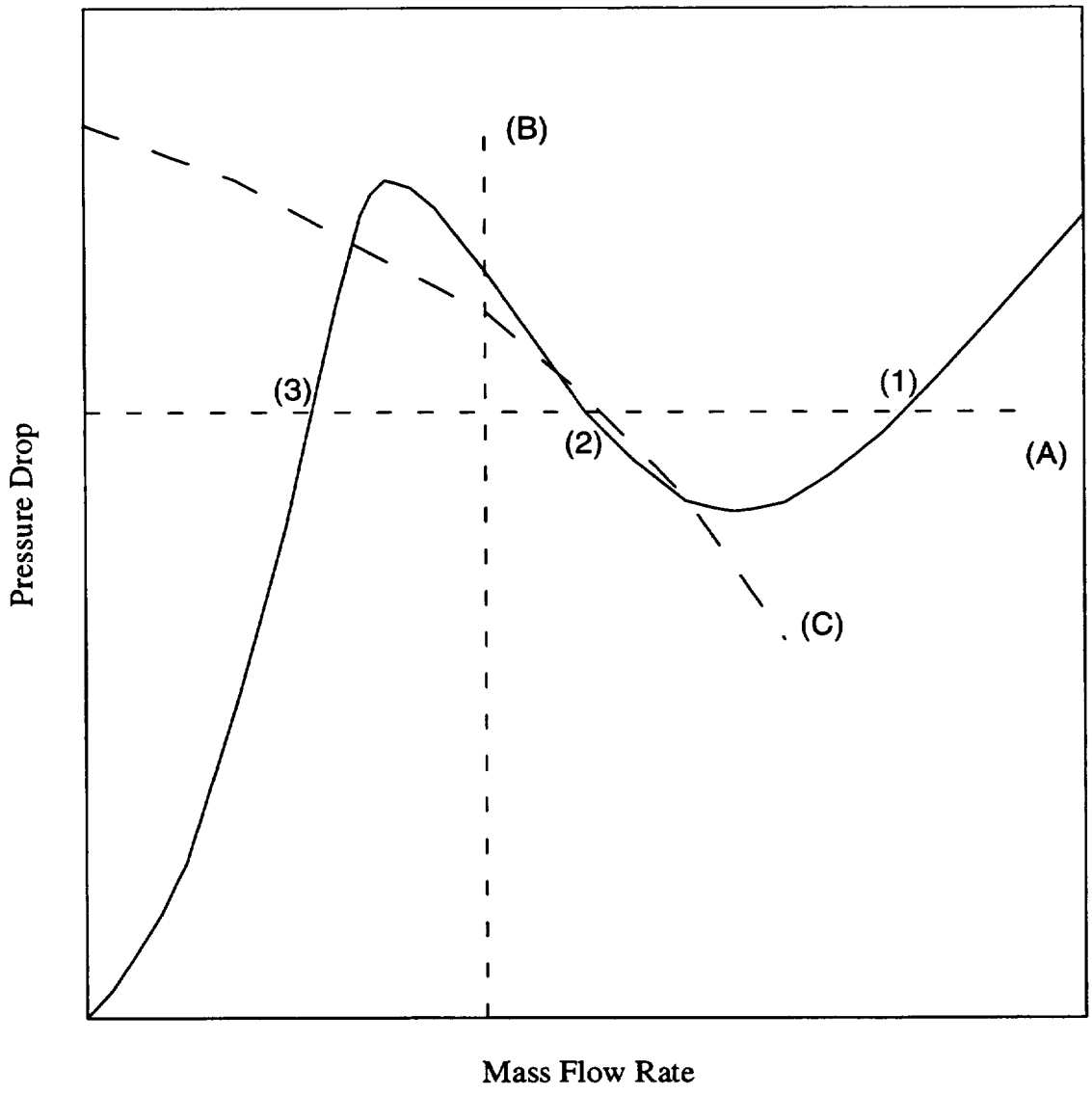

Figure 1.1 Pressure Drop - Flow Characteristic of a Two-Phase Channel

flow is expected to become unstable at the onset of subcooled void generation which is very close to the minimum point. The reason is that for upward flow, vapor generated initially at the exit will be swept away by buoyancy, while in downward flow buoyancy will sweep vapor upstream into the channel which will increase the pressure drop (more negative slope) and start oscillations. Therefore, the onset of oscillatory instability in downward flow will correspond to the minimum in the pressure drop-flow characteristic, while for vertical upward flow (without a compressible volume) it moves up in the negative slope region. High accelerations ($g > g_o$) in the direction of the flow would even be more severe than downward flow since the bubbles will be swept upstream with higher velocities. On the other hand, higher accelerations in the direction opposite to the flow will be stabilizing.

Generally, systems should be designed to avoid operation in the negative slope region completely. This is particularly important when several channels with multivalued characteristics operate in parallel. Due to the imposed constant pressure across the channels, severe flow maldistribution may result which could lead to unstable behavior and burnout. At normal gravity, this situation is usually avoided by restricting the flow at the entrance so that single-phase pressure drop is comparable to two-phase pressure drop. Restricting the flow will shift the minimum to lower flow rates and lower negative slopes, therefore stabilizing the system. Two-phase systems for spacecraft applications probably cannot afford to have such a large pressure drop (orifice or throttling valve) in the loop to stabilize the flow.

1.2 Scope of Work

The main objective of this study was to design and construct a modular two-phase loop to generate data on the onset of hydrodynamic instability and the critical heat flux under reduced gravity conditions. This effort consisted of a series of laboratory and aircraft trajectory tests to finalize the design and the method of testing, as well as generating preliminary data for the above two-phase flow parameters. The test loop was designed to serve as a test bed for component testing and also generating data for other two-phase flow parameters. In addition to the above primary parameters, data on pressure drop and two-phase heat transfer coefficients were also generated.

The laboratory tests were performed with the test section in vertical up (+1g) and vertical down (-1g) configurations to bound the reduced gravity conditions. In addition, the laboratory tests were used for system checkout, to set the operating procedure, and to establish the test matrix. Two sets of aircraft trajectory tests were planned to evaluate the test loop and its operational performance under the actual reduced gravity conditions, and to produce preliminary data for the test parameters.

2.0 DESCRIPTION OF EXPERIMENT

As mentioned earlier, the test apparatus for this project was designed to perform a series of normal gravity laboratory tests with vertical upflow and downflow configurations as well as a set of aircraft trajectory tests with a horizontal test section configuration. The schematic of the test loop is shown in Figure 2.1.

The test apparatus is a closed loop consisting of a magnetically coupled gear pump, a bladder type accumulator, a preheater section, a heated and an adiabatic test section, and a tube-in-tube condenser. Basically, the heated section is used to boil the working fluid and the measured test section surface temperatures is used to measure sudden rise in the wall temperature which indicates CHF or drop in flow rate due to instabilities. The adiabatic section is two feet long and is intended for two-phase pressure drop measurements over a region where the vapor phase content is known and does not change with distance. This section has the same diameter as the heated section and is thermally isolated from it with a Teflon flange. Differential pressures across two sections of the adiabatic tube is measured and recorded. A purge system is provided which will run subcooled liquid through the sense lines prior to pressure measurements.

The condenser is a single pass tube-in-tube design which uses standard tube fittings for the end connections. It consists of a 40 inch long 1/2 inch diameter inner tube and 3/4 inch diameter outer tube. Pumped water is used as the heat rejection source.

A magnetically coupled gear pump is used for the main loop to provide nearly constant flow at varying pressure heads. This is a variable speed pump and was selected to be oversized in order to provide a wider range of flow for possible future experiments. The bypass loop across the pump, with the solenoid valve SV1, is provided for safety purposes and is activated when the pump exit pressure is larger than a pre-set value. The regulating bypass loop, with regulating valve RV1, and the accumulator downstream of the pump are not needed for a positive displacement pump. They were provided for modularity purposes, in case a centrifugal pump replaces the existing pump. The accumulator contains a Buna-Nitrile bladder and is used to charge and pressurize the system in the present configuration.

All the sections of the test loop plumbing with the exception of the test section and the condenser are made up of 1/2 inch diameter stainless steel tubing connected using Swagelok fittings. The pre-heater was 1/2" wide, 8 foot long heating tape with a total power of 627 watts wrapped around a section of the stainless steel tubing upstream of the test section. All the tubing from the pre-heater to the condenser was insulated with polyethylene pipe insulation. The test section was insulated using Carborundum Fiberfax insulation material. Two drain lines with toggle valves were installed at the lowest and the highest elevation points of the test loop. These drain points are intended to drain the loop to the aircraft outboard vents in the case of an accidental leak, and to charge the system with the working fluid.

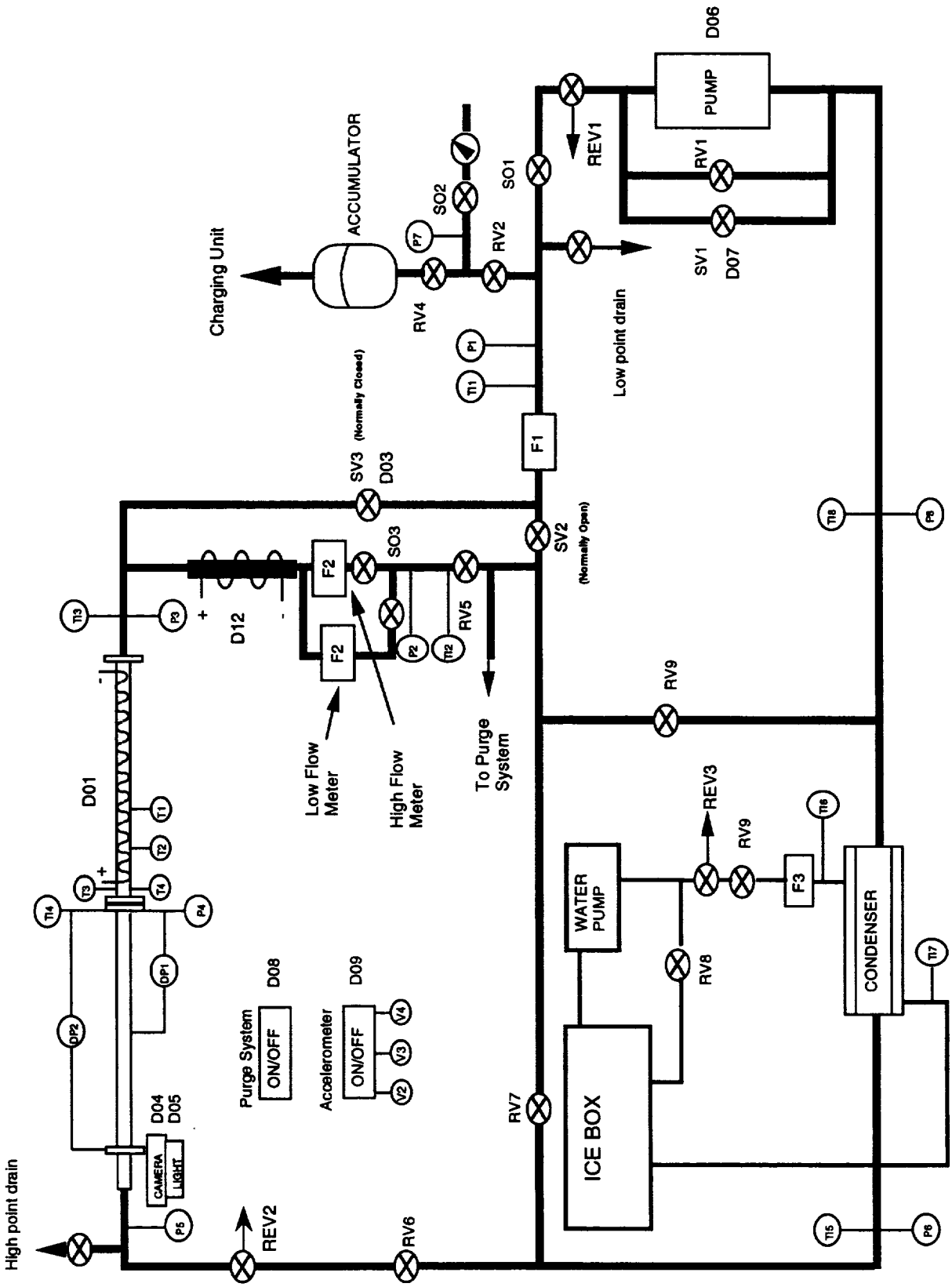

Figure 2.1 - Test Loop Schematic

The test section flow rate and system pressure are controlled by two regulating valves, RV5 and RV6, and the pump speed controller. The test section leg contains two turbine flow meters to cover the range of anticipated flow rates. Two isolation valves are used to select the applicable flow meter. In order to protect the test loop when CHF is reached, a bypass leg containing a solenoid valve is provided parallel to the test section. When over-temperature is sensed by the data acquisition system, SV3 is opened and SV2 is closed to use the maximum flow to flood the heated section. Two relief valves were used and the set points were adjusted to 10% over the maximum system operating pressure. It should be noted that a number of safety issues identified and controlled by the data acquisition software, which will be discussed later.

2.1 Test Parameters

The test variables for the critical heat flux and instability tests are the power level across the heated section and the flow rate. The critical heat flux tests were performed by gradually increasing the power input for a given flow rate until CHF, which follows a sudden rise in wall temperature, is reached. At every power setting, the system is brought to steady state and the pressure drop across the adiabatic section is recorded. The instability tests are performed by gradually decreasing the flow rate to the test section, at a given power level, until flow fluctuations and sudden rise in the wall temperature is observed.

The range of variation of power is set by the critical heat flux tests, since CHF sets the upper bound of power to the test section. The upper bound for the flow rate through the test section is set by the instability tests. The instability tests for a given power will be initiated with flow rates which will result in no voiding or small voiding in the test section. The stability tests will also set the pump head requirement.

3.0 TEST LOOP DESIGN

As mentioned earlier, modularity was one of the criteria in design and selection of the components for this experiment. This loop can serve as a test bed for generating data for other two-phase flow parameters as well as evaluating the performance of the loop components. Early in the design process it was decided to build this experiment as packaged in the aircraft racks to minimize the modifications from the laboratory configuration to the aircraft trajectory tests.

The test loop design process consisted of the selection of working fluid, component selection and design, instrumentation, mechanical layout, and design analysis.

3.1 Working Fluid Selection

The working fluid affects the sizing, as well as component design and selection. Several criteria were considered for selection of the working fluid. These are briefly described below.

Operating Pressure and Temperature

The most desirable operating conditions are close to the atmospheric conditions with a temperature approximately 10° F to 20° F above the highest expected ambient temperature. Operating at a saturation temperature of 80 to 100° F will reduce the heat loss to environment, eliminate the need for pre-cooling the fluid, and reduce the power requirement for pre-heating. In addition, operation close to the atmospheric pressure will minimize the possibility of sealant breakdown and leakage. Among the refrigerants, R-11 and R-114 have saturation pressures closest to the atmospheric pressure in the above temperature range. At 100° F the saturation pressure for R-11 is 23 psia, for R114 it is 46 psia and for R-12 it is 132 psia. .

Compatibility with Elastometers

This is a very important factor in selection of the working fluid because it allows reliable operation of the components with standard seals and barriers. Among the refrigerants, R-115, R-114, and R-12 are most compatible with polymers and elastomers, and result in the least amount of linear swell. With the exception of Viton, R-11 causes considerable swell to most elastomers.

Toxicity

Due to operation of this experiment in the university laboratories and within an aircraft, the working fluid should have a low toxicity level. Most of the Freon products have a Threshold Limit Value (TLV) of over 1000 ppm. Freon 114 has a TLV of >1000 ppm and an IDHL (Immediately Dangerous to Health or Life) limit of 50,000 ppm. This makes R-114 suitable for this experiment.

Power Requirement

As mentioned earlier, the upper bound for the power requirement is set by the critical heat flux which varies linearly with the heat of vaporization. R-11 has a heat of vaporization which is nearly 40% larger than R-12 and R-114. In order to estimate the power requirements, the model developed by Katto and Ohno, Ref. 1, was used. For saturation temperature of 100° F and a mass flow rate of 0.02 lb/s, the predicted critical heat fluxes for R-11 and R-114 are 1360 and 940 watts, respectively. The predicted heat flux with this model is a weak function of the surface tension and the liquid density.

Slope of pressure vs. Flow Curve

The stability tests will be initiated from a flow rate which, for the given power, will result in single phase flow or small voidage within the test section. This will correspond to a flow rate which causes the Net Vapor Generation (NVG) point to be at the exit of the heated section. The model of Saha and Zuber, Ref. 2, was used to predict the mass flow rate at NVG. For a heat flux of 500 watts, the predicted mass flow rates were 0.26 for R-114 and 0.30 lb/s for R-11. As the flow rate is reduced during the stability tests, two-phase flow will develop along a portion of the heated section and the pressure drop will increase.

Two-phase pressure drop was predicted by using the correlation developed by Freidel, Ref. 3. Although R-11 will generate smaller exit quality for the same flow rate and power, the two-phase pressure drop would still be higher than R-114. Therefore starting from the NVG, R-11 will have a steeper pressure drop vs. flow curve and will become unstable at lower flow rate. The larger pressure drop for R-11 also imposes a higher head requirement for the pump which may be difficult to satisfy with a magnetically sealed gear pump.

Based on the above discussion, R-114 was selected for the working fluid.

3.2 Component Design

Most of the components used for this experiment were off-the-shelf equipment and instrumentation. The loop was designed to be modular and several of the components, although not needed for the present experiments, were mainly incorporated for modularity purposes. Component specifications are provided in Appendix A. The component design consisted of developing the heater section and the condenser. Packaging the set-up within the racks was actually the most involved task in the building process.

Heated Section

Design of the heated section basically consisted of developing the method of heating and sizing the tubing accordingly. Direct electrical current was originally considered for heating the fluid in the test section. Due to low electrical resistance of the tube wall, direct heating will require very thin tubes and high electrical currents. For example, a 2 ft. long 1/4" Sch. 40 pipe will need a current of 384 amps for 1000 watts power input. The wall electrical resistance for a 1/4" stainless

steel tubing with a wall thickness as small as 0.007" is 0.16 ohm. This tubing will require approximately 80 amps at 12 volts, for 960 watts power. Since stainless steel tubing with the above specifications was not a stock item, it was decided to grind the test section wall to the required thickness. Stainless steel tubing of this size can be safely used for at least 1000 psi pressure. However, since flanges were needed at the end of the heated section to connect to other components and to provide electrical leads, machining and brazing of such a thin walled tube was a major concern. Several lengths of the test section were special ordered to be ground down within a tolerance of 0.001". Examination of the thin wall test pieces still showed localized wall thickness variation and the possibility of hot spots. In addition, since the end flanges had to be used as the electrical leads, the hottest spot would fall within the flanged section, away from the wall thermocouples. One method to avoid these problems was to use a tapered tube where the sections which were to be brazed to the flanges would have a thicker wall. Maximum power would then be supplied over a controlled distance away from the flanges, and brazing would be done on a section of the tube with a thicker wall. The problem with this approach was that the required tolerance could not be maintained to within a 3" length from the tapered section. Therefore, the location of the highest wall temperature would not be known and there was a possibility of hot spots at the end of the test section.

Another method of heating consisted of wrapping heating tape around the test section. For this purpose, a larger outside diameter is preferable to increase the heat transfer area. In addition, the piping should be as thick as possible to provide a smaller inside diameter, and therefore a smaller length requirement for a given L/d. It was calculated that we would need at least a 1/2" diameter piping for this type of heating. For 1000 watts of power input, approximately 85 square inches of heating area with a high temperature heating tape will be needed. Even with 1/2" Sch. 160 piping (OD=0.84"), we needed at least 3 ft. of piping (L/d=77). The disadvantages of this approach are the long test section length requirements and the expected low velocities due to larger inside diameters. At higher velocities the critical heat flux will be higher and a longer section will be needed.

The method that proved to be the most practical was to wrap resistance heater wires over the heater section. Standard tube sizes can then be used for all the components, which eliminates the concerns on bending and buckling of the heated section and use of special flanges. In addition, due to the high electrical resistance of the heater wire, only a low current power supply will be needed. The main challenge was to find a material to electrically insulate the test section from the wire, while permitting good heat conductance. A Magnesium Oxide based cement, which has an excellent dielectric strength and a thermal conductivity close to MgO (6 Btu/hr-ft-F), was selected for the insulation purposes. This material can be used at temperatures of up to 2600°F and has a coefficient of thermal expansion close to stainless steel ($13x10^{-6}$ in/in-F compared to $17x10^{-6}$ in/in-F for stainless steel). Several tests were performed to evaluate the feasibility of this approach and develope procedures for wrapping the wires without contacting with the tube wall. It was also noted that wrapping the wire with a lathe caused cracks in the cement and contact between the wire and the wall resulting in lower resistance and higher currents. Instead, it was decided to wrap the wire on a different tube and then screw/slide it onto the coated test section which resulted in no cracks or contacts with the wall.

The length and the thickness of the heater wire was selected to result in total resistance of approximately 7 ohms. This will generate around 1600 watts of power with 15 amps, 110 volt line power. We needed 14 inches of wrapped wire to get this resistance. The voltage/current combination will eliminate the need for a power supply, and standard line hook-up in the laboratory and the aircraft could be directly used for our tests.

Figure 3.1 shows the as-built heated section design. It consists of 17.38" long 5/16" ID, 0.035" thick 304 stainless steel with 14" of heating tape. A Swagelok fitting is used to connect the test section to the upstream piping. A set of mating flanges and O-rings, seal the heated and adiabatic sections together, as shown below. A 0.375" Teflon gasket is used to thermally isolate the two sections.

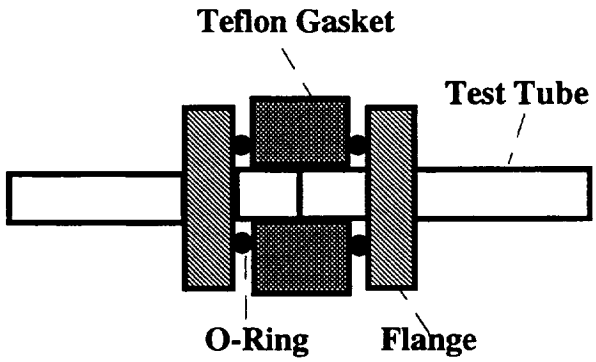

Figure 3.2 - Heated and Adiabatic Section Flange and Sealing

The main difficulty in using the resistance wire heating was the problem with measuring the surface temperature. Two arrow type ribbon thermocouples were used to monitor the surface temperature at the end of the heated section. Ribbon thermocouples are sturdier than conventional thermocouples, have fast response time, and can be shaped in different configurations. These thermocouples were cemented to the test section wall at opposing circumferential locations. In addition, two other flat ribbons which are joined at 180 degree angle (ribbons joined at the test section and the other end joined at the measuring instrument) were installed between the heater wires. 30 gage wire was used to make these ribbons which are 2 mil thick and 20 mil wide. These ribbons were placed in the 40 mil gap between the heater wires. Since the temperature rise will occur at the test section exit, the variation of the surface temperature near the exit is important.

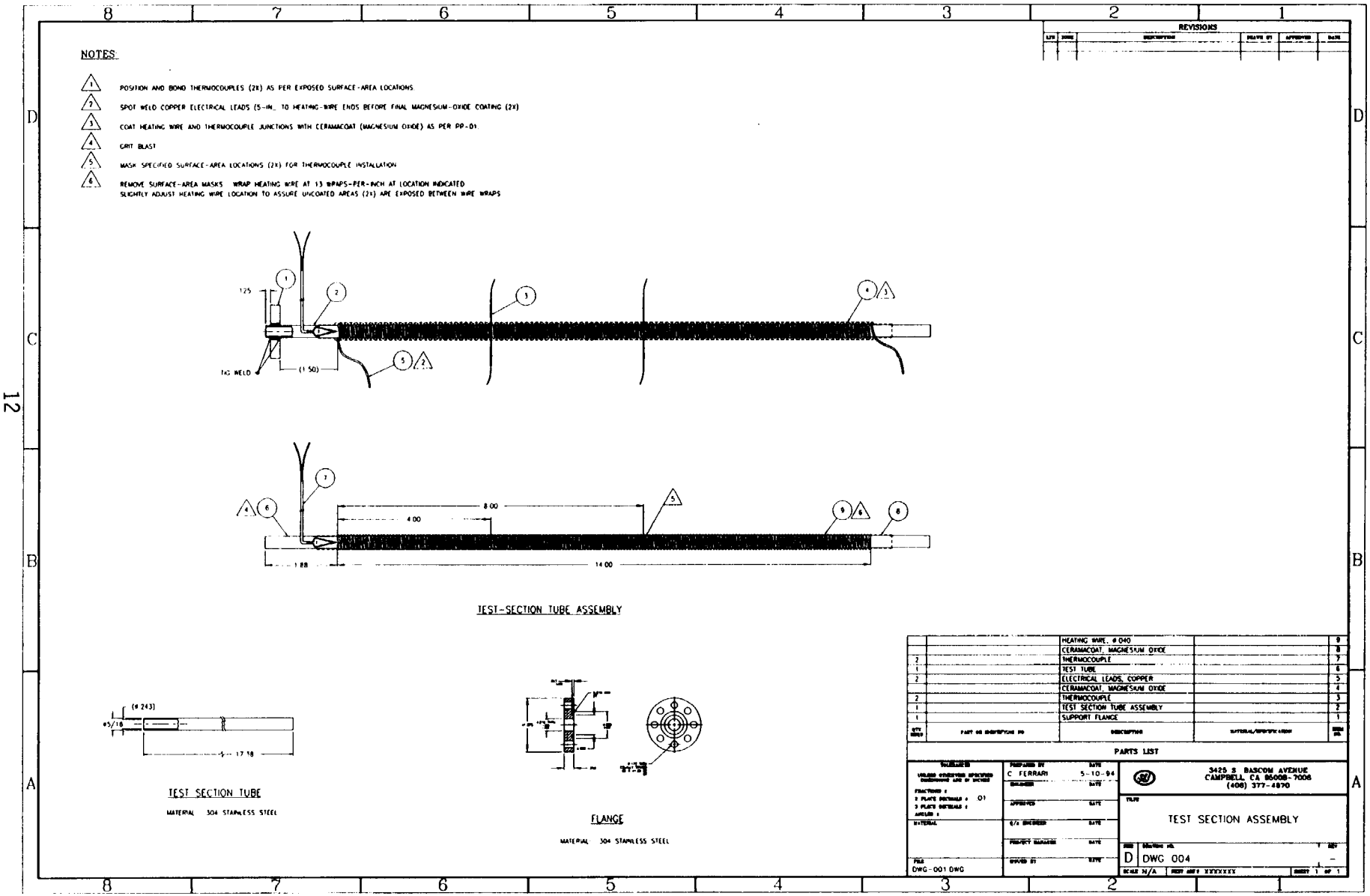

Figure 3.1 - Heated Test Section

Adiabatic Test Section

The adiabatic section is a two foot long section of 5/16" tubing which is used to measure the pressure drop over a fixed length of the test section with known vapor quality. The tubing is the same size as the heated section to minimize flow disturbances. Bored through Swagelok union Tees were used to connect sections of 5/16" tubing, as shown in Figure 3.3, in order to avoid tapping, drilling, and brazing the pressure transducer sense lines to the adiabatic section. One of the features of this test loop is a purge system which flows subcooled liquid through the pressure sense lines. This will purge out any bubbles which will cause errors in the differential pressure measurements. As shown in Figure 2.1, the purge system connects the sense lines to a point in the main loop piping upstream of control valve RV5. The adiabatic section and the purge system are shown in Figure 3.3. Every purge line is equipped with a solenoid and a regulating valve which is intended to reduce the pressure drop in the purge line and to avoid damage to the transducer. Prior to pressure recording, the solenoids open and flow the subcooled liquid into the sense lines and out of the adiabatic section.

In order to provide a wide range of differential pressure measurements with reasonable accuracy, two pressure transducers are utilized across the adiabatic section which share the same sense lines. A set of three way ball valves is used to switch between the appropriate transducers.

Condenser

The condenser is a single pass, cross flow tube-in-tube design which uses standard tube fittings for end connections. It consists of a 40 inch long 1/2 inch diameter inner tube and a 3/4 inch diameter outer tube. Condenser sizing analysis was performed by using a model based on the calculational method outlined in Ref. 4. The overall heat transfer coefficient , U, is given by

$$1/U = 1/h_c + R_i \, \mathrm{Log}(R_0 / R_i) / K_w + R_i / (R_0 \, h_0)$$

where h_C is the condensation heat transfer coefficient given in Ref. 4, h_0 is the outer surface heat transfer coefficient given by the Dittus-Boelter correlation, Ref. 5, and K_w is the wall thermal conductivity. For a given inlet quality, X, the condenser length is broken down into several regions of equal ΔX. Starting from the inlet, the length for each region to change the quality by ΔX is calculated from

$$\Delta Z = \frac{G \, h_{fg} \, D \, \Delta X}{4 \, U \, (T_{sat} - T_0)}$$

where G is the mass flux, D is the condenser inner diameter, and T_0 is the secondary side temperature. In addition, the pressure drop within the condenser primary side and the change in the coolant temperature is also evaluated.

This model was used to predict the required condenser length and pressure drop for different combinations of inner and outer tube sizes, and coolant flow rates and temperatures. The calculations were performed for the conditions expected for both the CHF and the stability tests. Basically, larger diameter inner tubes will result in smaller pressure drop and smaller clearance

between the inner and outer tubes will increase the secondary side heat transfer coefficient and result in shorter condenser length. The best combination was found for a 1/2" diameter inner tube and 5/8" diameter outer tube which required a condenser length of 32". However, the clearance between the tubes is so small that the secondary side pressure drop would be very large. A compromise combination of 1/2" diameter inner and 3/4" diameter outer tubing was found to satisfy all the criteria with a condenser length of 40 inches.

Figure 3.4 shows the condenser design drawings.

3.3 Mechanical Layout

Early in this experimental program, it was decided to utilize the NASA Learjet for the reduced gravity tests due to its availability. The plan was to package the experiment on two learjet racks which would be bolted down to the plane. Each rack can accommodate four shelves with approximately 6 to 8 inch clearance. The shelves were made of 1/4" aluminum plates with appropriate brackets to connect to the racks. Packaging the test components, plumbing the loop, and securing the entire assembly to the shelves proved to be a major task. Due to the size and the number of components, a set of middle shelves had to be used to accommodate the entire package. Since the middle shelves were supported by the rack shelves, the entire assembly had to be treated as one piece for the evaluation of the moment arm. The data acquisition system, the electronic controls, and the variacs were mounted on two aluminum plates which were separately bolted to the floor of the aircraft. The power supplies, relays, temperature controller, and the flow meter integrator were packaged in a single box, which along with two variacs, were mounted on one plate. The data acquisition system consisting of the multiplexers and the computer CPU were mounted on another plate. Figures 3.5 and 3.6 show the final package from two views as installed within the NASA DC9 aircraft. The layout drawings are shown in Appendix B.

The weight and moment calculation on each rack had to be performed to assure the integrity of the racks under all the anticipated conditions during the flight. The weight limit for each rack is 188 lbs and the limit for the moment is 3268 in.-lb. As mentioned earlier, the racks are connected together by the center shelves. Therefore, for the purpose of weight and moment calculations, the weight and moment of the center shelves are equally distributed between the two racks. Table B.1 shows the structural load evaluation on the racks.

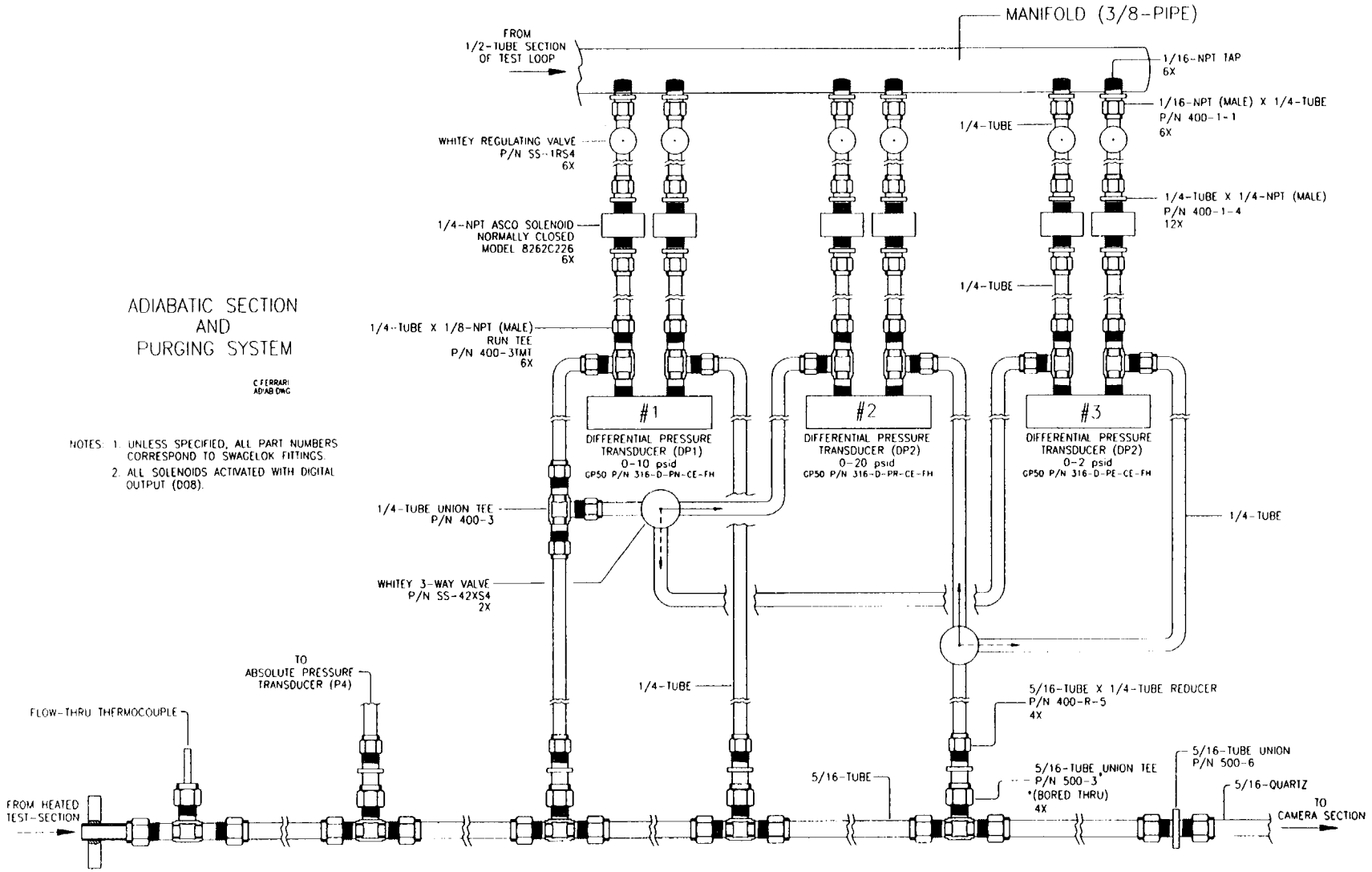

Figure 3.3 - Adiabatic Test Section

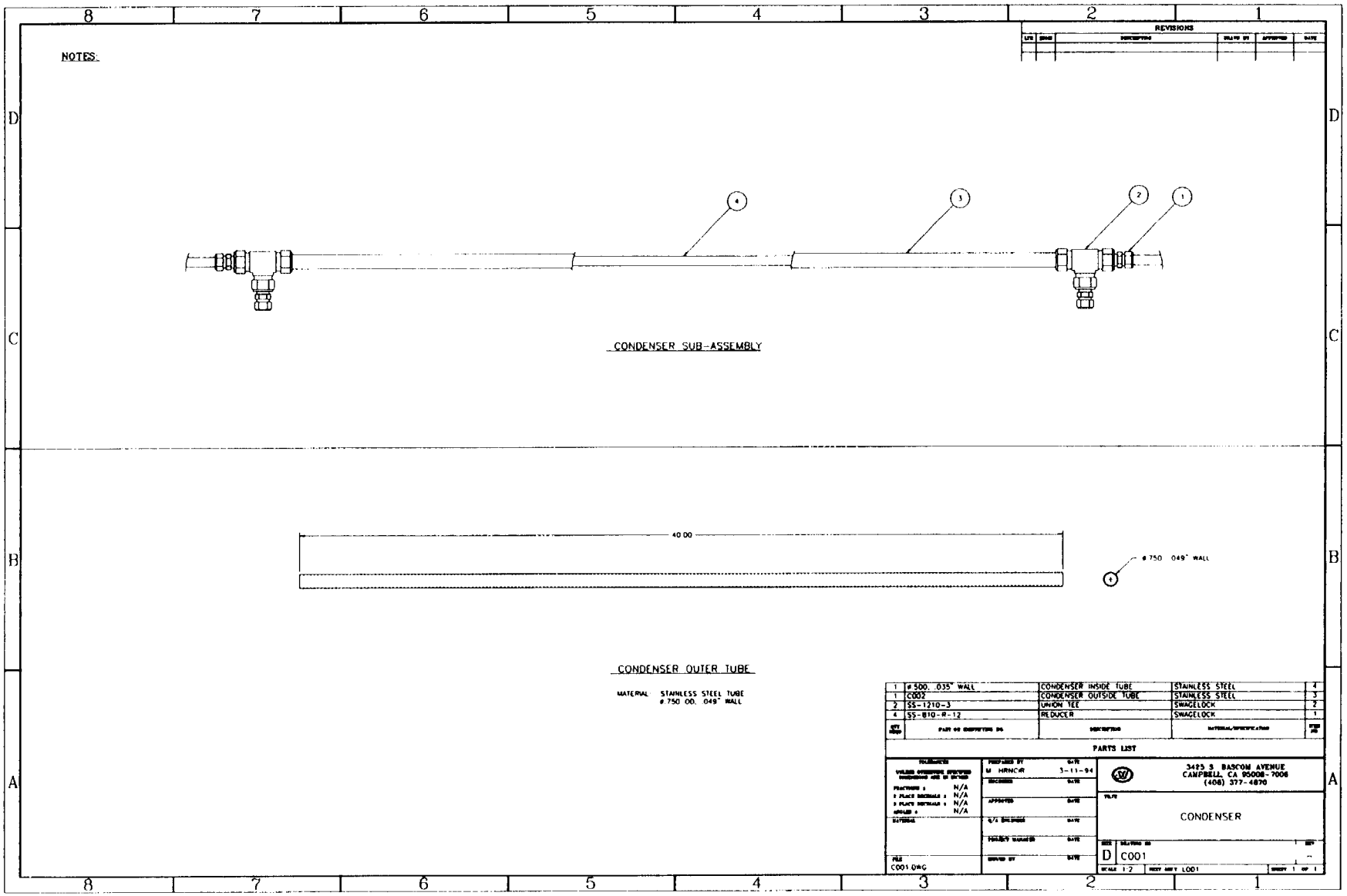

Figure 3.4 - Condenser

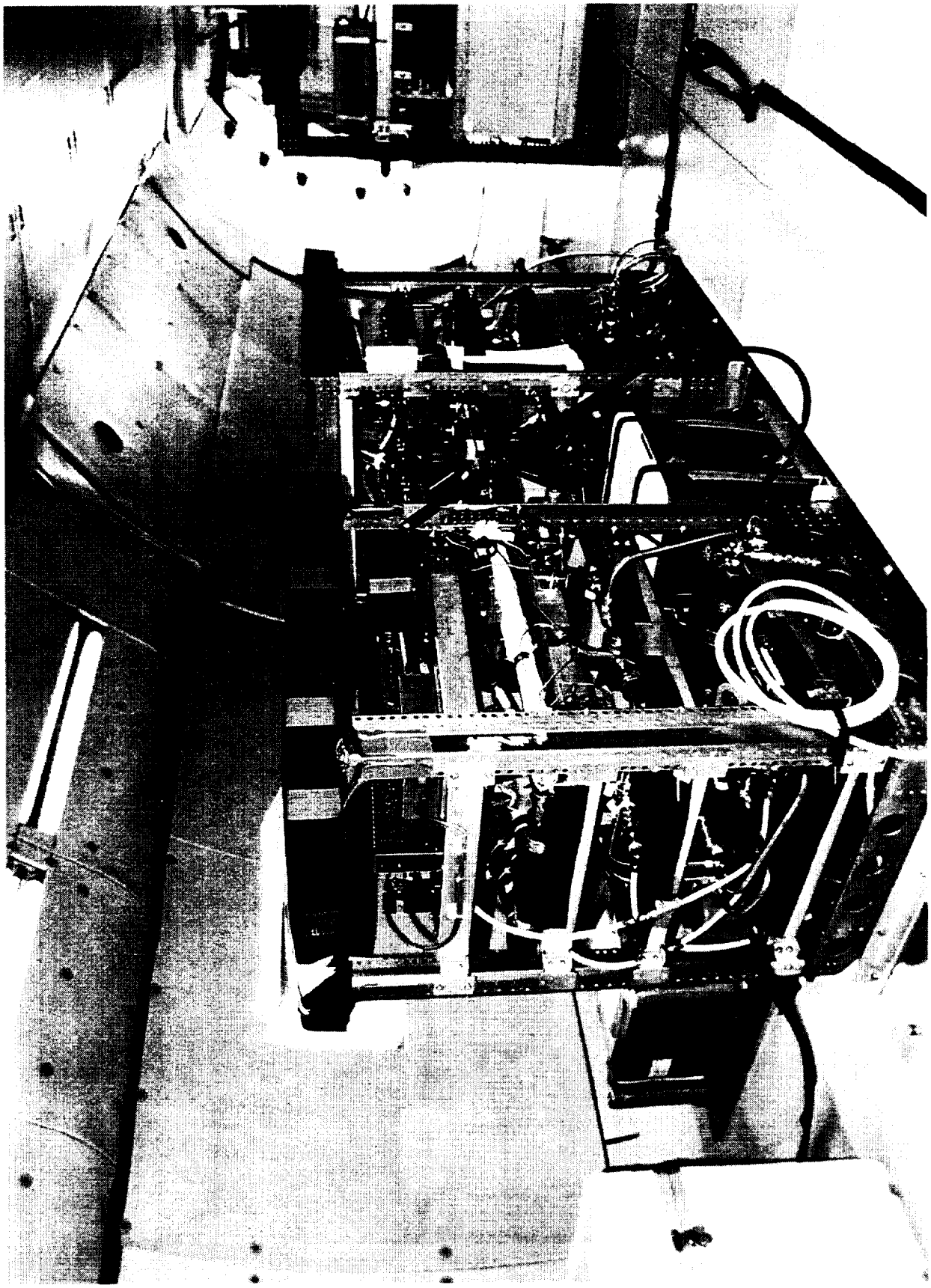

Figure 3.5 - Final Test Packages

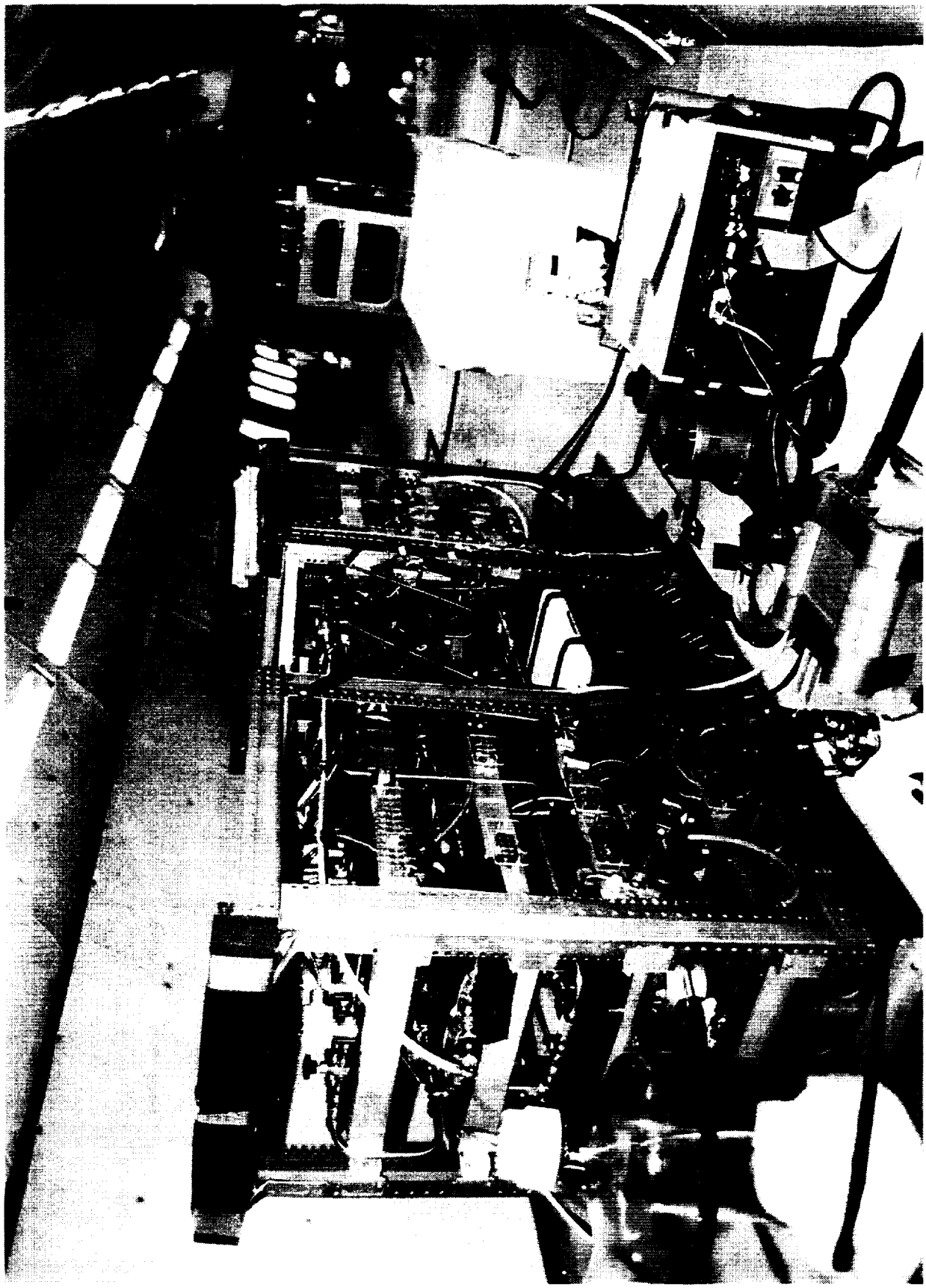

Figure 3.5 - Final Test Packages

3.4 Instrumentation

The specific instrumentation with the manufacturer, model number, and the range of measurement are listed in Table A.1. As mentioned earlier, the measurements for both the CHF and instability tests included the fluid temperature and pressure, differential pressure along the adiabatic section, flow rates, surface temperature, and heater wire input voltage and current. Fluid temperature is measured by NANMAC flow-through thermocouples which use ribbon type thermocouples flush with the inner surface and result in minimal flow disturbance. These thermocouples have minimal conduction error and have a response time of 20 milliseconds. The surface temperatures along the heated section are measured by NANMAC ribbon thermocouples. The absolute pressures are measured by GP:50 absolute pressure transducers with a range of 0-250 psi and accuracy of 0.01% of full scale. The differential pressures along the adiabatic section are measured with a GP:50 transducer with a range of 0-10 psid across an 11" section, and two transducers with ranges of 0-2 psid and 0-20 psid across a 22" inch length of the adiabatic test section. Turbine flow meters are used to measure the volumetric flow rates of the working fluid in the main leg and test section leg, as shown in Figure 2.1. Two interchangeable turbine meters are used to measure flow ranges of 0.02-0.7 and 0.13-3.0 gpm. A turbine flow meter with a range of 0.75-5.0 gpm is used to measure the condenser secondary side flow rate.

The heater wire current is measured by a model A100 Neilsen-Kuljian AC current sensor. The heater voltage is measured by a custom circuit card mounted near the heated section. This is discussed in a later section.

3.5 Electrical Sub-System

The electrical sub-system consists of electrical distribution, variacs, the water pump motor starter, the Freon pump controller, the heater controller, and connections to the data acquisition system. The electrical sub-system uses several power strips to distribute the electrical loads and allow the experiment to be connected to the AC sources in the aircraft. The power strips provide switching, filtering, and fuses for each load group. A power strip is provided for the computer, external power supplies, and the data acquisition components. Other power strips are provided for the larger electrical loads for the experiment rack, namely, the pre-heater and the main experiment heater. The electrical loads are fused at the instrument box (the water circulating pump is an exception and is fused at the motor starter box).

The data acquisition system controls the ON and OFF status of the electrical loads through the solid state relays in the instrument box. For several loads (heater, preheater, and water circulating pump), the solid state relays control additional slave relays in the instrument box.

The heater and pre-heater power are adjusted through variacs (variable auto transformers). The instrument box contains +24vdc and +5vdc power supplies for the current loop process sensors, flow sensor electronics, and the solid state relays. The accelerometer has a separate +/-15vdc power supply.

The electrical drawings are provided in Appendix C, Figures C.1 to C.5, and a listing of the electrical loads is given in Table C.1.

4.0 Data Acquisition and Control

A Personal Computer (PC) based Data Acquisition System (DAS), and common vendor supplied hardware and software were used for developing the DAS for this project. Considering the possibility of increasing the number of the analog inputs, a multiplexed analog and discrete digital architecture was chosen. An external interface box is used for signal conditioning and as a connection point. The National Instruments family of PC based instruments was chosen, due to the availability of a wide range of products and our familiarity with the software.

The PC system contains a multi-function analog/digital interface card. The interface card cable splits into a discrete digital and a multiplexed analog cable. The discrete digital cable is connected to an Opto-22 style optical isolator card which performs the isolation for both the input and output signals. The multiplexing of the analog inputs (and outputs) are performed by the SCXI chassis, SCXI input modules, and SCXI termination modules.

There are two identical SCXI analog input modules which are different in the termination and the range of the signals. The first card is the thermocouple input card which contains 32 channels and is set for a gain of 500. Only 12 of the 32 channels are initialized and scanned. The module is configured for ungrounded thermocouples at the experiment, and they are grounded at the SCXI input module. Cold Junction Compensation (CJC) voltage is provided by an additional channel.

The second analog input card is for normal voltage and current loop inputs. There are 32 channels on this input card which are set to a gain of 1. Only 22 channels are initialized and scanned. An analog input is scanned, corrected for voltage calibration constants, and is converted to engineering units. The current to voltage conversion is performed on the module that has been configured for grounded measurement only.

A list of the major data acquisition system components is given in Table 4.1. It should be noted that all the component part numbers refer to National Instrument components.

Table 4.1 - Data Acquisition and Control System Components

Component Part Number	Description/Function
AT-MIO-16D-H	Data acquisition I/O board. 16 single ended or 8 differential channels. Two 12 bit analog and 24 digital I/O channels
SCXI-1100	32 channel multiplexer amplifier
SCXI-1300	Terminal block
SCXI-1303	Thermocouple terminal block with 0.65 C accuracy CJC
SCXI-1000	120 V Chassis

The software for the data acquisition system is based on LabVIEW 3.1 running under Windows and the NIDAQWIN software for the National Instruments Data Acquisition equipment.

The software provides the following functions:

- Allows the user to control various pumps and solenoids within the Data Acquisition System.
- Converts the sensor data from voltage inputs into engineering units.
- Provides monitoring functions for the user with selectable channel sensor outputs.
- Provides a capability to record the sensor data.
- Provides equipment protection and safety features through the use of interlock logic.

4.1 Hardware Interfaces

The hardware interface for different channel types is provided below:

Thermocouples

The thermocouple channels are the first twelve channels (0 to 11) of the data acquisition system. These channels use ungrounded thermocouples which are grounded at the SCXI instrumentation. Additional low pass filtering has been added to the SCXI-1100 module to help filter noise on the thermocouple channels. Cold junction compensation is based on measuring the temperature at the SCXI termination module and all the unused thermocouple channels are grounded to the local SCXI ground.. The temperature is sensed as a voltage by the software and input to a conversion module. The engineering unit conversion factors convert the degree Celsius reading to Fahrenheit.

There are several types of thermocouples that can be accommodated, however the software presently is based on the K-type thermocouples used for this experiment.

Current to Voltage Converted Channels

Most of the process sensors are connected to a 24vdc power supply and a 232 ohm shunt resistor. The shunt resistor (within the SCXI 1100 module) converts the loop current into a sensed voltage. The shunt conversion ratio is compensated within the software with the engineering unit conversion factors.

It should be noted that the selection of the low or high range flow meter must be done before starting the LabVIEW software. The reason is that the engineering unit conversion factor for the high range flow meter is in a different location (line 33, channel # 32).

Standard Voltage Channels

For these channels, a 0 to 10v range is converted to a biased and scaled engineering unit. The standard voltage range of -10 to +10v is used with the heater overtemperature controller and the accelerometer.

Heater Voltage

Special conditioning electronics is used for measuring the heater voltage. The 120VAC heater voltage is stepped down through a 6.3V AC filament type transformer. The output of the transformer is rectified and filtered. The DC value is then clamped at 8vdc. The engineering unit conversion factor is applied to the measured RMS voltage.

Relay Outputs

The 24vdc and 120vac digital outputs are controlled by an Opto-22 solid state relay card. This card converts the National Instrument +5vdc signal to a closed or open output contact. There are 24 output channels. Each output channel is configured by the plug-in solid state relay for the type of output (+24vdc, 120vac).

4.2 PC Based Software (Data Acquisition)

As mentioned earlier, the DAS software is based on LabVIEW 3.1 (running under Windows) and the NIDAQWIN software for the National Instruments Data Acquisition equipment. NIDAQWIN utility sets up the hardware information to link the software drivers to the AT-MIO-16D and SCXI external Analog multiplexers.

The LabVIEW based software performs the following functions:

- DAS Configuration
- Analog Sampling
- Conversion of Analog Sampled Data into Engineering Units
- Front Panel Display
- Data Recording
- Interlock and Shutdown Conditions

The DAS Configuration is performed in two steps. The NIDAQWIN software driver connects the DAS hardware to Windows software services. This includes addressing, DMA control, and Interrupt processing. The second step is done through the executable software. The software sets up a background data acquisition and buffering task. The data acquisition tasks are provided with 2000 scan buffers.

The Analog Sampling is done based on the configuration described above. The analog channels are sampled at a rate controlled by the executable software (100 Hz). Since the thermocouple channels are amplified in the computer, a slower sample rate is selected to prevent capacitive

interference between the channels. All channels are scanned at a single rate to simplify the software. The sampled data is then placed in the data acquisition buffer.

The buffered data is filtered and converted to engineering units. The unit conversion constants are kept in a data file and consist of offset and gain parameters for both the voltage and the engineering unit conversion. The software contains constants to control the filtering of the raw data buffers. The present software uses 10Hz for the output data rate.

The Front Panel display uses the converted data and calculates interlocks to display the experiment status. The front panel contains a decimation factor to select one out of "n" samples to be displayed. This method is used to allow a higher recorded data rate without having a proportional display overhead. The user may select specific variables for display and also view the standard status data. There are also controls for the front panel. These controls access specific tasks; start / stop data recording, turn ON/OFF digital outputs, and display user selected parameters. In addition, an emergency shutdown is provided which causes the experiment to be placed in a specified condition with one button access.

The Data recording is used to set up the output file and to accept a user-defined number of experimental data sets. The software maintains file numbering throughout the experiment for up to 100 sequential data runs. The user maintains the file path, base file name, and data record size. The data is stored in an "EXCEL" compatible file format.

The software maintains interlocks for the preheater, heater, and Freon pump. The Freon pump has a bypass valve which is activated if the discharge pressure is too high.

The preheater and heater have several interlocks that turn off the heat if:

- the experiment section has low flow,
- the Freon pump has too high or too low a discharge pressure,
- the circulating water pump is not on,
- the experiment overtemperature setpoint is exceeded (latched condition).

A view of the LabVIEW front panel display is shown in Fig. 4.1.

4.3 PC Based Software (Analysis)

Two software packages were developed to aid in the data analysis. A data viewer was developed to display the recorded data. Another software package was developed to correct for sensing errors and to provide property look-up tables for the working fluid. The corrected data and the fluid properties were also used with heat transfer correlations to graph the experimental data results.

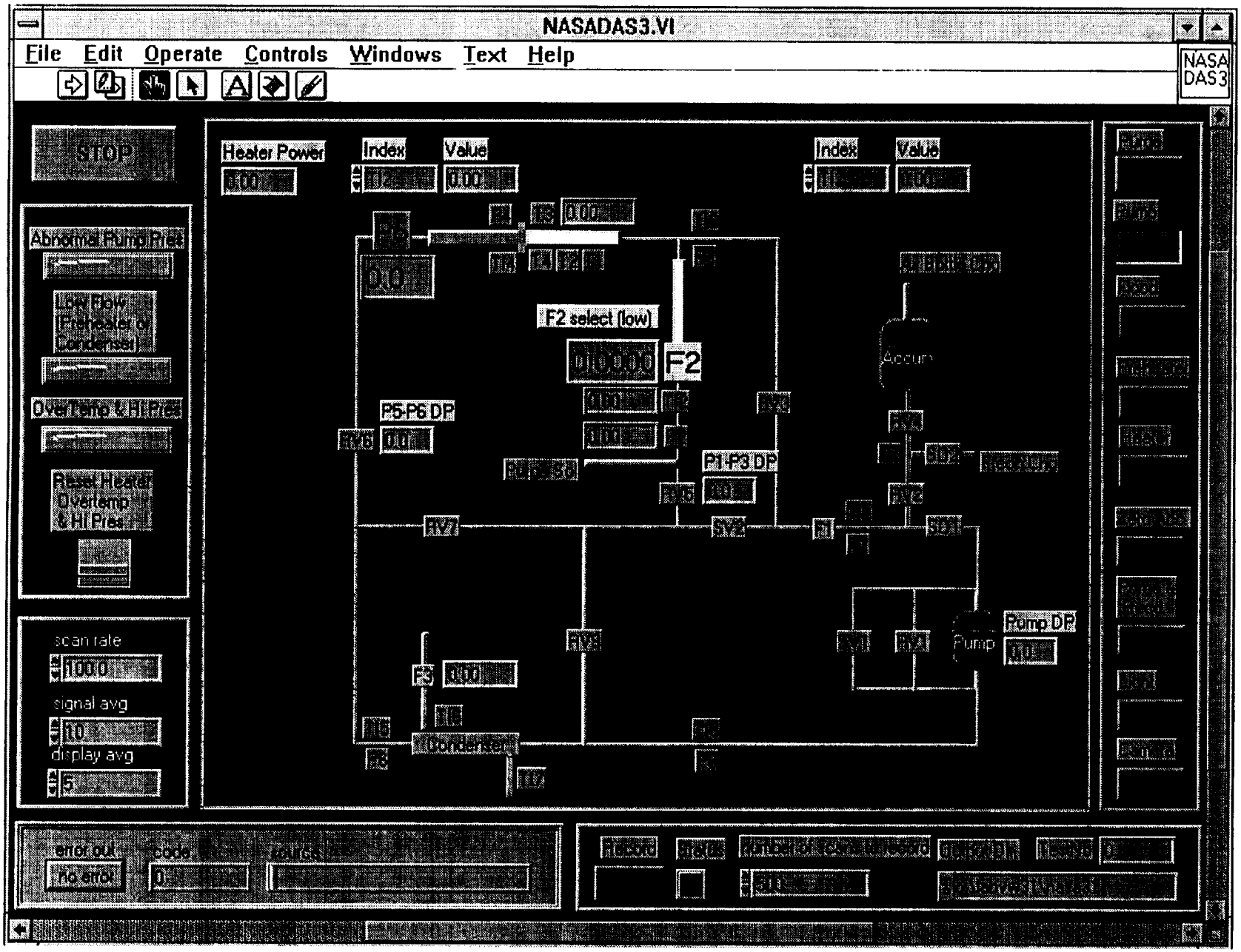

Figure 4.1 - LabView Display

5.0 TEST RESULTS

The tests performed in this program were aimed at generating data for the critical heat flux and the onset of hydrodynamic instability under reduced gravity conditions. All the tests were carried out by supplying a known power level to the heated section in order to boil the fluid up to certain vapor quality, measuring the pressure drop within a specified length of test section, and then condensing and circulating the flow. The critical heat flux tests were carried out at fixed flow rates, by increasing the heat input until a sudden surge in temperature was detected at the exit of the heated section. The instability tests were performed at fixed power levels, by reducing the flow rate until flow fluctuations and subsequent rise in temperature resulted in system shut down. In the laboratory tests, the system was brought to a steady-state condition for any combination of flow and power level, and the data was recorded.

Every aircraft trajectory was performed at a given flow rate and power level. They were developed to produce steady-state conditions during the level flight. It was believed that the system will become more stable during the instability tests, or get farther from CHF, as the plane goes into the high gravity portion of the trajectory. The critical heat flux tests were planned such that the power level was increased during subsequent trajectories until system shutdown due to temperature rise would occur. The plan was to drop back in power level in smaller increments until the critical heat flux is determined. A similar procedure would be used for the instability experiments, but with flow as the main test variable. As will be discussed later, the first series of tests showed pre-mature system shutdown which is believed to be due to orientation of the test section and occurrence of CHF during the 2g portion of the trajectory.

The test parameters consisted of the pressure drop information for every power/flow, or rather flow and quality, combination and the CHF or onset of instability. It should be noted that, although the two-phase pressure drop data is produced at every power/flow combination, only one CHF data point is produced for a set of tests at a given flow rate. Similarly, one data point for the onset of instability is obtained from the set of tests at given power and varying flow rates.

5.1 Normal Gravity Tests

The normal gravity tests consisted of a series of laboratory experiments with the test section in vertical up (+1g) and vertical down (-1g) configurations. As noted earlier, the test loop was packaged in the aircraft racks and only the test section was placed outside the racks in vertical orientation. These tests consisted of a series of steady-state experiments intended to bound the conditions expected under reduced gravities. The critical heat flux tests were performed at nominal volumetric flow rates of 0.05, 0.075, 0.1, 0.125, and 0.15 GPM. The instability tests were performed at 600, 700, and 800 watts for vertical up, and 600, 700, 800, and 900 watts input power for vertical down configuration.

All the laboratory tests were carried out with the fluid temperature at the test section inlet (TI3 in Fig. 2.1) set to 100 ± 1 °F and the test section exit pressure (P5 in Fig. 2.1) at approximately 60 psia. The test procedure consisted of setting the flow rate and exit pressure by adjusting the

regulating valves RV5 and RV6, in Fig. 2.1, with some adjustment from the Freon pump controller, if necessary. For certain flow and power combinations, the gas pressure in the accumulator had to be varied in order to reach the desired conditions. The preheater power was adjusted to achieve the required test section inlet temperature. The power to the heated section was set by adjusting the input voltage. Due to void generation, the test section exit pressure and, therefore, the flow rate would be different after the power level was established. RV5 and RV6 had to be re-adjusted to establish the desired operating conditions. When steady state was achieved, the record button on the LabVIEW screen was pushed to record 500 samples of data.

The critical heat flux tests were performed with all the bypass lines across the heat section closed off. This means that the regulating valves RV7 and RV1 were completely closed to eliminate a parallel line across the heated section. The instability tests were carried out with RV7 open to impose a fixed pressure drop across the heated section.

The critical heat flux tests were performed at five flow rate settings, and the measured critical heat flux along with the mass flux are listed below. Figure 5.1 shows the critical heat flux versus the mass flux for vertical up and down configurations.

Table 5.1 - Measured Critical Heat Flux for Normal Gravity Tests

Vertical Up		Vertical Down	
Mass Flux ($lbm/s\text{-}ft^2$)	Critical Heat Flux ($Btu/s\text{-}ft^2$)	Mass Flux ($lbm/s\text{-}ft^2$)	Critical Heat Flux ($Btu/s\text{-}ft^2$)
32.00	6.17	32.73	5.972
47.79	7.72	48.57	7.964
62.74	11.37	64.05	10.12
77.82	12.57	78.59	10.91
97.88	13.00	94.93	11.16

As shown in Table 5.1, flow orientation does not affect CHF at low mass flow rates. At higher flow rates, CHF occurred at a lower heat input for the vertical downflow configuration. As long as the flow velocity is larger than the bubble rise velocity, the bubbles generated at the wall will be swept by the flow. However, for vertical downflow configuration, the buoyancy force is against the flow direction and bubbles will tend to have a longer residence time in the channel, resulting in larger void fractions and CHF at smaller power levels.

As mentioned earlier, the instability experiments were performed at given test section power levels, by gradually reducing the flow rates. Generally, it was expected that with a parallel single phase line which imposes a fixed pressure drop across the heated section, departure from nucleate

boiling will occur at smaller power levels. In fact it was believed that, for vertical down configurations, instability and subsequent critical heat flux would occur very close to the onset of net vapor generation.

The test results showed that, imposing a fixed pressure drop across the test section by opening a bypass valve resulted in a lower critical heat flux for vertical upflow. There were significant flow oscillations close to CHF which resulted in sudden surface temperature rise. However, the existence of a parallel channel seemed to make the downflow configuration more stable and the test section flow rate had to be substantially reduced to show any surface temperature rise. The measured critical heat flux (or the onset of instability) for vertical upflow configuration is shown in Table 5.2.

Table 5.2 - Measured Onset of Unstable Heat Flux for Normal Gravity Tests.Vertical Upflow

Power Input		Flow Rate at Shut-Off	
(watts)	(Btu/s-ft^2)	GPM	(lbm/s-ft^2)
500	6.40	0.055	33.78
600	7.68	0.09	55.27
700	8.96	0.11	67.55
800	10.24	0.15	92.12

In order to compare the above results with the data for stable CHF, Table 5.1, the flow rates should be interpolated to get similar mass fluxes. These results show that for similar mass flow rates, flow becomes unstable and shut-off occurs at lower power levels when a parallel single-phase flow path exists.

Although these tests have provided only limited CHF data, a large number of pressure drop data points were extracted at intermediate power settings. This data will be used to reduce the two-phase friction multiplier and compare with the existing correlations. The two-phase friction multiplier is defined as the ratio of the two-phase to the corresponding single-phase pressure drop. The single-phase friction pressure drop can be obtained based on the total flow rate, or the gas or liquid flow rate. In the present analysis, the two phase multiplier (ϕ^2_{LO}) is defined based on liquid only (LO) definition, which means that the single-phase pressure drop is calculated based on the total flow rate.

$$\phi^2_{LO} = \frac{\left(\frac{dP}{dZ}\right)}{\left(\frac{dP}{dZ}\right)_{LO}} \tag{5.1}$$

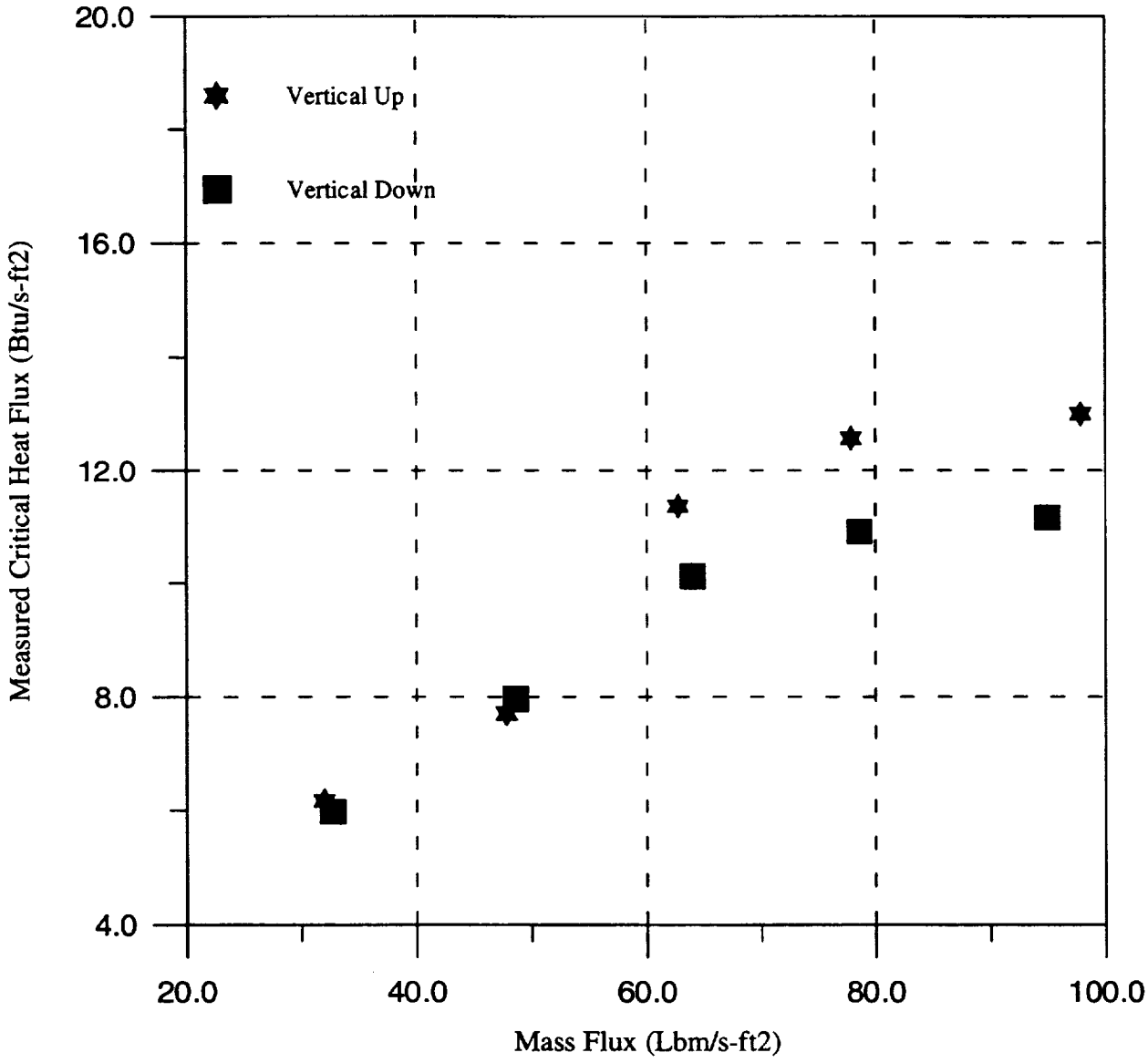

Figure 5.1 - Experimental Critical Heat Flux vs. Mass Flux for Vertical Up and Down Flow Configurations.

$$\left(\frac{dP}{dZ}\right)_{LO} = \frac{2 f_{LO} G^2}{D \rho_L} \tag{5.2}$$

$$f_{LO} = \frac{C}{(Re)_{LO}^{n}} \tag{5.3}$$

$$(Re)_{LO} = \frac{G D}{\mu_L} \tag{5.4}$$

In the above equations,

μ_L = Liquid viscosity

ρ_L = Liquid density

D = Test section diameter

G = Total mass flux

f_{LO} = Single phase friction coefficient

C and n are the constant and the exponent used for the definition of the single-phase friction coefficient. In the present analysis, values of C= 0.316 and n =0.25 were used for turbulent flow conditions.

Since all the tests were performed at the same system pressure and inlet liquid temperature, the only parameters for the variation of the two-phase multiplier would be the mass flux and the quality (or void fraction). Figure 5.2 shows the two-phase friction multiplier for vertical upflow, as a function of quality at the entrance to the adiabatic section for three flow rates. This figure shows that the two-phase friction multiplier is independent of the flow rate and increases with quality for equilibrium qualities less than ~0.4. Although a flow regime map analysis was not made in this study, it is believed that a flow regime transition occurs around an equilibrium quality of 0.4. For larger qualities, the mass flow rate affects the two-phase friction multiplier, and lower mass flow rates result in larger multipliers.

Two-phase friction, based on the measured pressure drop for downflow configuration, is plotted in Figure 5.3. The two-phase multiplier is independent of the flow rate for equilibrium qualities larger than 0.1-0.2. Although this is believed to be due to a flow regime transition, reduction of two-phase pressure drop with quality in the low quality range cannot be explained.

ERRATA

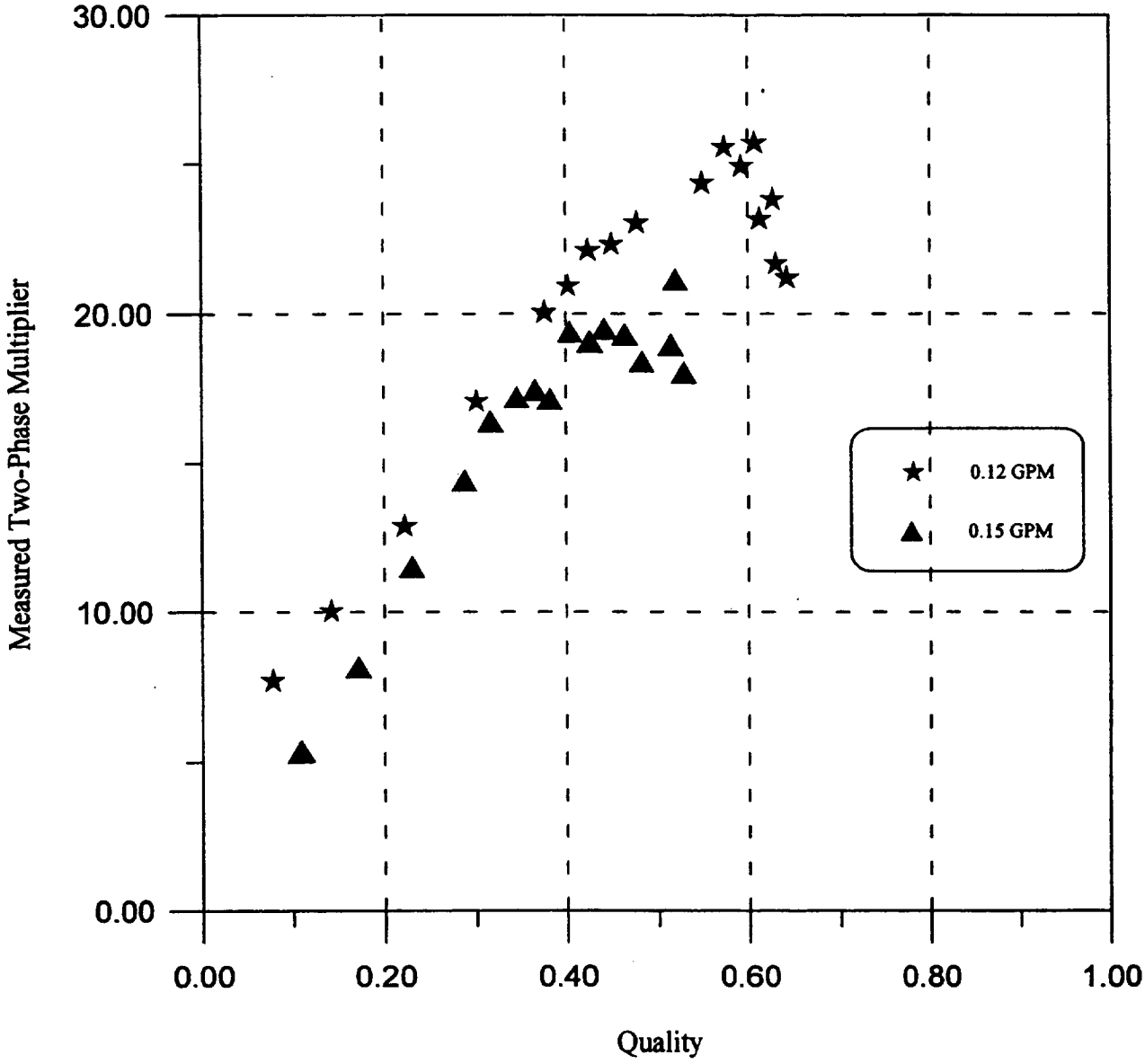

Figure 5.2 - Two-Phase Friction Multiplier Based on Measured Pressure Drop vs. Quality for Upflow Configuration.

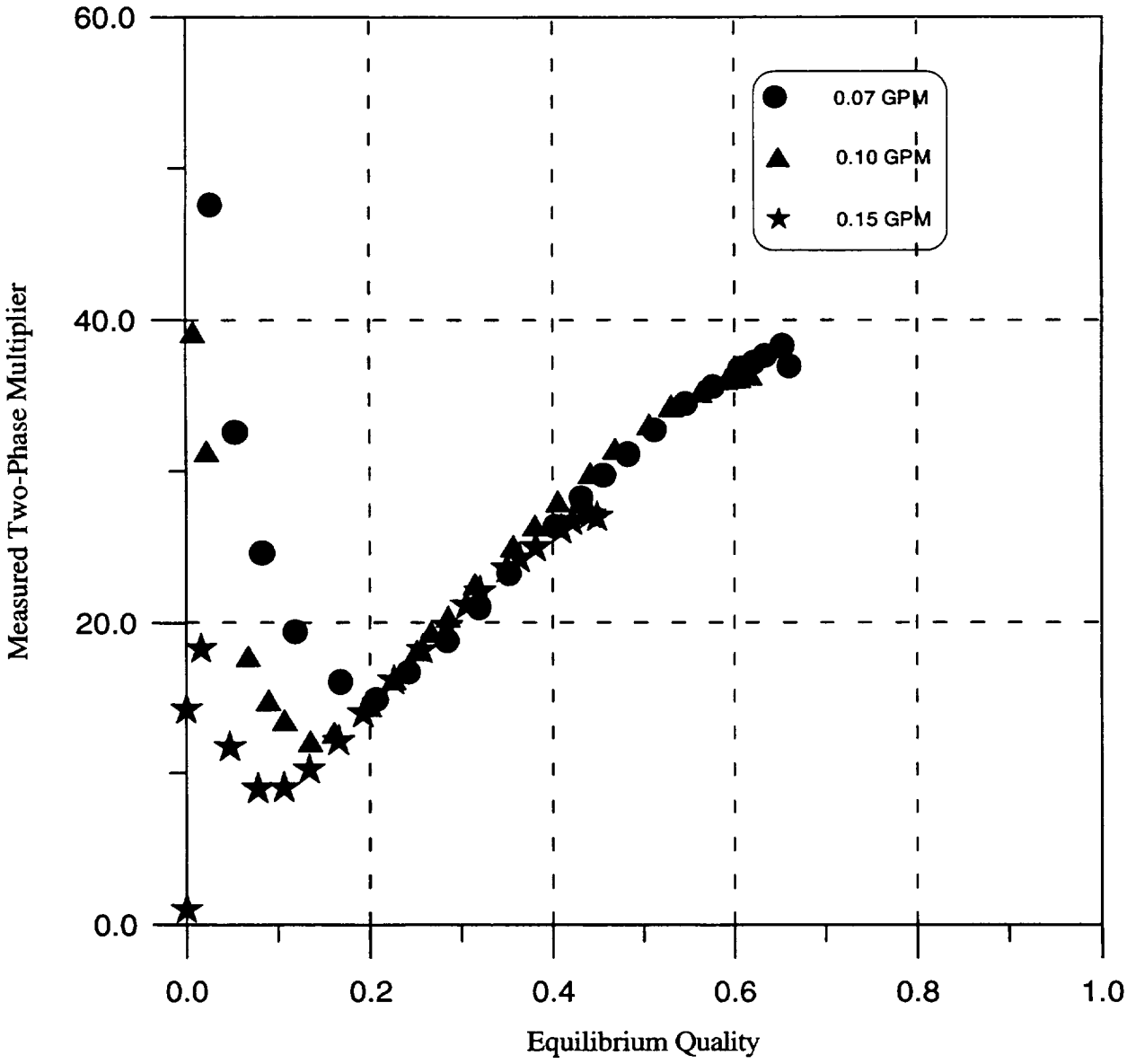

Figure 5.3 - Two-Phase Friction Multiplier Based on Measured Pressure Drop vs. Quality for Downflow Configuration.

5.2 Reduced Gravity Tests

As mentioned earlier, the first set of the aircraft trajectory tests was mainly aimed at evaluating the loop and the test procedures. These experiments consisted of four flight days aboard NASA DC-9 over a period between March 26 and April 4, 1996. A procedure was developed for the reduced gravity period tests which is given in Appendix D.

The first day of testing showed several problems with the condenser ice box which resulted in modification of the condenser secondary loop. The ultimate heat sink for the condenser cooling water consisted of an off-the shelf cooler, filled with a mixture of ice and water. The condenser cooling water was extracted from the bottom of the cooler, and the return water was injected through a hole close to the top of the cooler. A wire mesh was placed in the cooler which kept the ice above the water extraction line to avoid passing ice through the pump. Although it was believed that the cooler cap was water tight, under reduced gravity conditions extraction of water from this open system proved to be very difficult. First, there were leaks from the cooler to the aircraft cabin, and secondly air/water mixture intake into the pump caused system shut-down on low water flow rate signal. The open condenser cooling loop was modified by NASA and a closed copper coil was utilized. This coil was cooled by bags of ice and water which were placed around the coil inside the ice box. The testing was stopped on March 28 due to aircraft mechanical problems and resumed on April 3.

The packaging of the loop and the procedure for the low gravity testing were developed based on the idea that the 2g acceleration at the start of the low gravity trajectory was directed towards the tail of the aircraft. Therefore, the test section was placed in a horizontal position with flow direction towards the front of the plane (opposite the assumed gravity vector). This was intended to avoid flow stratification during the 2g portion of the flight which would result in temperature rise along the portion of the test section covered by vapor, and subsequent system shutdown. Actually, most of the gravity vector during the 2g acceleration was towards the floor of the plane which resulted in system shutdown prior to reduced gravity dive. Although the preliminary tests provided only a few CHF data points at zero g, there is sufficient data for the two-phase pressure drop which can be used to evaluate the applicability of the normal gravity models.

One of the main concerns with any reduced gravity aircraft trajectory experiment is whether the conditions become stable during the 20 to 30 seconds of low gravity dive. Figure 5.4 shows a plot of data directly extracted from the data acquisition system for one of the reduced gravity tests. The volumetric flow rate, test section exit pressure, and the X-component of the acceleration which is perpendicular to the floor of the aircraft, are plotted vs. time. It can be seen that the pressure drop increases and remains fairly stable throughout the low gravity portion of the flight. The data was averaged over the time period during the reduced gravity conditions when the pressures and flow rate remained stable. For some tests like the one shown in Figure 5.4, the entire reduced gravity period was represented with one average condition. For some other tests, several average representative conditions were obtained.

It should be noted that due to the short duration between two trajectories, there was not sufficient time to adjust the regulating valves to maintain a constant flow rate while varying the power.

During the tests, the volume expansion due to evaporation caused the test section exit pressure, and therefore the pump inlet pressure, to rise. Since the accumulator forced a constant pressure at the pump exit, the pressure drop across the pump dropped as more vapor was generated. This variation in pressure drop across the pump affected the pump flow rate, and there was not sufficient time to re-adjust the flow following heat-up. Therefore, the tests were carried out at different flow rates, as shown in Table 5.3. However, Figure 5.5 shows that the two-phase friction multipliers fall on the same curve and vary only with quality. This suggests that all the recorded tests were at the same flow regime, probably annular flow.

Table 5.3 - Reduced Gravity Two-Phase Friction Multiplier Based on Measured Pressure Drop

Quality	Mass Flux ($lbm/s\text{-}ft^2$)	ϕ^2_{LO}
.558	50.463	28.450
.637	45.306	30.506
.571	60.289	27.048
.711	50.428	34.814
.751	48.145	35.600
.795	45.851	36.678
.871	42.384	38.108
.387	88.884	17.829
.455	78.048	21.591
.539	68.157	26.033
.380	90.571	14.127
.228	79.678	13.406
.245	85.736	9.766
.237	86.253	11.504
.630	59.456	25.760
.596	62.225	25.019
.594	62.408	26.197
.181	117.459	10.840
.376	94.326	19.825
.424	97.048	20.291
.459	91.063	22.029
.492	85.745	23.600
.533	80.309	24.374
.571	75.984	25.877
.200	82.288	11.111

Table 5.3 - Reduced Gravity Two-Phase Friction Multiplier Based on Measured Pressure Drop (continued)

Quality	Mass Flux (lbm/s-ft^2)	ϕ^2_{LO}
.205	80.667	11.717
.206	80.405	12.312
.205	80.650	12.574
.153	105.921	11.129
.149	107.087	11.490
.400	83.657	21.868
.402	82.608	22.933
.109	117.246	7.243
.108	7.771	7.771
.125	122.941	9.434
.274	104.449	15.561
.276	103.206	16.341
.188	112.219	11.453
.192	110.298	12.122
.402	97.444	20.965
.192	109.575	12.622
.556	80.658	24.273
.491	99.158	19.539
.343	53.295	19.523
.377	54.528	20.909
.288	76.221	17.102
.305	75.753	17.139
.556	53.583	28.130
.172	105.107	11.932
.193	102.290	13.200
.227	98.615	14.625
.286	88.349	17.240
.440	66.647	23.670
.371	83.608	20.936
.401	83.472	21.559

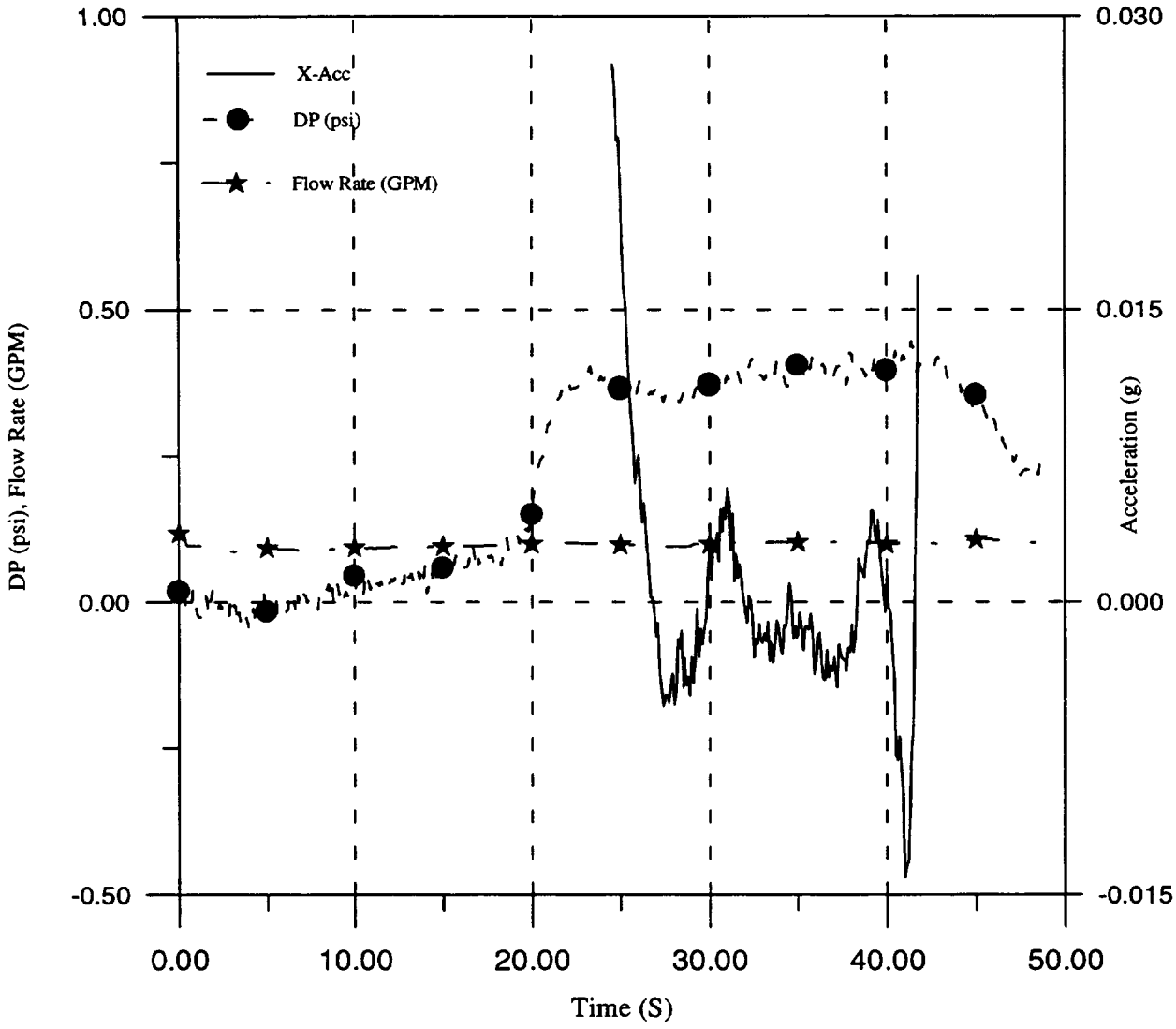

Figure 5.4 - Pressure Drop, Flow Rate, and X-Acceleration vs. Time for Flight Test 17.

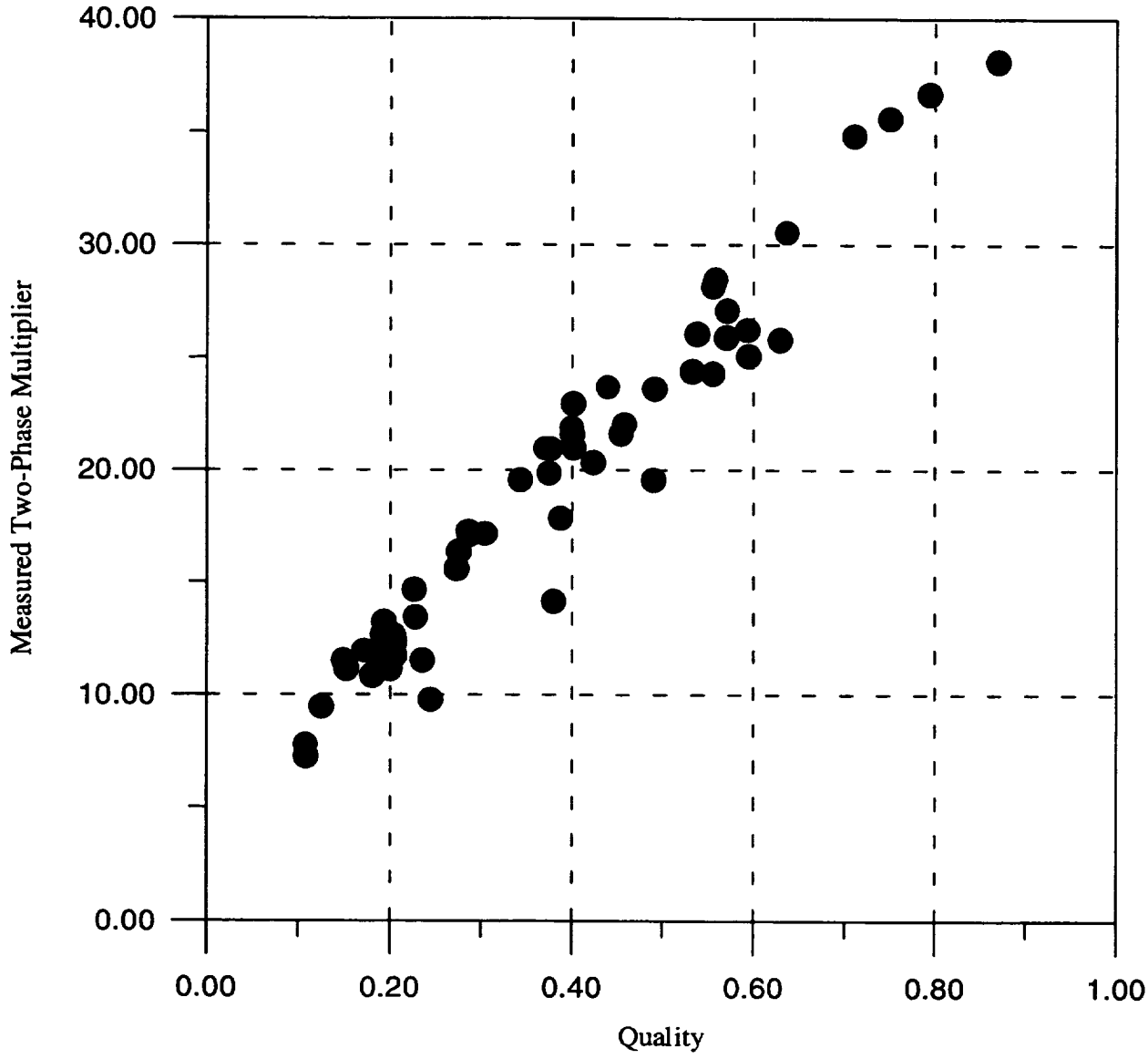

Figure 5.5 - Two-Phase Friction Multiplier Based on Measured Reduced Gravity Pressure Drop vs. Quality.

As mentioned earlier, most of the tests intended to produce critical heat flux under reduced gravity conditions, resulted in system shut-down during the 2g portion of the flight. However, a few CHF data points were obtained which were due to flow changes following the heat-up and evaporation. As noted above, the void generation in the test section resulted in a reduction in the flow, because of changes in the pump head. For a few of the tests performed during the last two flight days, the flow and power conditions were sufficiently different from CHF which system shut-down did not occur during the 2g portion of the flight. However, the drop in the flow rate just prior to the reduced gravity dive, resulted in reaching CHF during reduced gravities. Figure 5.6 shows the variation of the pressure drop and flow rate during one of these tests. These data points will be compared to the normal gravity data and CHF models in the following sections.

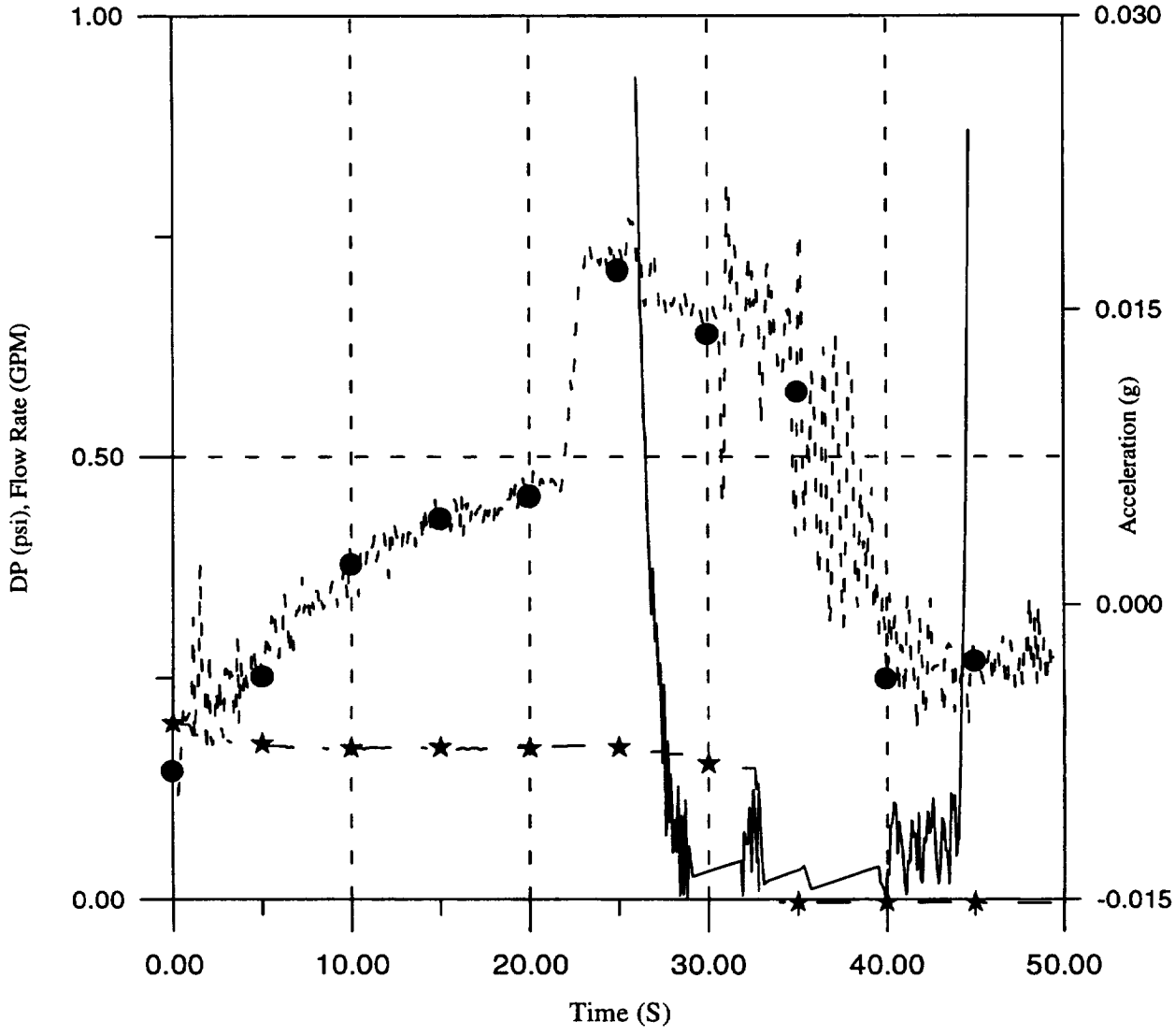

Figure 5.6 - Pressure Drop, Flow Rate, and X-Acceleration vs. Time for Flight Test 23.

5.3 Prediction of Two-Phase Pressure Drop

Following the pioneering study performed by Heppner et al., Ref. 6, it was generally believed that, under equivalent flow conditions, two-phase pressure drops at reduced gravities are significantly higher than they would be at the normal gravity. Heppner's study was mainly aimed at flow regime identification and quantitative pressure drop data was not reported. With renewed interest in application of two-phase flow to spacecraft thermal management systems, several studies were initiated in the mid-80's. Although the majority of these studies were aimed at flow regime identification, some pressure drop behavior was also reported. One of the studies performed by Sunstrand Corp. aboard NASA KC-135, Ref. 7, also confirmed Heppner's conclusion regarding the higher two-phase pressure drops at reduced gravities. Detailed measurements performed by Foster-Miller and Texas A&M University aboard NASA KC-135, Ref. 8, has shown that there is essentially no difference between the ground test results and the reduced gravity pressure drops. The best overall prediction of the two-phase pressure drop was obtained by an annular flow model, although it is not clear which model was used for the predictions.

Prediction of the two-phase pressure drop is one of the main concerns in design and analysis of any system operating with a two-phase flow. Although there are a large number of publications on this subject, there is no completely satisfactory procedure for evaluating two-phase pressure drop under all the conditions. The majority of the commonly used models are empirical and account for the effect of the controlling parameters within their range of applicability. These models can predict the two-phase pressure drop, if they are properly used for the geometries and flow conditions that they are intended for. Most of these models do not differentiate between different flow regimes, boiling or adiabatic conditions, and the flow orientation. Several commonly used models were applied for prediction of the two-phase friction multiplier, as defined by equation 5.1. A brief description of these models is provided here.

Homogeneous Equilibrium Model (HEM)

The simplest form of the two-phase multiplier is based on the assumption of a homogeneous flow where the phases are treated as a mixture with their corresponding properties. The two-phase multiplier is given by:

$$\phi_{LO}^2 = 1 + \left(\frac{\rho_L}{\rho_G} - 1\right) X \tag{5.5}$$

where X is the equilibrium quality, ρ is the density and the subscripts L and G refer to liquid and vapor phases.

Chisholm Correlation

The Chisholm correlation, Ref. 9, was developed in an attempt to generate an analytical basis for the Lockhart-Martinelli correlation, Ref. 10. Later, the effect of property variation was incorporated through the parameter Γ, and the resulting correlation predicted the data used by a number of other correlations. The Chisholm-B correlation is given by:

$$\phi_{LO}^2 = 1 + (\Gamma^2 - 1)\{B\,[X(1-X)]^{\frac{2-n}{2}} + X^{2-n}\} \tag{5.6}$$

$$\Gamma = \left(\frac{\rho_L}{\rho_G}\right)^{0.5} \left(\frac{\mu_G}{\mu_L}\right)^{n/2}$$

μ is the viscosity and the exponent n is in the range of 0.2 to 0.25. B is given by the following table

Γ	G (lbm/s-ft^2)	B
$\Gamma \le 9.5$	$G \le 102$	4.8
	$102 < G < 390$	492/G
	$G \ge 390$	$25/(G)^{0.5}$
$9.5 < \Gamma < 28$	$G \le 123$	$\frac{235}{\Gamma G^{0.5}}$
	$G > 123$	$21/\Gamma$
$\Gamma > 28$		$\frac{6788}{\Gamma^2 G^{0.5}}$

In addition, Chishlom has proposed a correlation which is cast similar to the Lockhart-Martinelli correlation. This correlation is known as Chisholm-C and is given below.

$$\phi_{LO}^2 = (1-X)^{2-n}\left[1 + \frac{C}{\chi_{tt}} + \frac{1}{\chi_{tt}^2}\right] \tag{5.7}$$

where C = 26 and χ_{tt} which is the Lockhart-Martinelli parameter is given by

$$\chi_{tt} = \left(\frac{\rho_G}{\rho_L}\right)\left(\frac{\mu_L}{\mu_G}\right)^n \left(\frac{1-X}{X}\right)^{2-n} \tag{5.8}$$

Fit to Lockhart Martinelli

Chisholm has also suggested a fit to Lockhart-Martinelli which actually uses equation 5.7 with C=21.

Friedel Correlation

Using a large data bank containing over 25,000 data points, Friedel developed the following correlation which is valid for horizontal and vertical upflow, Ref. 3. It should be noted that, apparently there is also a Friedel downflow correlation which we have not been able to locate.

$$\phi_{Lo}^2 = E + \frac{3.24\ FH}{Fr^{0.045}\ We^{0.035}}$$

$$E = (1-x)^2 + x^2\ \frac{\rho_L\ f_{Go}}{\rho_G\ f_{Lo}}$$

$$F = x^{0.78}\ (1-x)^{0.24}$$

$$H = \left(\frac{\rho_L}{\rho_G}\right)^{0.91} \left(\frac{\mu_G}{\mu_L}\right)^{0.19} \left(1-\frac{\mu_G}{\mu_L}\right)^{0.7} \qquad (5.9)$$

$$Fr = \frac{G^2}{gD\rho_{TP}^2}$$

$$We = \frac{G^2 D}{\rho_{TP}\ \sigma}$$

$$\rho_{TP} = \left(\frac{x}{\rho G} + \frac{1-x}{\rho_L}\right)^{-1}$$

All of the above models were used to predict the two-phase friction multiplier based on the measured ΔP. Figures 5.7 to 5-11 show the comparison of the measured and predicted two-phase friction multipliers using the above models for the normal gravity tests with vertical upflow configuration. The best agreement is obtained by the HEM and the Friedel models.

The comparisons of the measured and predicted two-phase friction multipliers by the above models for the downflow configuration are shown in Figures 5.12 to 5.16. Although the HEM and Friedel models result in closer agreement with data, predictions by none of these models are satisfactory. This was expected since the flow regime for downflow is considerably different and none of the above correlations had included downflow data in their development.

The predictions for the reduced gravity two-phase friction multipliers are shown in Figures 5.17 to 5.21. Basically, the data and predictions are very similar to vertical upflow normal gravity tests and HEM and Friedel models provide the best agreement. This may be caused by similarity in flow regimes between the two cases.

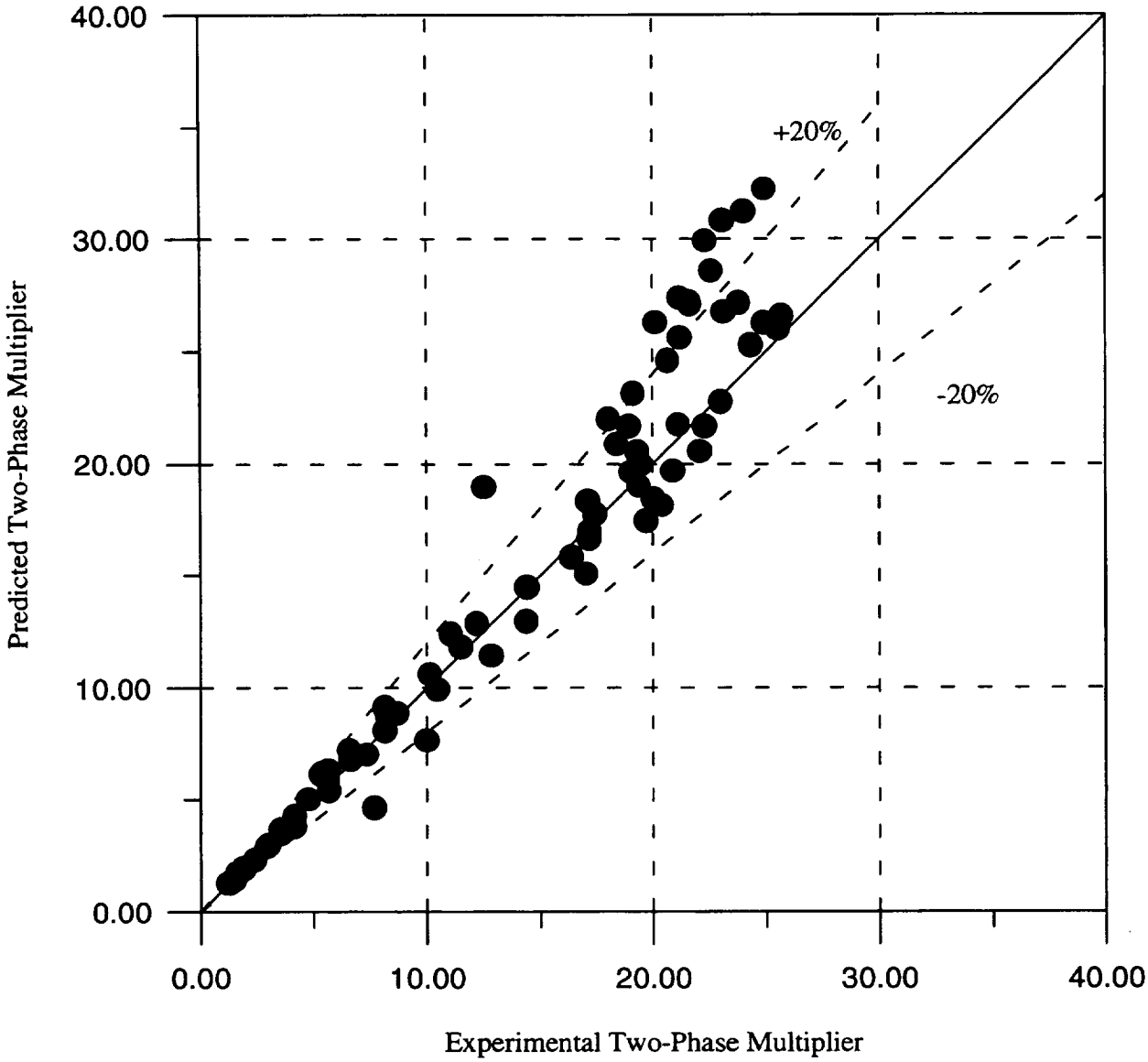

Figure 5.7 - Comparison of the Predicted and Experimental Two-Phase Friction Multipliers Using HEM for Vertical Upflow.

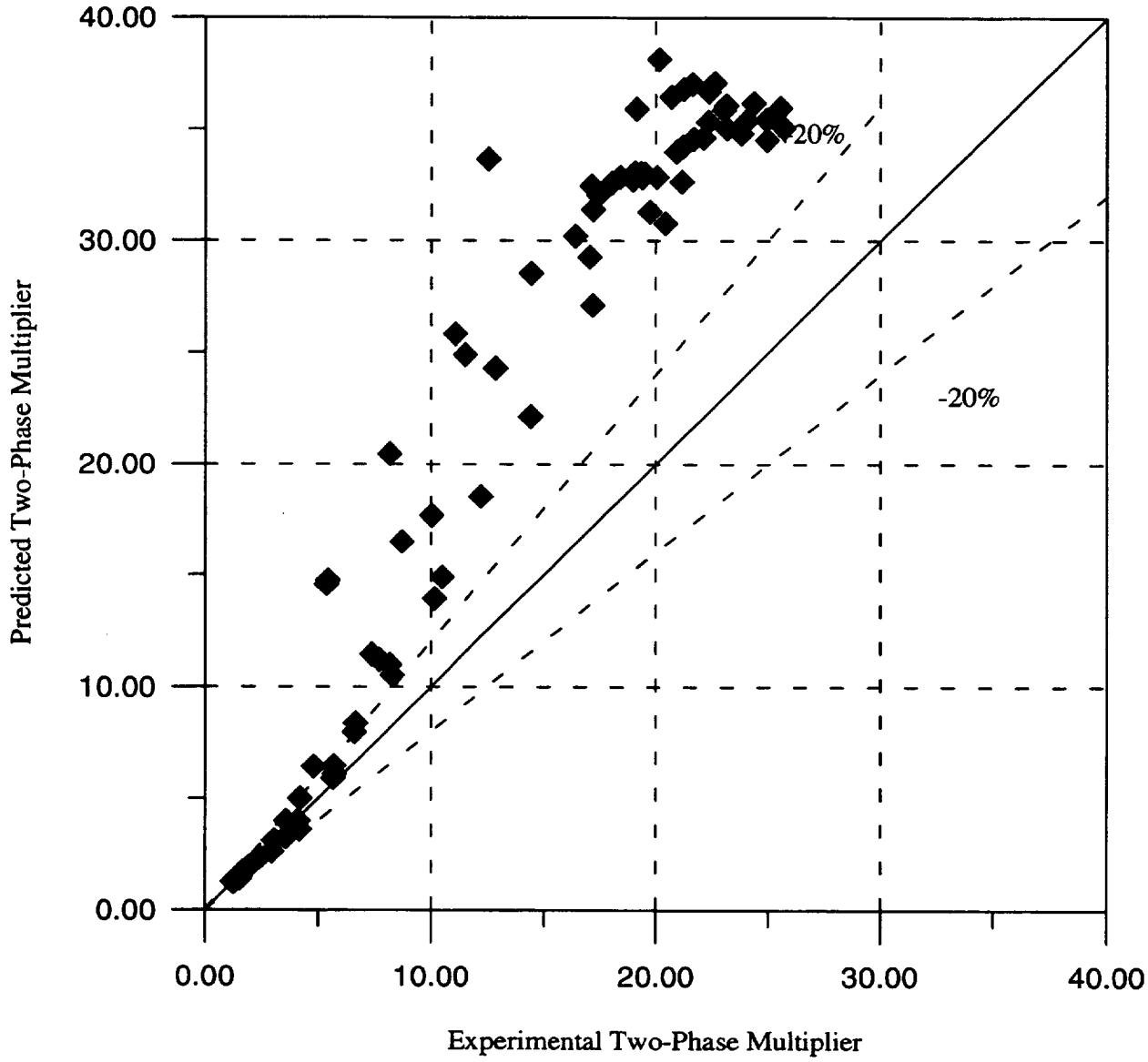

Figure 5.8 - Comparison of the Predicted and Experimental Two-Phase Friction Multipliers Using Chisholm -B Model for Vertical Upflow.

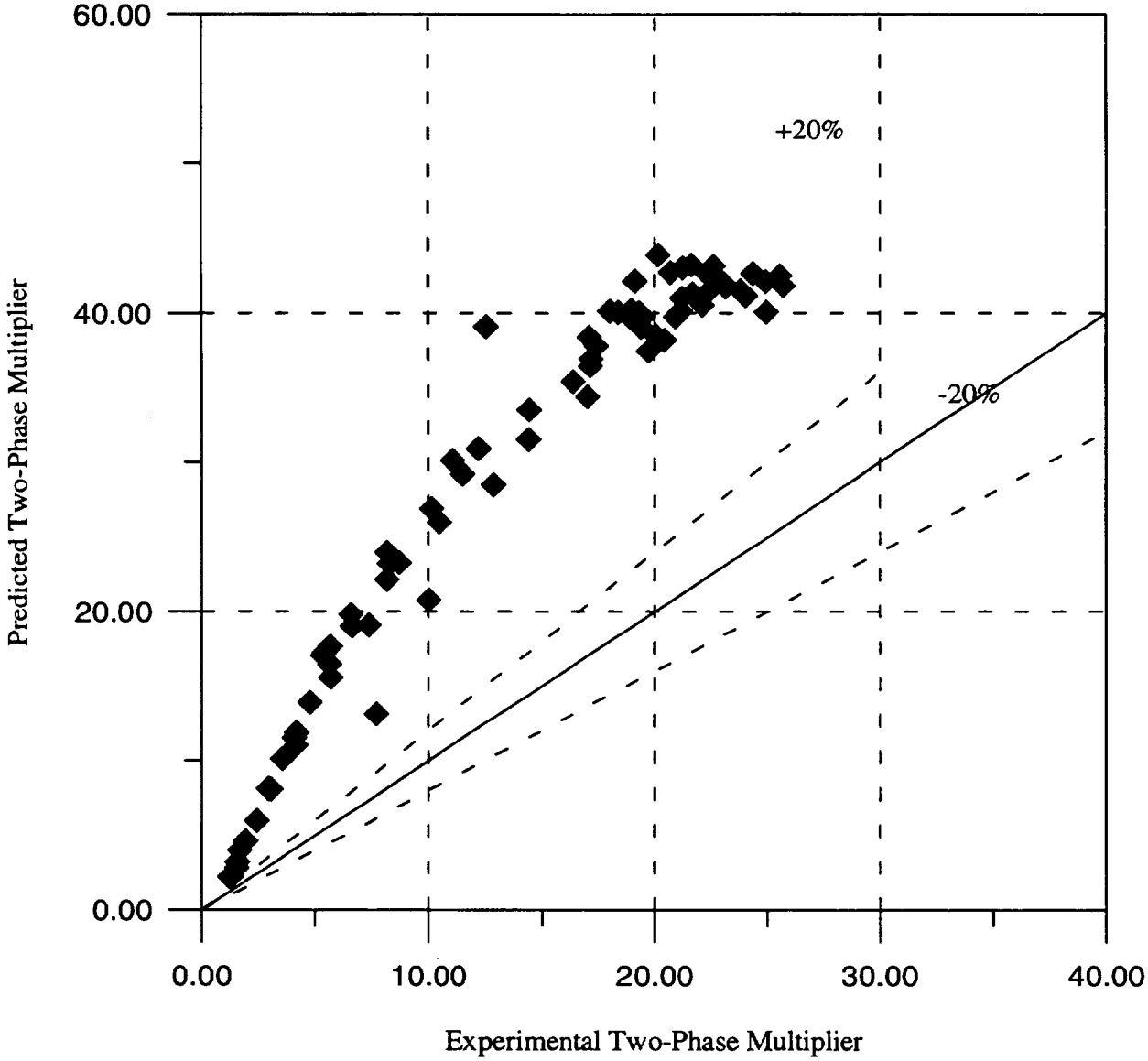

Figure 5.9 - Comparison of the Predicted and Experimental Two-Phase Friction Multipliers Using Chisholm-C Model for Vertical Upflow.

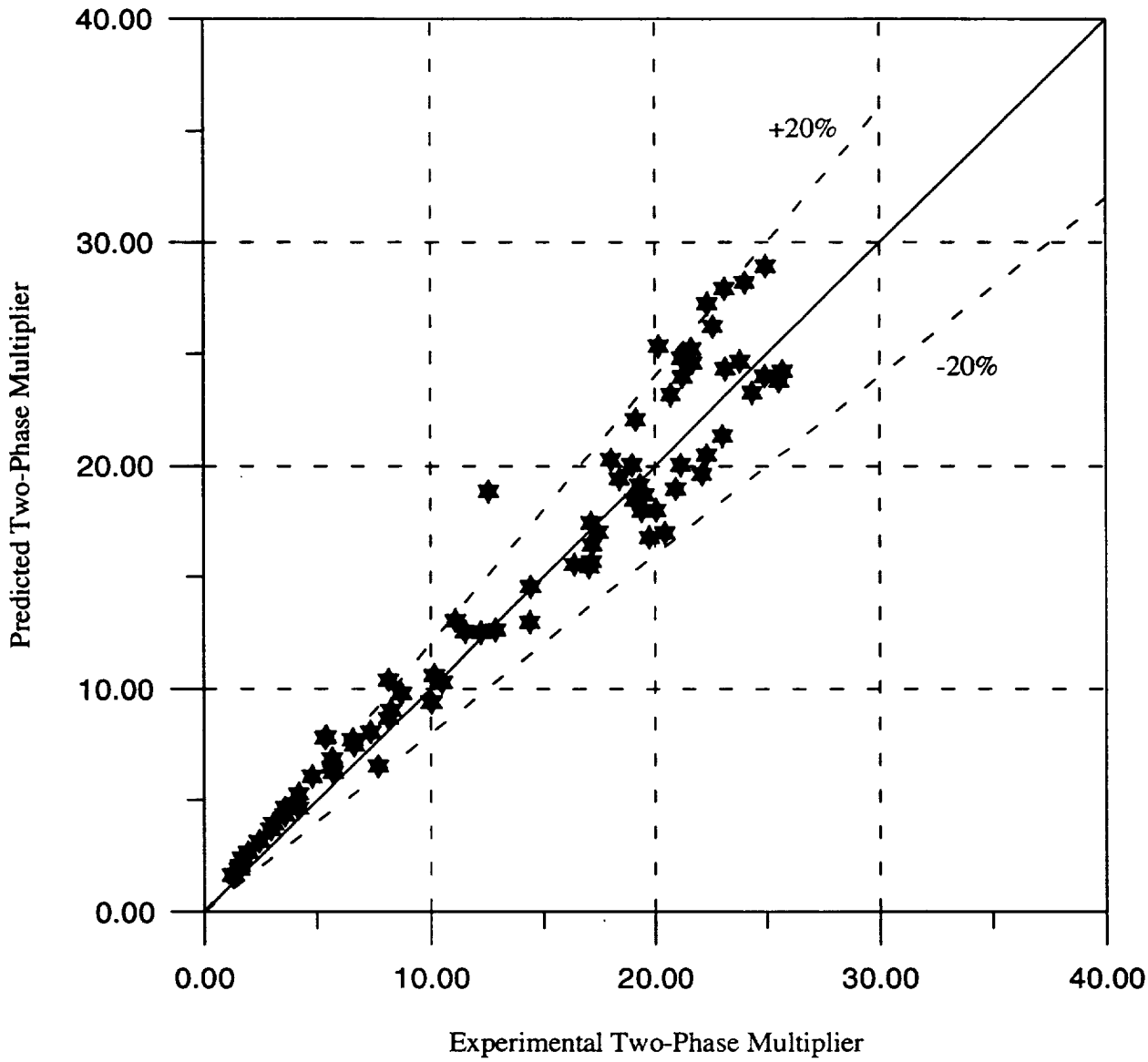

Figure 5.10 - Comparison of the Predicted and Experimental Two-Phase Friction Multipliers Using Friedel Model for Vertical Upflow.

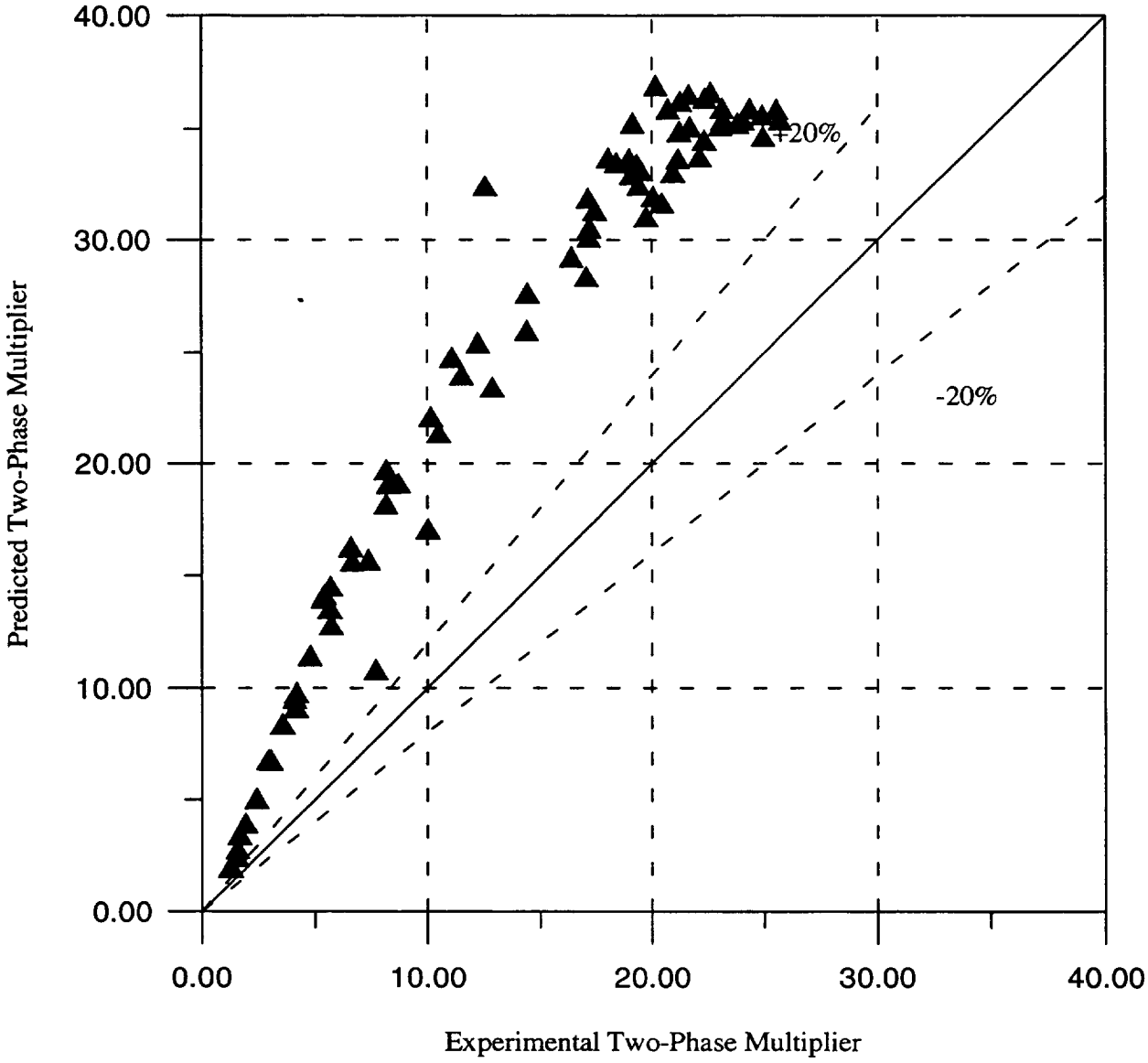

Figure 5.11 - Comparison of the Predicted and Experimental Two-Phase Friction Multipliers Using Lockhart-Martinelli Model for Vertical Upflow.

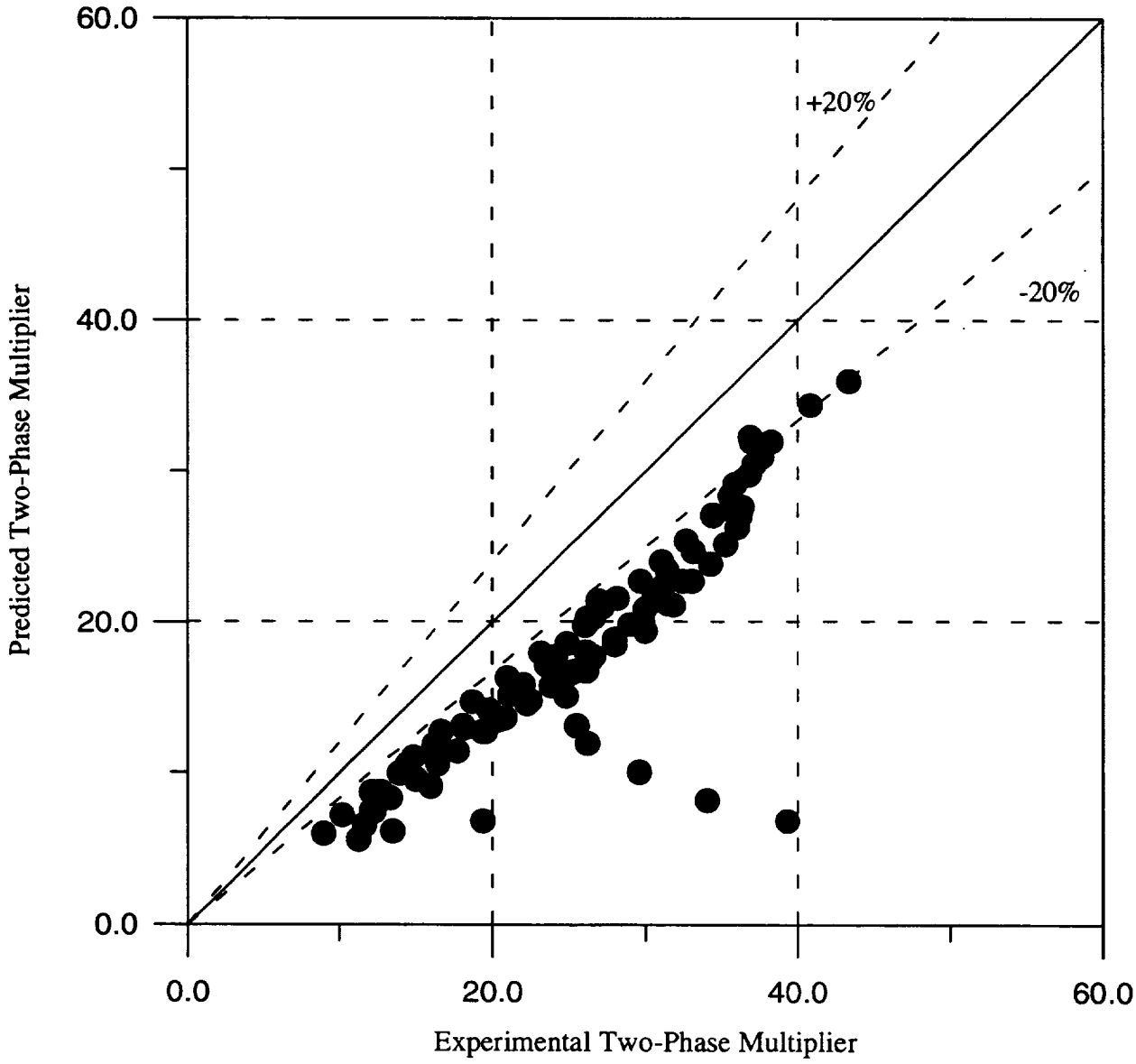

Figure 5.12 - Comparison of the Predicted and Experimental Two-Phase Friction Multipliers Using HEM for Vertical Down Flow.

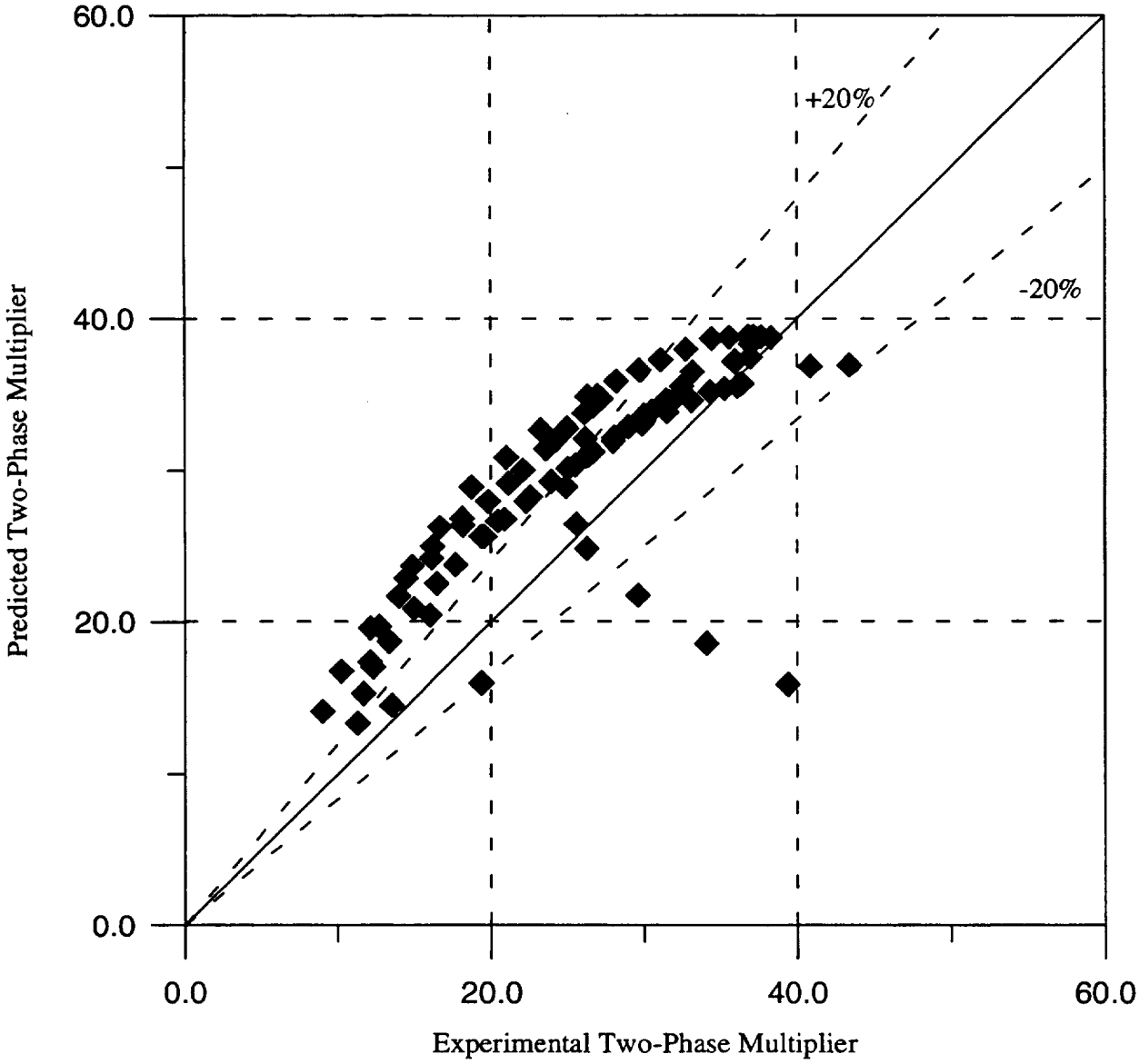

Figure 5.13 - Comparison of the Predicted and Experimental Two-Phase Friction Multipliers Using Chisholm-B model for Vertical Down Flow.

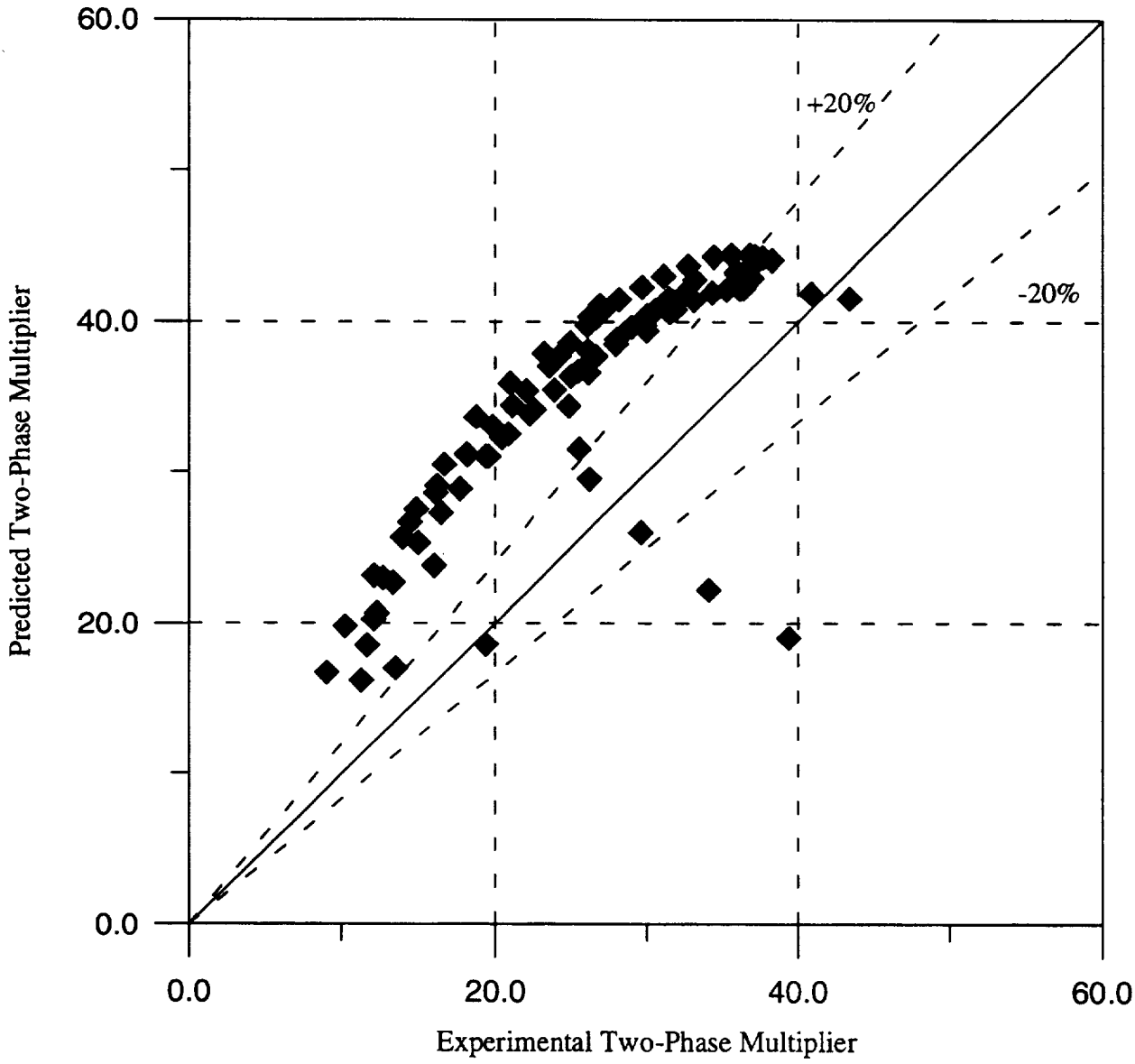

Figure 5.14 - Comparison of the Predicted and Experimental Two-Phase Friction Multipliers Using Chisholm-C model for Vertical Down Flow.

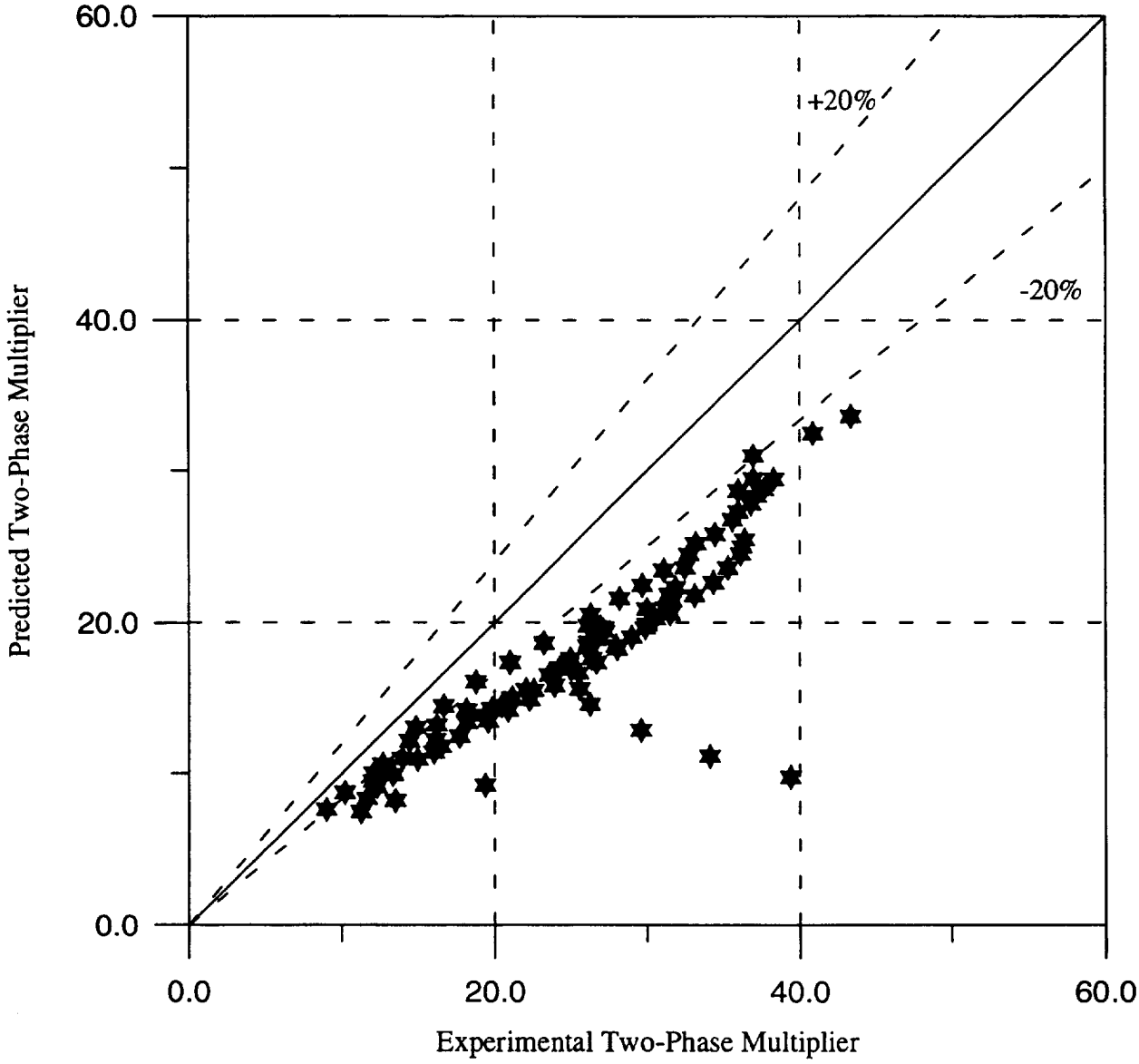

Figure 5.15 - Comparison of the Predicted and Experimental Two-Phase Friction Multipliers Using Friedel model for Vertical Down Flow.

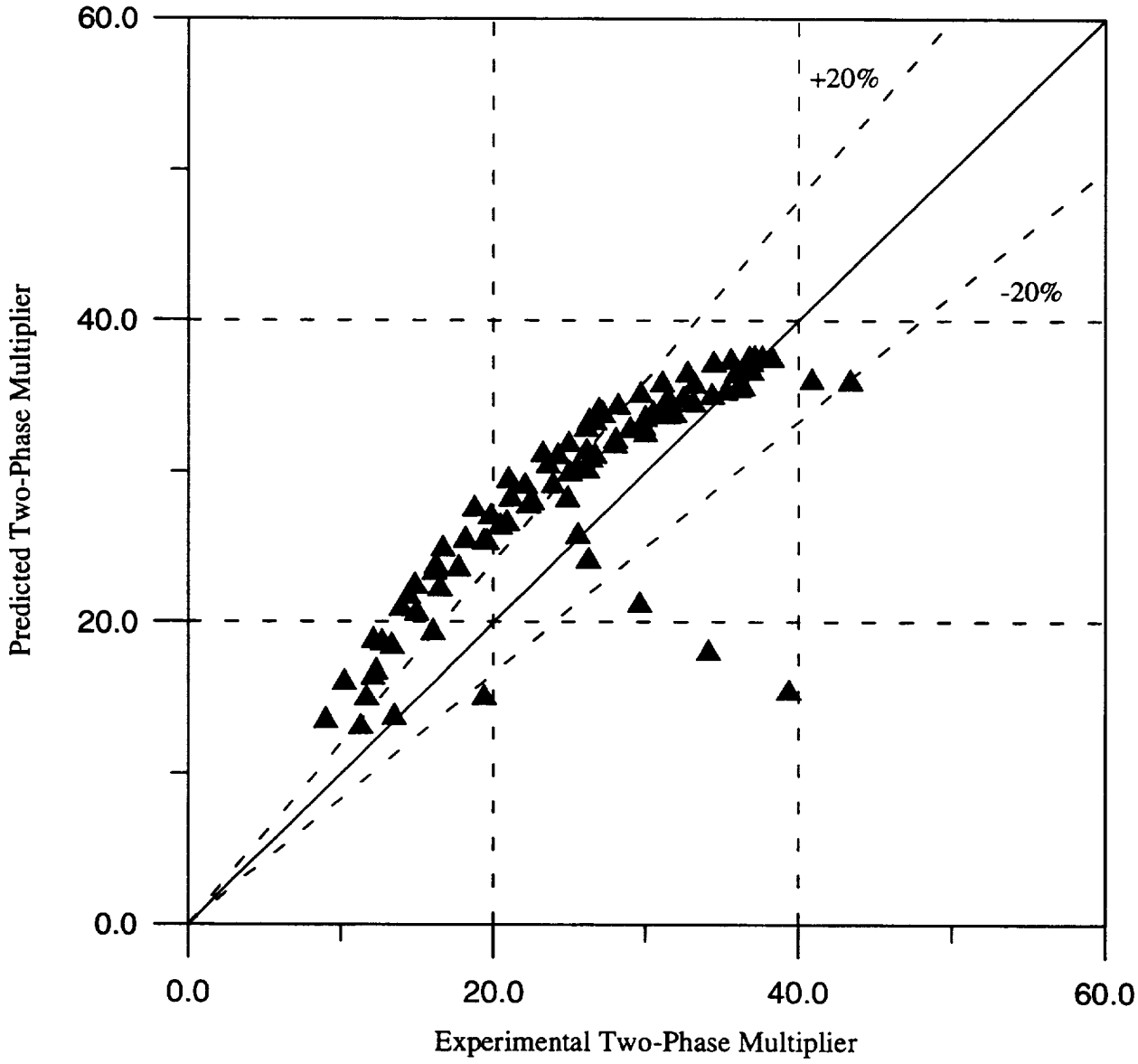

Figure 5.16 - Comparison of the Predicted and Experimental Two-Phase Friction Multipliers Using Lockhart-Martinelli model for Vertical Down Flow.

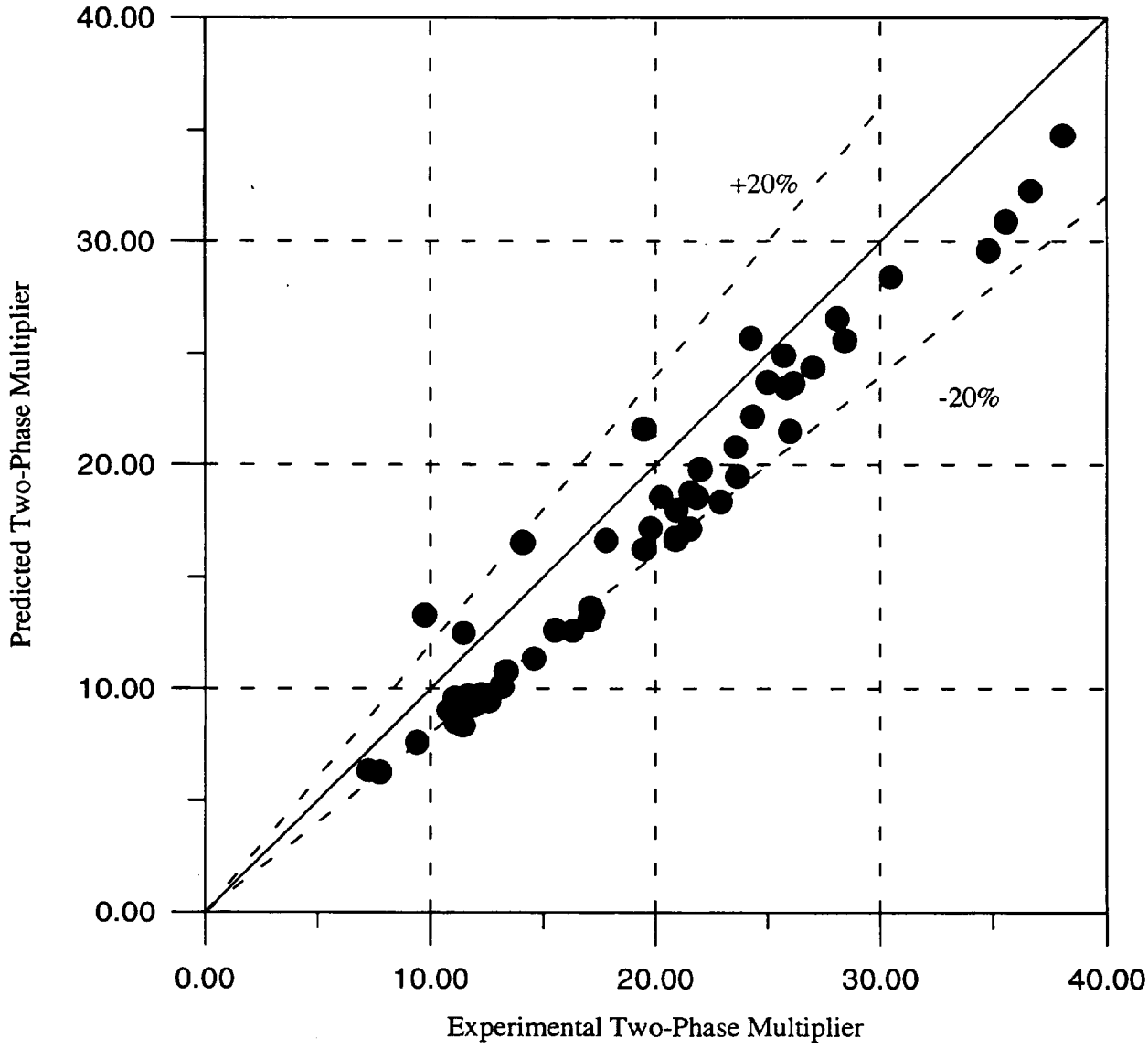

Figure 5.17 - Comparison of the Predicted and Experimental Two-Phase Friction Multipliers for Reduced Gravity Using Homogeneous Equilibrium Model.

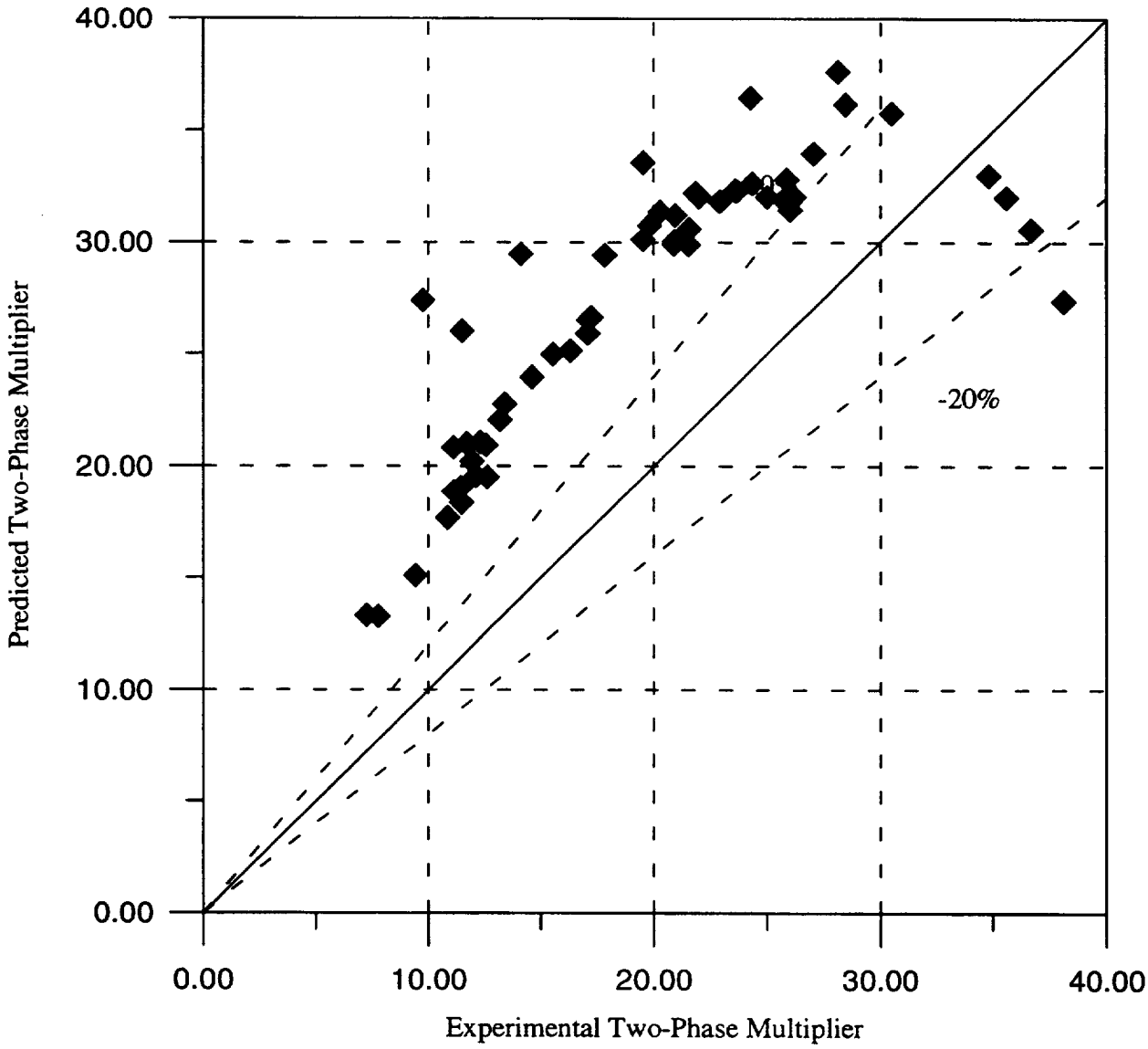

Figure 5.18 - Comparison of the Predicted and Experimental Two-Phase Friction Multipliers Using Chisholm B Model for Reduced Gravity.

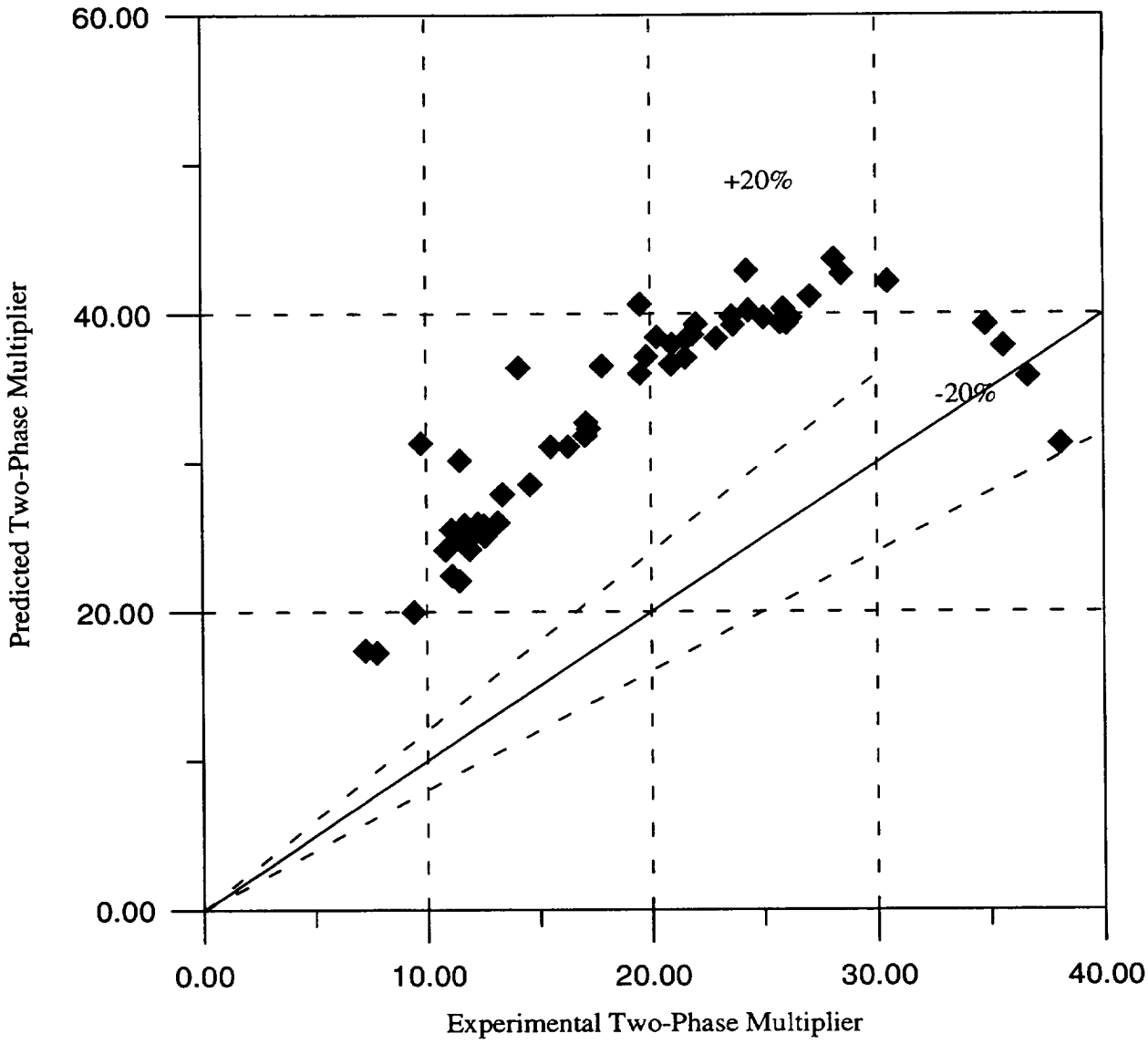

Figure 5.19 - Comparison of the Predicted and Experimental Two-Phase Friction Multipliers Using Chisholm-C Model for Reduced Gravity.

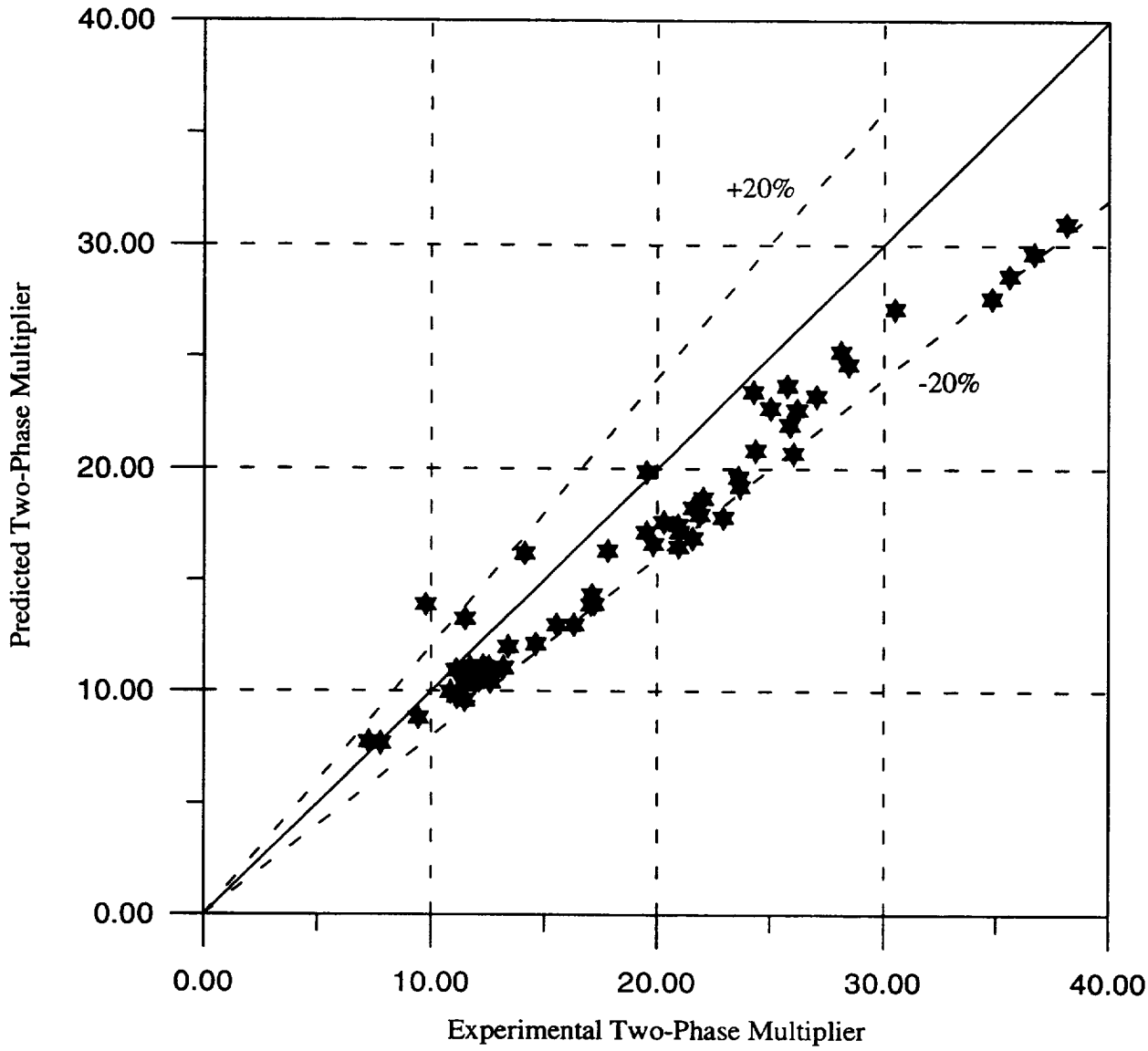

Figure 5.20 -Comparison of the Predicted and Experimental Two-Phase Friction Multipliers for Reduced Gravity Using Friedel Model.

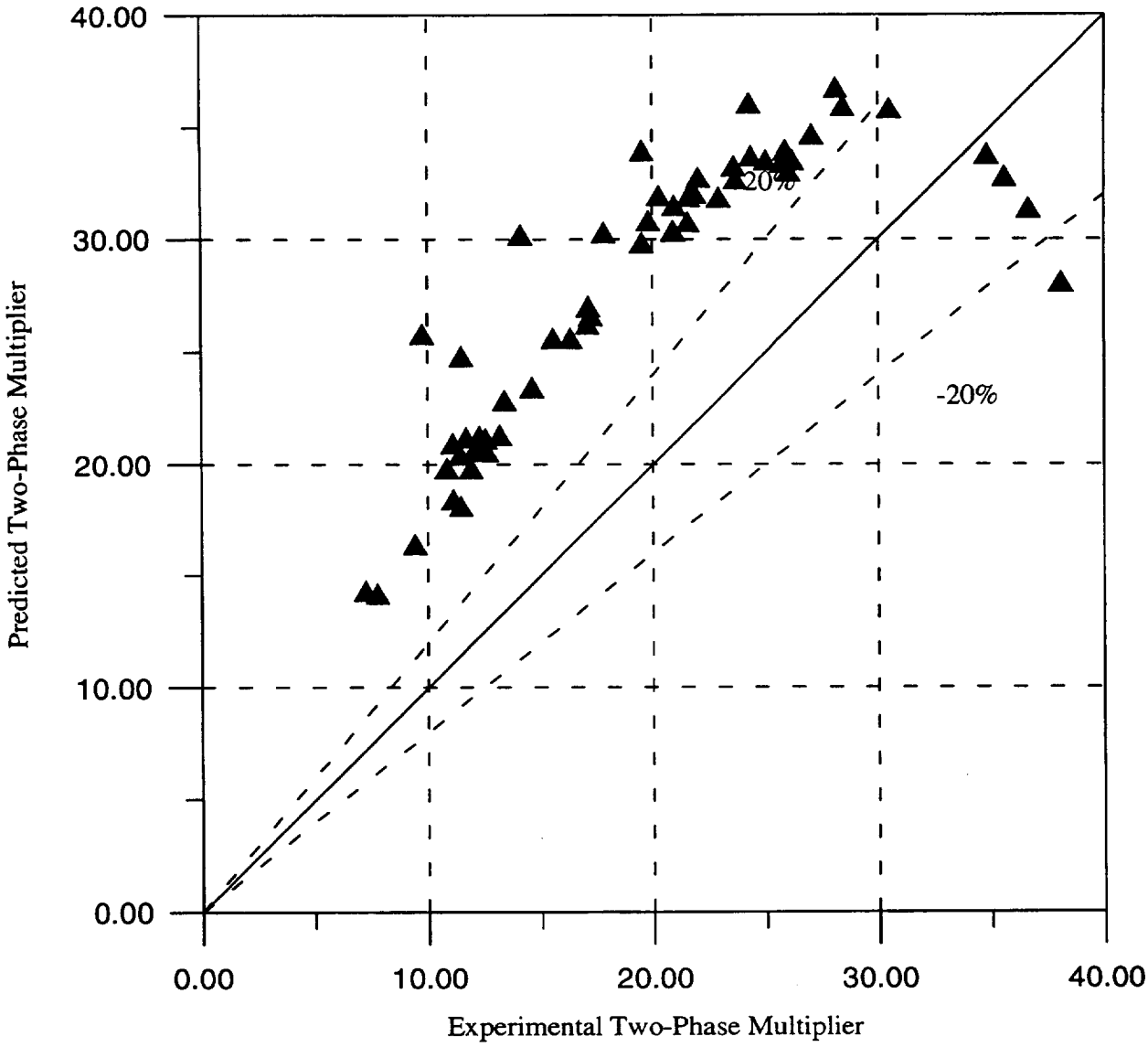

Figure 5.21 -Comparison of the Predicted and Experimental Two-Phase Friction Multipliers Using Fit to Lockhart-Martinelli for Reduced Gravity.

5.4 Prediction of the Critical Heat Flux

Theoretically based CHF models can be categorized based on the underlying mechanism which depends on the type of flow pattern at CHF. One class of models assumes annular flow regime when CHF occurs due to dryout of a liquid film at the wall. Another class of models assumes bubbly or dispersed flow pattern where a vapor film forms at the wall and prevents the liquid from contacting the surface. Models based on both of the above mechanisms should be considered for evaluating the reduced gravity data, as it becomes available. In the meantime, applicability of a correlation which is based on dimensional analysis and has been successfully applied to several fluids is evaluated here. The correlation developed by Katto and Ohno, Ref.1, was used to predict the data for vertical up and downflow configurations as shown in Figure 5.22. Three points which are believed to be CHF at zero g are also shown in this figure. These points were obtained due to reduction in the flow rate which was resulted from system pressure rise at reduced gravities. Generally, CHF is overpredicted by the Katto and Ohno correlation. The reduced gravity data points are close to CHF obtained under vertical upflow configuration, possibly indicating the same type of flow pattern.

5.5 Conclusions and Recommendations

A test loop has been designed and procedures were developed for generating data for the critical heat flux, onset of instability, and two-phase pressure drop under reduced gravities. Several design and procedural changes were identified following the first series of aircraft trajectory tests. Basically, the test loop should be modified to accommodate a test section in vertical upflow configuration, and the accumulator should be moved to a point downstream of the test section. This will impose a specified pressure at test section exit and reduce flow variations due to pump response.

As with the vertical upflow configuration, the pressure drop data can be successfully predicted by HEM or Friedel models. Mechanistic models based on the flow regime at CHF or as a consequence of bubble coalescence should be evaluated for the reduced gravity conditions.

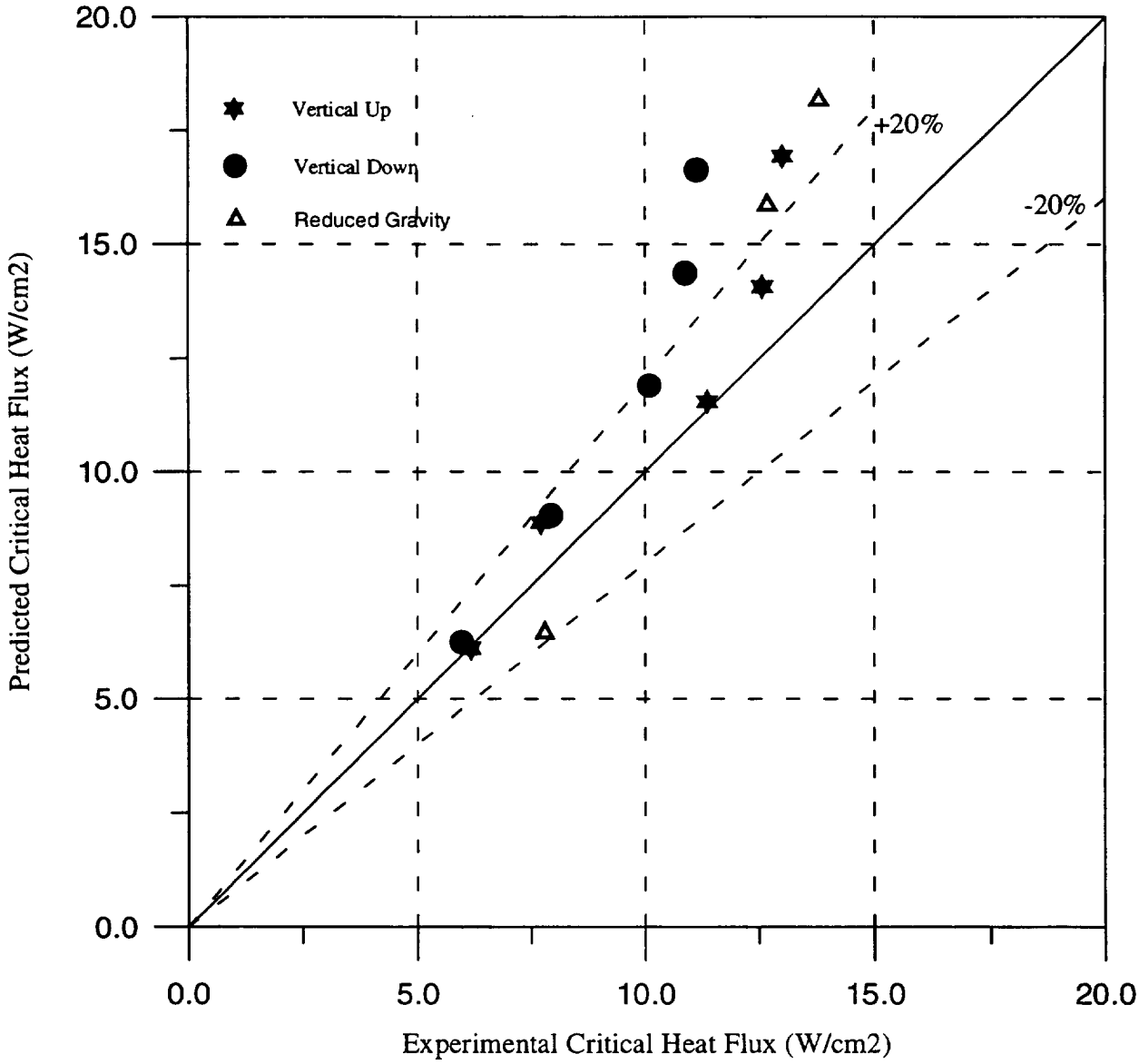

Figure 5.22 - Comparison of the Predicted and Experimental Critical Heat Flux Using Katto Model for Vertical Up, Down, and Reduced Gravity.

6.0 REFERENCES

1. Katto, Y. and Ohno, H., "An Improved Version of the Generalized Correlation of Critical Heat Flux for the Forced Convection Boiling in Uniformly Heated Vertical Tubes," Int. J. Heat Mass Transfer, Vol. 27, 1983.

2. Saha, P., and Zuber, N., "Point of New Vapor Generation and Vapor Void Fraction in Subcooled Boiling," Proc. of 5th Int. Heat Transfer Conf., Tokyo, Vol. IV, 1974.

3. Hewitt, G. F. and Hall-Taylor, N., Annular Two-Phase Flow, Pergamon Press, 1970.

4. Rohsenow, W. M., and Hartnett, J. P., Handbook of Heat Transfer, McGraw Hill, 1973.

5. Dittus, F. W. and Boelter, L. M. K., University of California Engineering Publications, Vol. 2, 1930.

6. Heppner, D. B. et al., "Zero-G Experiments in Two-Phase Fluid Flow Regimes," ASME Paper 75-ENAS-24, 1975.

7. Hill, D. and Downing, R. S., A Study of Two-Phase Flow in a Reduced Gravity Environment - Final Report, Sunstrand Energy Systems Report, Contract NASP-17195, October 1987.

8. Hill, W. S. and Best, F. R., Definition of Two-Phase Flow Behavior for Spacecraft Design, Air Force Report AFK-0062-FM-8933-418, June 1991.

9. Chisholm, D., Two-Phase Flow in Pipelines and Heat Exchangers, George Godwin, 1983.

10. Lockhart, R. C. and Martinelli, R. C., "Proposed Correlation of Data for Isothermal Two-Phase Two-Component Flow in Pipes," Chem. Eng. Prog., 45, 39, 1949.

Appendix A

COMPONENT LISTING

Table A.1 - COMPONENT LISTING

ITEM	DESCRIPTION	MANUFACTURER	PART NO.	SIZE	WORKING PRESSURE	NOTES
REV1	Relief Valve	Nupro	SS-8CPA2-50	1/2" NPTM	3000 psig	Cracking Pressure: 100 psi
		Sunnyvale Valve & Fitting Co.				
SO1	Shut-Off Ball Valve	Whitey	SS-45S8	1/2" Swagelock	2500 psig	Cv = 12.0
		Sunnyvale Valve & Fitting Co.				
	Accumulator (1 qt.)	Oil Air	A-1QT-3100	1-1/4" NPTF	3000 psi	
RV2	Regulating Valve	Whitey	SS-1RS8	1/2" Swagelock	5000 psi	Cv = 0.73
RV4	Regulating Valve	Whitey	SS-1RS8	1/2" Swagelock	5000 psi	Cv = 0.73
SO2	Shut-Off Ball Valve	Whitey				
P7	Absolute Pressure Transducer	GP:50	311-D-RE-CE-FH	1/8" NPTF	2000 psig	28 VDC, Range: 0-250 psi
P1	Absolute Pressure Transducer	GP:50	311-D-RE-CE-FH	1/8" NPTF	2000 psig	28 VDC, Range: 0-250 psi
TI1	Thermocouple	Nanmac	D4-83-K	1/2" Swagelock	2400 psi	
F1	Turbine Flow Meter	Sponsler	SP3/8	1/2" NPTF	4000 psig	
SV3	Solenoid	Asco	8030-A67	1/2" NPTF	max delta P = 15 psi	Cv=2.8, 120VAC, 60 Hz
SV2	Solenoid	Asco	8030-A67	1/2" NPTF	max delta P = 15 psi	Cv=2.8, 120VAC, 60 Hz
RV5	Regulating Valve	Whitey	SS-8RS8	1/2" Swagelock	5000 psi	Cv = 1.4
P2	Absolute Pressure Transducer	GP:50	311-D-RE-CE-FH	1/8" NPTF	2000 psig	28 VDC, Range: 0-250 psi
TI2	Thermocouple	Nanmac	D4-83-K	1/2" Swagelock	2400 psi	
SO3	Shut-Off Ball Valve	Whitey	SS-45S8	1/2" Swagelock	2500 psig	Cv = 12.0
SO4	Shut-Off Ball Valve	Whitey	SS-45S8	1/2" Swagelock	2500 psig	Cv = 12.0
F2	Turbine Flow Meter (High Flow)	Sponsler	MF70	1/2" NPTF	4000 psig	
F2	Turbine Flow Meter (High Flow)	Sponsler	MF175	1/2" NPTF	4000 psig	

Table A.1 (Cont.)- COMPONENT LISTING

ITEM	DESCRIPTION	MANUFACTURER	PART NO.	SIZE	WORKING PRESSURE	NOTES
	Pre-Heater Tape	Omega	STH051-080			
P3	Absolute Pressure Transducer	GP:50	311-D-RE-CE-FH	1/8" NPTF	2000 psig	28 VDC, Range: 0-250 psi
TI3	Thermocouple	Nanmac	D4-83-K	1/2"Swagelock	2400 psi	
T1-T4	Thermocouple	Nanmac	Ribbon			
P4	Absolute Pressure Transducer	GP:50	311-D-RE-CE-FH	1/8" NPTF	2000 psig	28 VDC, Range: 0-250 psi
TI4	Thermocouple	Nanmac	D4-83-K	1/2" Swagelock	2400 psi	
DP1	Diff. Pressure Transducer	GP:50	316-D-PN-CE-FH	1/8" NPTF	2000 psig	28 VDC, Range: 0-10 psi
DP2	Diff. Pressure Transducer	GP:50	316-D-PN-CE-FH	1/8" NPTF	2000 psig	28 VDC, Range: 0-20 psi
DP3	Diff. Pressure Transducer	GP:50	316-D-PN-CE-FH	1/8" NPTF	2000 psig	28 VDC, Range: 0-2 psi
P5	Absolute Pressure Transducer	GP:50	311-D-RE-CE-FH	1/8" NPTF	2000 psig	28 VDC, Range: 0-250 psi
	Drain Valve	Whitey	SS-1GS8	1/2" Swagelock		
REV2	Relief Valve	Nupro	SS-8CPA2-50	1/2" NPTM	3000 psig	Cracking Pressure: 100 psi
RV6	Regulating Valve	Whitey	SS-8RS8	"1/2"" Swagelock"	5000 psi	Cv = 1.4
RV7	Regulating Valve	Whitey	SS-8RS8	1/2" Swagelock	5000 psi	Cv = 1.4
P6	Absolute Pressure Transducer	GP:50	311-D-RE-CE-FH	1/8" NPTF	2000 psig	28 VDC, Range: 0-250 psi
TI5	Thermocouple	Nanmac	D4-83-K	1/2" Swagelock	2400 psi	
TI6	Thermocouple	Nanmac	D4-83-K	1/2" Swagelock	2400 psi	
REV3	Relief Valve	Nupro	SS-8CPA2-50	1/2" NPTM	3000 psig	Cracking Pressure: 150 to 350 psig
F3	Turbine Flow Meter (High Flow)	Sponsler	SP1/2	1/2" NPTF	4000 psig	
RV8-RV9	Regulating Valve	Whitey	SS-18RS8	1/2" Swagelock	5000 psig	Cv = 1.8
P8	Absolute Pressure Transducer	GP:50	311-D-RE-CE-FH	1/8" NPTF	2000 psig	28 VDC, Range: 0-250 psi

Table A.1 (Cont.)- COMPONENT LISTING

ITEM	DESCRIPTION	MANUFACTURER	PART NO.	SIZE	WORKING PRESSURE	NOTES
TI8	Thermocouple	Nanmac	D4-83-K	1/2" Swagelock	2400 psi	
	Condenser Pump 1/3 HP	Eastern	ECD1-ASACAYSS	1/4" NPTF	150 psig	head = 50 ft, gpm = 7.9
	Freon Pump	Tuthill Magnet Drive	TXCM79MCNK	3/8" NPTF	500 psig	gph = 475, delta P = 60 psi"
RV1	Regulating Valve	Whitey	SS-18RS8	1/2" Swagelock	5000 psig	Cv = 1.8
		Sunnyvale Valve & Fitting Co.				
SV1	Solenoid	Asco	8030-A67	1/2" NPTF	max delta P = 15 psi	Cv=2.8, 120VAC, 60 Hz

Appendix B

MECHANICAL LAYOUT

Table B.1 Aircraft Rack Weight and Moment Arm Calculation

LEFT RACK					
	Shelf	Weight (gm)	Weight (lbs)	Distance (in)	Moment Arm (in lbs)
Tubing + Fluid	1	1254	2.8	8	22.1
Fittings	1	1426	3.1	8	25.1
Valve	1	454	1.0	8	8.0
Low Point Drain Valve	1	312	0.7	8	5.5
Solenoid Valve	1	907	2.0	10	20.0
Pressure Transducer	1	454	1.0	8	8.0
Pump	1	13608	30.0	11	329.7
Accumulator + Fluid	1	5796	12.8	10	127.7
Valve	1	595	1.3	10	13.1
Valve	1	139	0.3	10	3.1
Shelf	1	7618	16.8	7.5	125.8
Tubing + Fluid	2	346	0.8	17	13.0
Fittings	2	967	2.2	17	37.0
Shutoff Valve	2	340	0.7	17.5	13.1
Relief Valve	2	125	0.3	17.5	4.8
Shelf	2	7618	16.8	16	268.5
Tubing + Fluid	3	476	1.0	23	24.1
Fittings	3	222	0.5	23	11.2
Thermocouple	3	300	0.7	23	15.2
Solenoid Valve	3	907	2.0	25	49.9
Shelf	3	7618	16.8	22	369.2
Total on Rack			113		1494
+ 1/2 of Center Section			38		920
Total Attributed to Rack			151		2414
Learjet Rack Limits			188		3268

CENTER SECTION					
	Shelf	Weight (gm)	Weight (lbs)	Distance (in)	Moment Arm (in lbs)
Tubing + Fluid	1	707	1.6	17	26.5
Fittings	1	383	0.8	17	14.3
Flow Meter	1	791	1.7	17.5	30.5
Shelf	1	6987	15.4	16	246.2
Tubing + Fluid	2	252	0.6	23	12.8
Fittings	2	332	0.7	23	16.8
Thermocouple	2	300	0.7	23	15.2
Flow Meters	2	1582	3.5	23	80.1
Shelf	2	6987	15.4	22.5	346.3
Tubing + Fluid	3	850	1 9	30	56.2
Fittings	3	840	1.9	30	55.5
Pressure Transducer	3	454	1.0	29	29.0
Delta-P Transducers	3	6804	15.0	30	449.6
Three way Valves	3	238	0.5	29	15.2
Shelf	3	6987	15.4	29	446.3
Total			76		1841

Aircraft Rack Moment Arm Analysis

Table B.1 (Cont.) Aircraft Rack Weight and Moment Arm Calculation

RIGHT RACK					
	Shelf	Weight	Weight	Distance	Moment Arm
		(gm)	(lbs)	(in)	(in lbs)
Tubing + Fluid	1	409	0.9	8	7.2
Fittings	1	549	1.2	8	9.7
Valve	1	907	2.0	8	16.0
Flow Meter	1	791	1.7	8	13.9
Pressure Relief Valve	1	125	0.3	8	2.2
Condenser Pump	1	13608	30.0	11	329.7
Shelf	1	7618	16.8	7.5	125.8
Tubing + Fluid	2	825	1.8	17	30.9
Fittings	2	941	2.1	17	35.2
Solenoid Valve	2	907	2.0	17.5	35.0
Valve	2	453	1.0	17.5	17.5
Shelf	2	7618	16.8	16	268.5
Tubing + Fluid	3	117	0.3	23	5.9
Fittings	3	583	1.3	23	29.5
Thermocouple	3	300	0.7	23	15.2
Pressure Relief Valve	3	125	0.3	23	6.3
Regulating Valve	3	595	1.3	23	30.1
Shelf	3	7618	16.8	22	369.2
Tubing + Fluid	4	764	1.7	30	50.5
Fittings	4	1362	3.0	30	90.0
Solenoid Valves	4	2722	6.0	30	179.9
Pressure Relief Valves	4	833	1.8	29	53.2
Drain Valve	4	312	0.7	29	19.9
Shelf	4	7618	16.8	28.5	478.2
Total on Rack			127		2220
+ 1/2 of Center Section			38		920
Total Attributed to Rack			165		3140
Learjet Rack Limits			188		3268

CENTER SECTION					
	Shelf	Weight	Weight	Distance	Moment Arm
		(gm)	(lbs)	(in)	(in lbs)
Tubing + Fluid	1	707	1.6	17	26.5
Fittings	1	383	0.8	17	14.3
Flow Meter	1	791	1.7	17.5	30.5
Shelf	1	6967	15.4	16	246.2
Tubing + Fluid	2	252	0.6	23	12.8
Fittings	2	332	0.7	23	16.8
Thermocouple	2	300	0.7	23	15.2
Flow Meters	2	1582	3.5	23	80.1
Shelf	2	6987	15.4	22.5	346.3
Tubing + Fluid	3	850	1.9	30	56.2
Fittings	3	840	1.9	30	55.5
Pressure Transducer	3	454	1.0	29	29.0
Delta-P Transducers	3	6804	15.0	30	449.6
Three way Valves	3	238	0.5	29	15.2
Shelf	3	6987	15.4	29	446.3
Total			76		1841

Aircraft Rack Moment Arm Analysis

TOP LEVEL 4
LEVEL 3
LEVEL 2
BOTTOM LEVEL 1
4 (RIGHT)
4 (CENTER)
3 (RIGHT)
3 (CENTER)
3 (LEFT)
2 (RIGHT)
2 (CENTER)
2 (LEFT)
1 (RIGHT)
1 (LEFT)
CONDENSER LOOP PUMP
FREON LOOP PUMP
ACCUMULATOR
CONDENSER
PREHEATER
TEST SECTION
SHUT-OFF
SOLENOID VALVES
REGULATING VALVES
HIGH POINT DRAIN
LOW POINT DRAIN

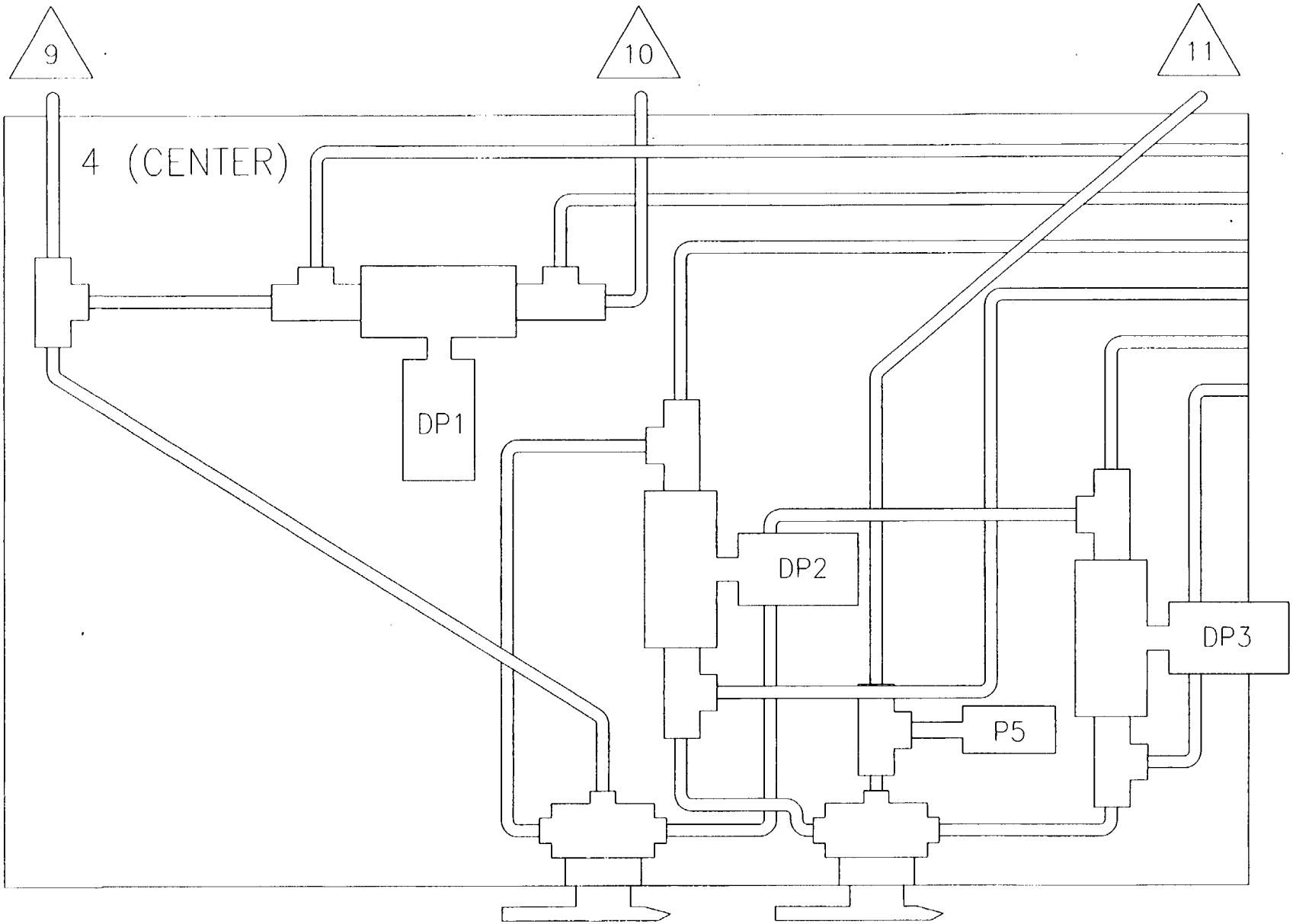
9
10
11
4 (CENTER)
DP1
DP2
DP3
P5

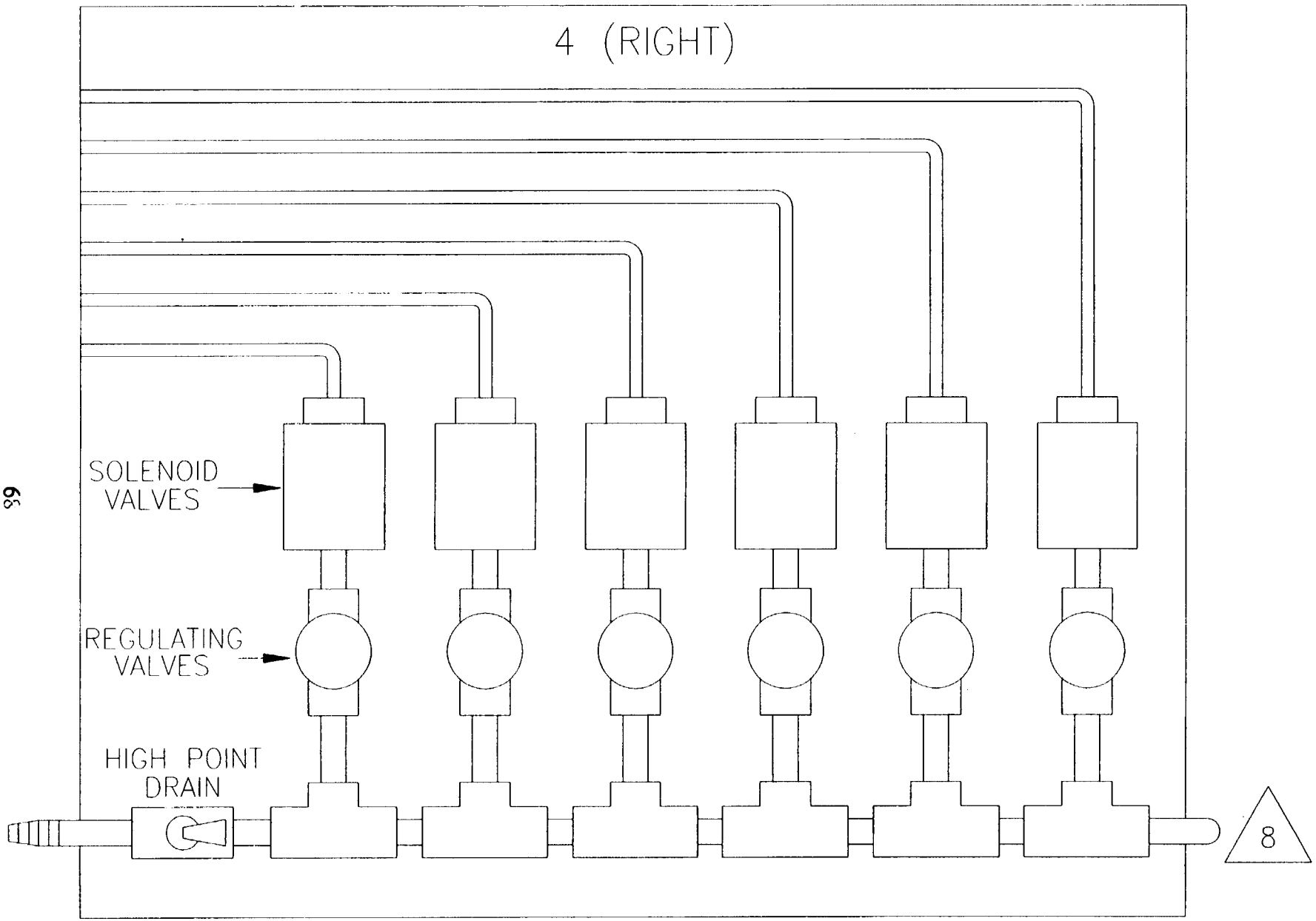
4 (RIGHT)
SOLENOID VALVES
REGULATING VALVES
HIGH POINT DRAIN
8

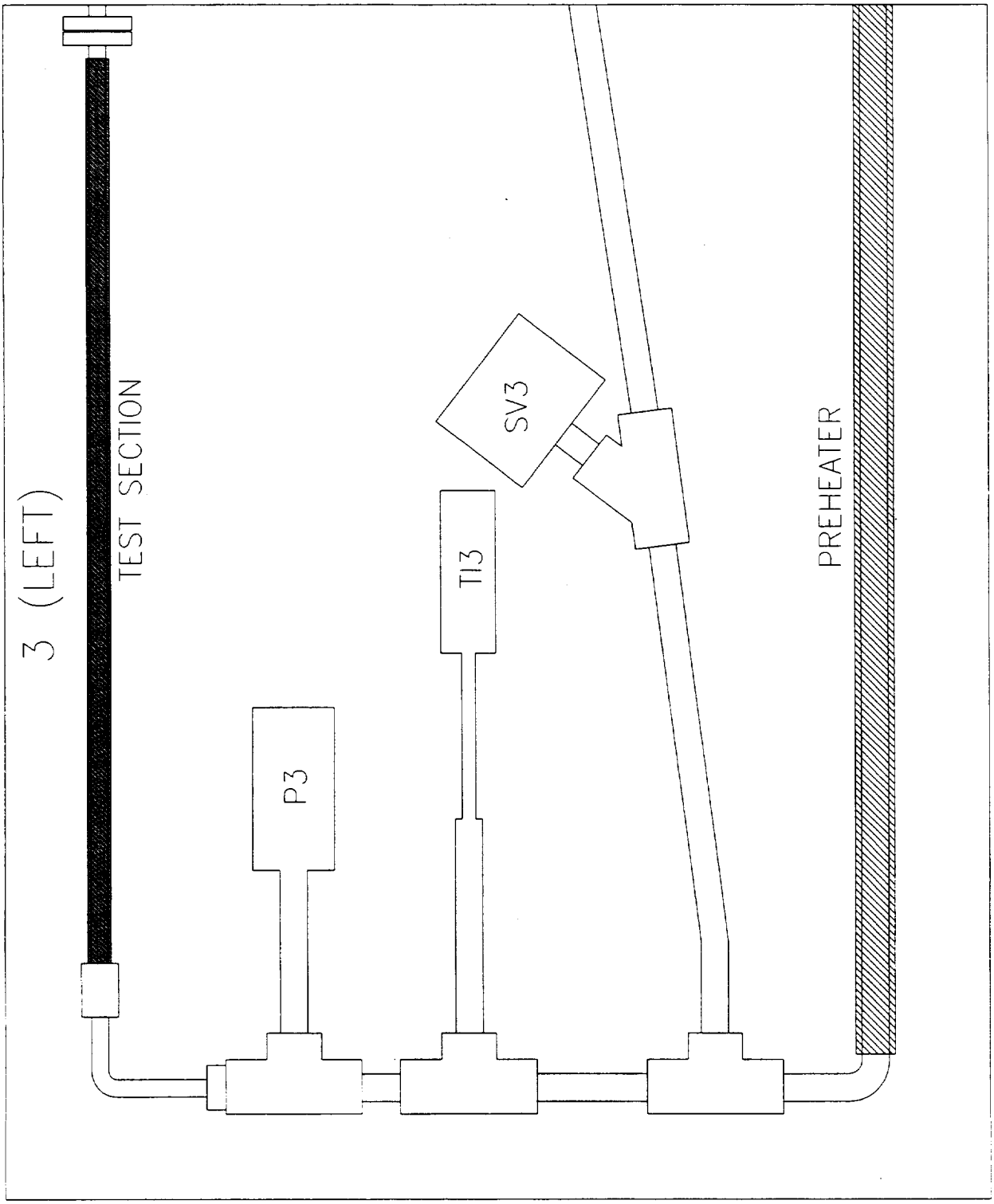
3 (LEFT)
TEST SECTION
P3
TI3
SV3
PREHEATER

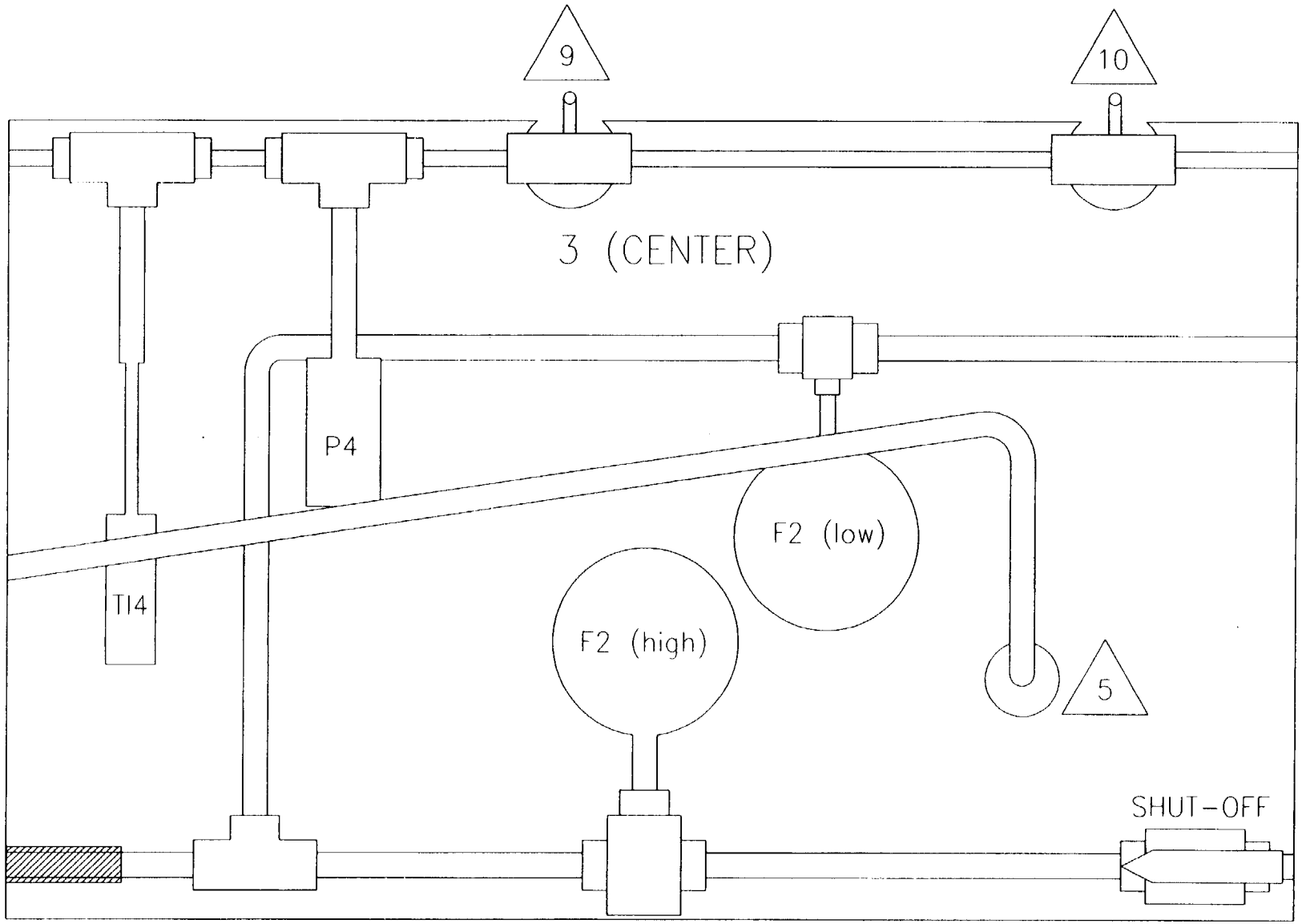
9
10
3 (CENTER)
P4
TI4
F2 (low)
F2 (high)
5
SHUT-OFF

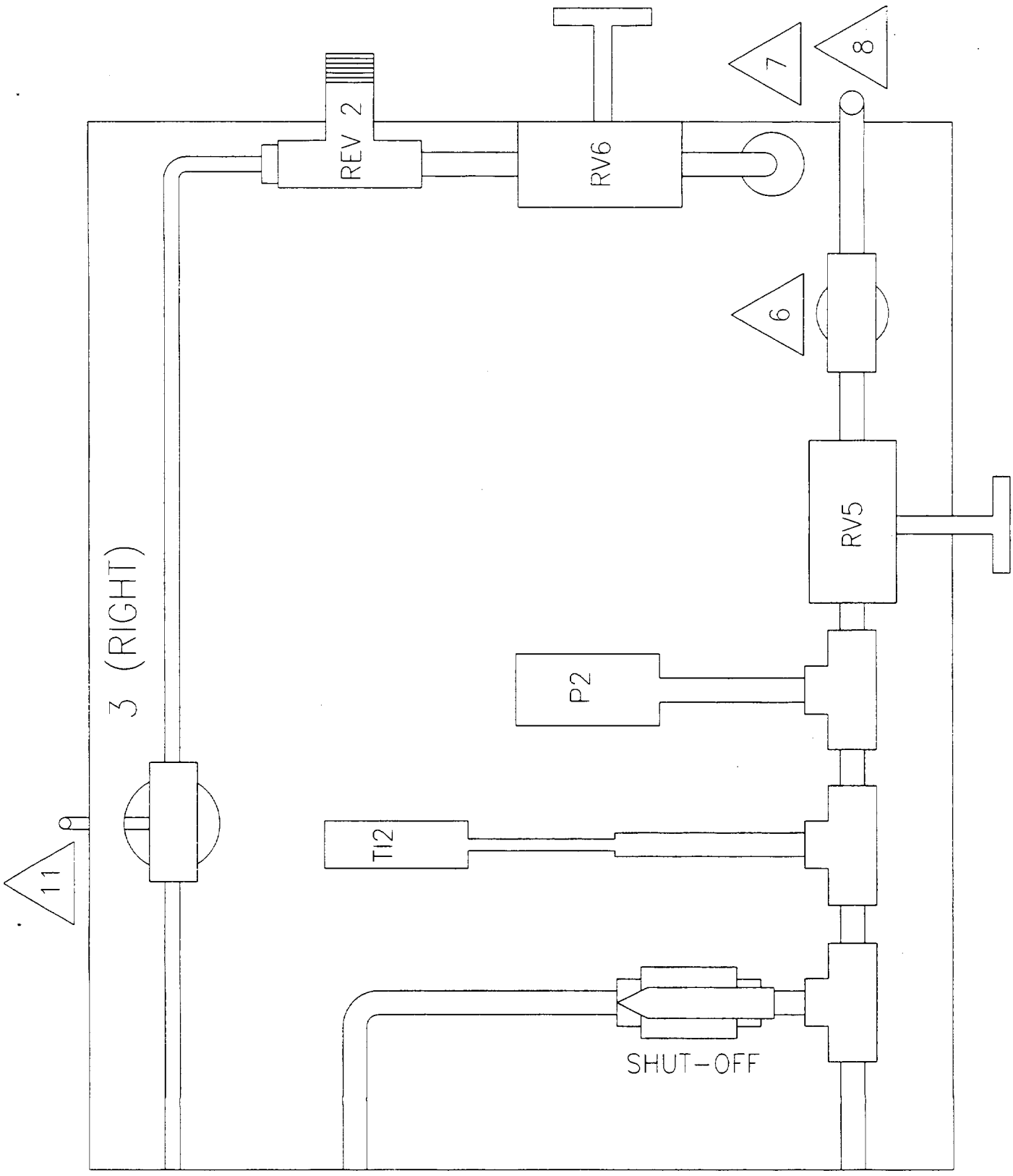
REV 2
RV6
7
8
6
RV5
3 (RIGHT)
P2
T12
11
SHUT-OFF

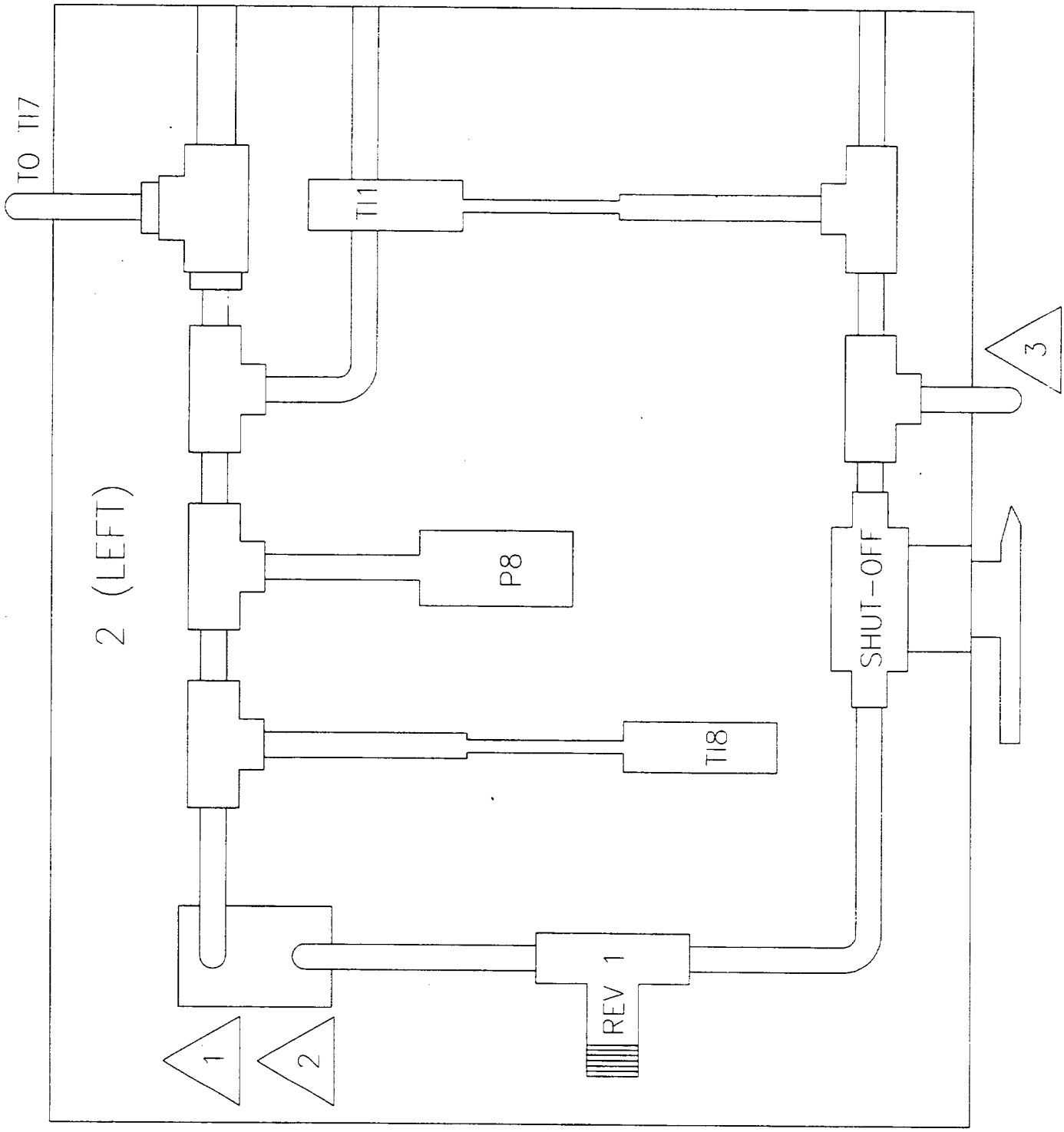
TO T17
T11
2 (LEFT)
P8
T18
SHUT-OFF
REV 1
1
2
3

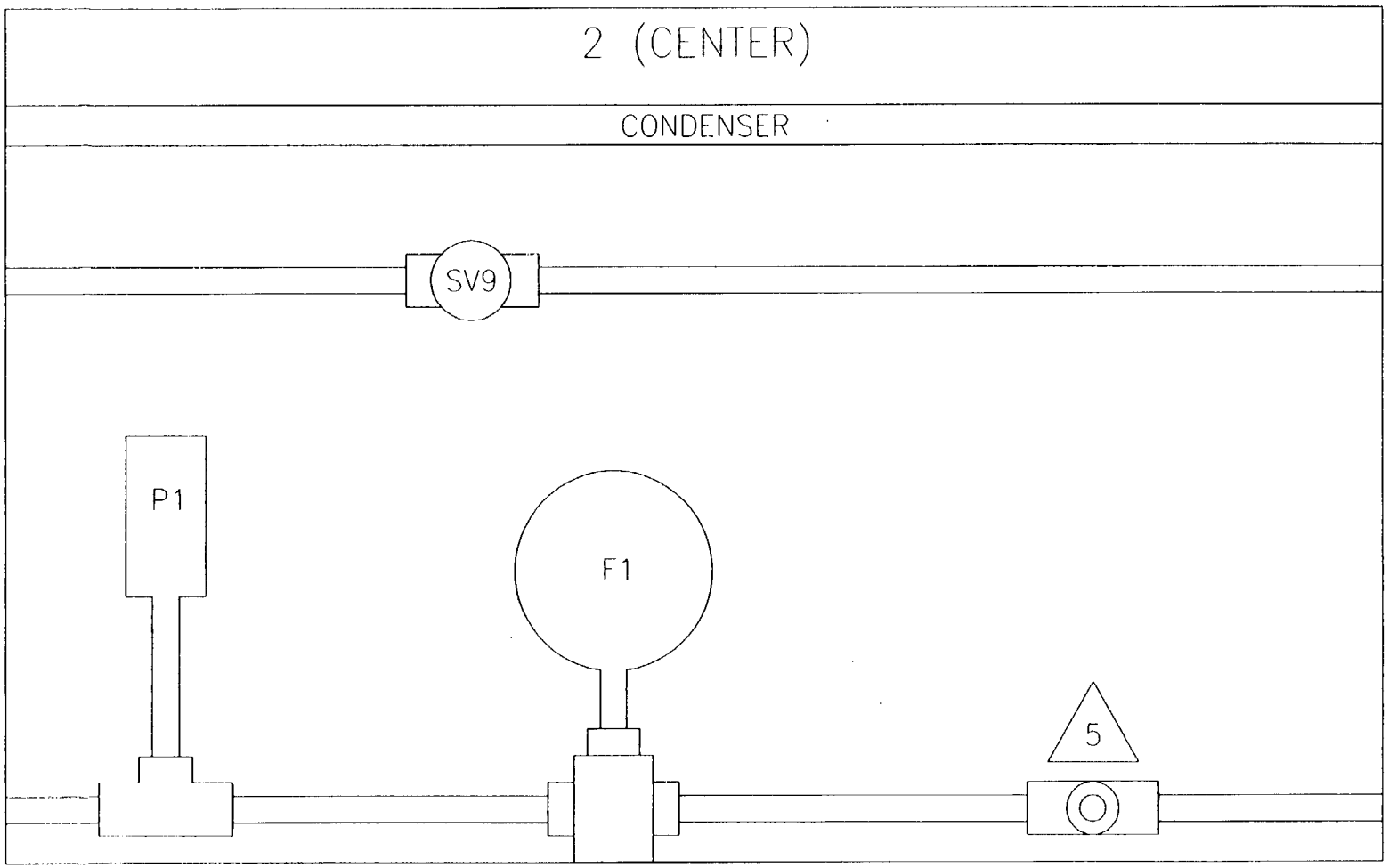
2 (CENTER)
CONDENSER
SV9
P1
F1
5

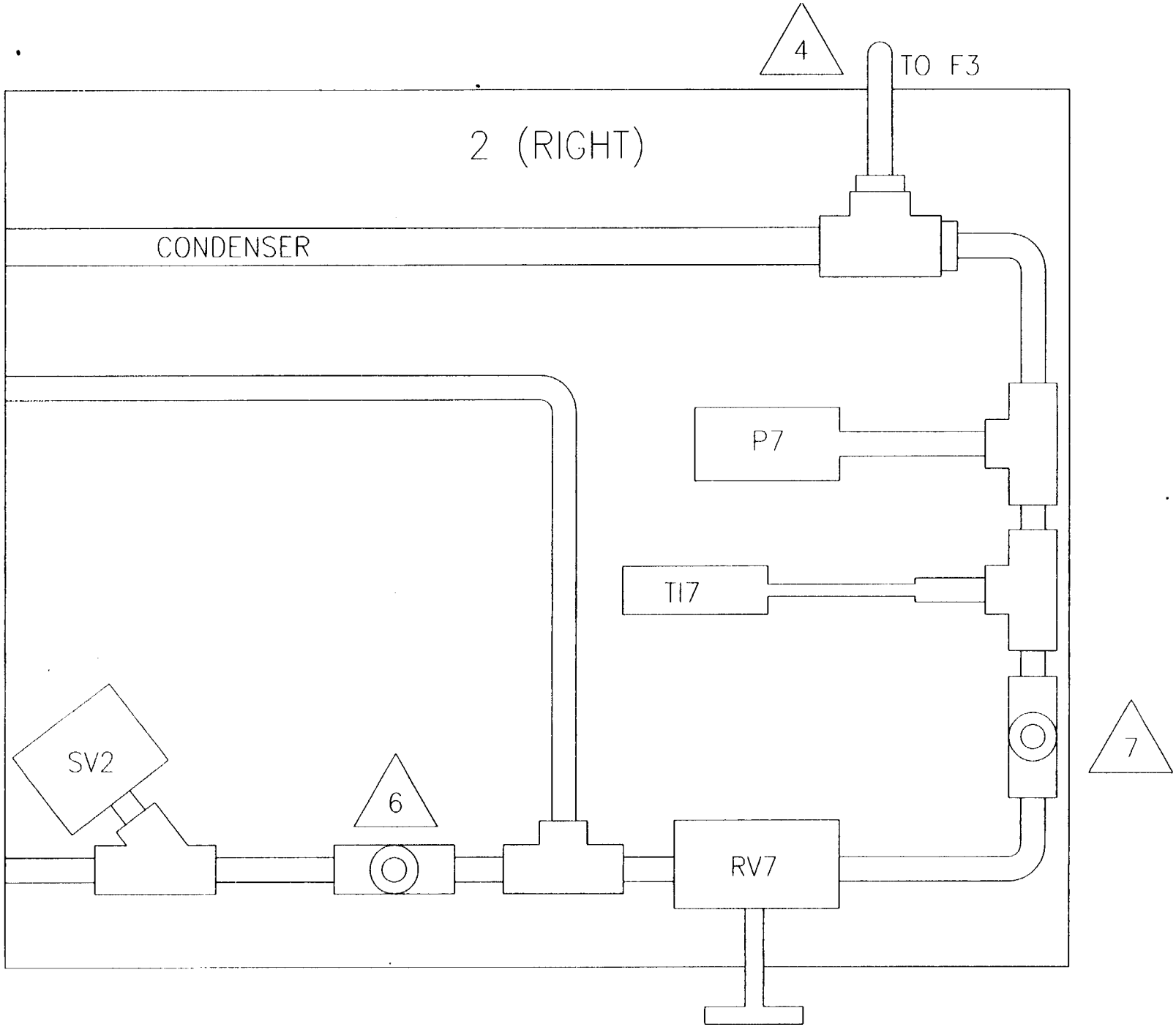
4
TO F3
2 (RIGHT)
CONDENSER
P7
TI7
SV2
6
RV7
7

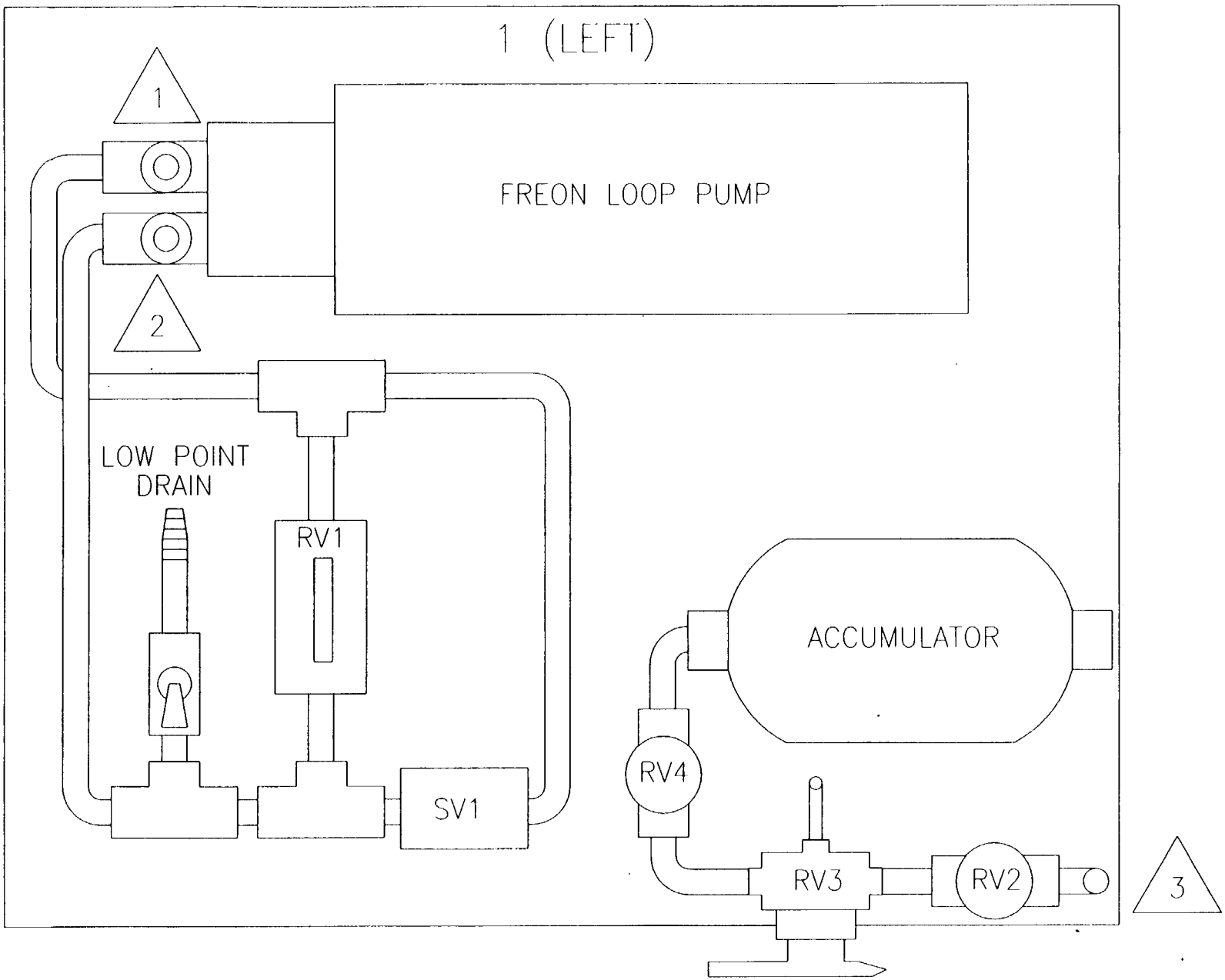
1 (LEFT)
1
2
FREON LOOP PUMP
LOW POINT
DRAIN
RV1
SV1
ACCUMULATOR
RV4
RV3
RV2
3

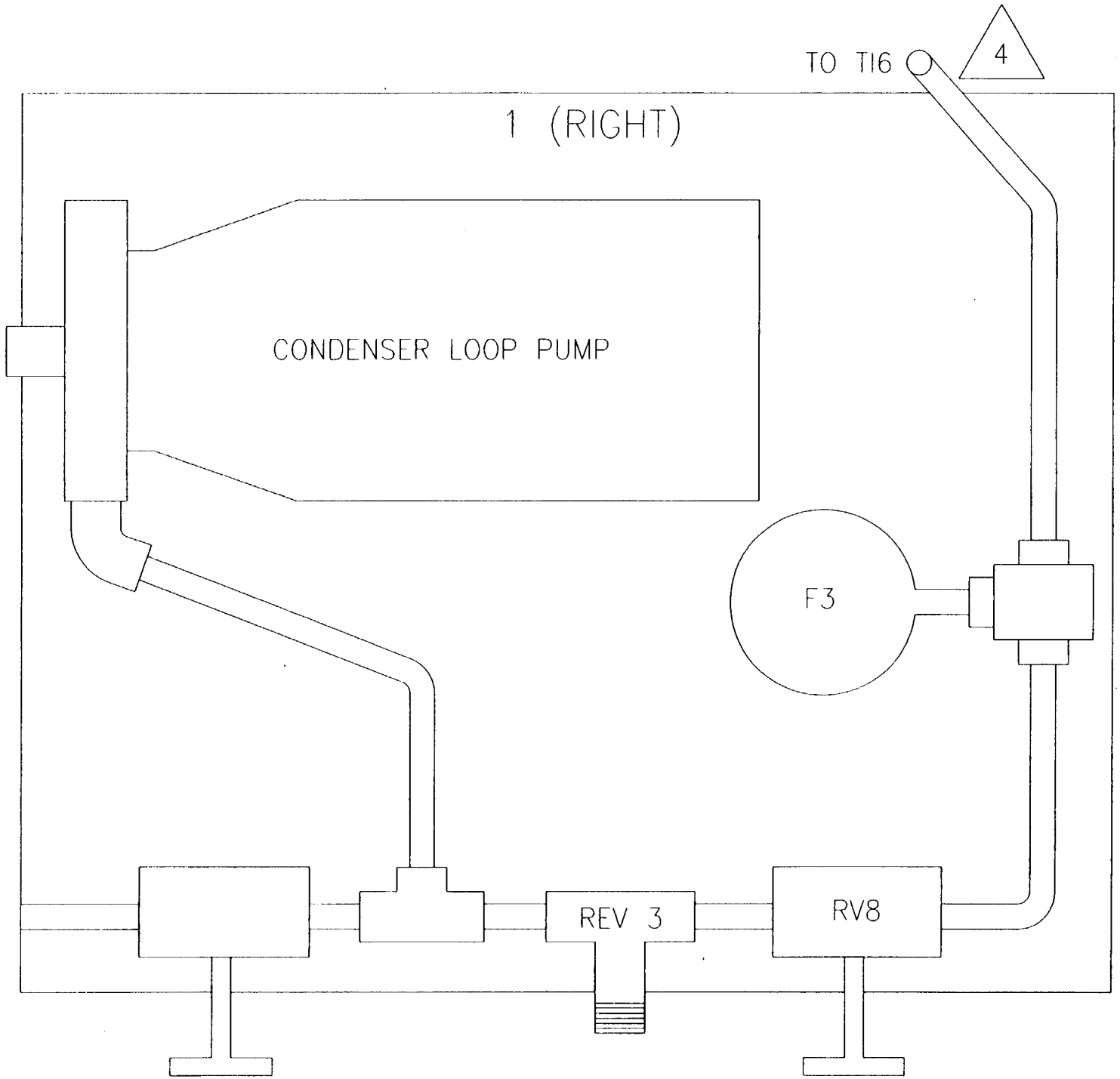
TO TI6
4
1 (RIGHT)
CONDENSER LOOP PUMP
F3
REV 3
RV8

Appendix C

ELECTRICAL SYSTEM

Table C.1 Electrical Load Analysis

Component	Power (VA)	Calculated Current (amp)
Heater	1512.5	12.6
Pre-Heater	627	5.23
Computer and Monitor	350	2.92
Data Acquisition	100	0.83
Over-temperature Controller	6	0.05
Solenoids, 2 floods and 6 purge (12 VA each)	96	0.80
Freon Pump and Controller	300	2.50
Water Pump	690	5.75
Sensor Power Supply 24 V, and Relay Power supply 5 V (includes sensors and amplifiers)	200	1.67
	Total Current	32.35
	Heater Current - Load 1	12.6
	Pre-Heater Current - Load 2	5.23
	Other - Load 3	14.52

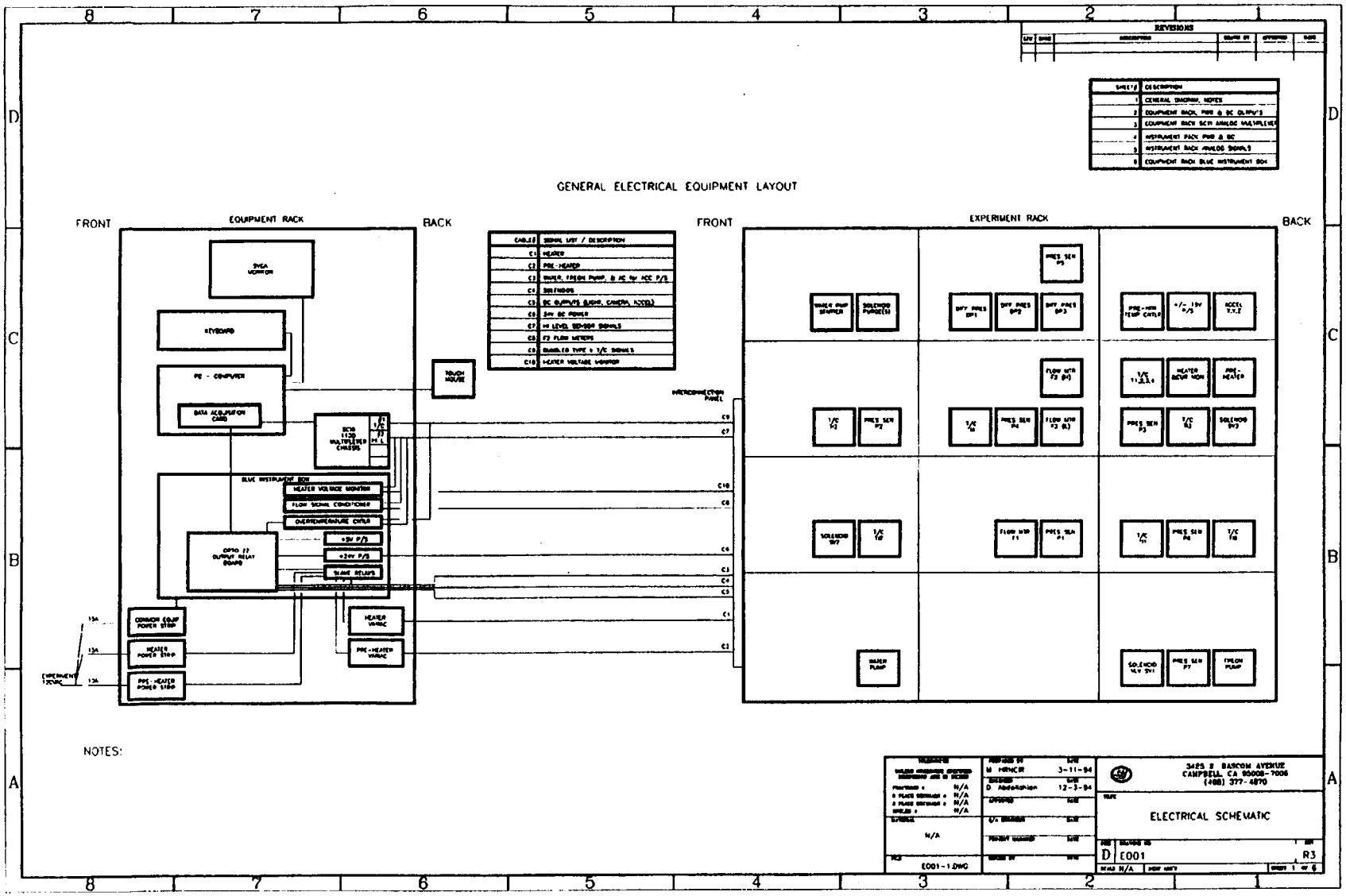

Figure C.1 - Schematic of Electrical Subsystem

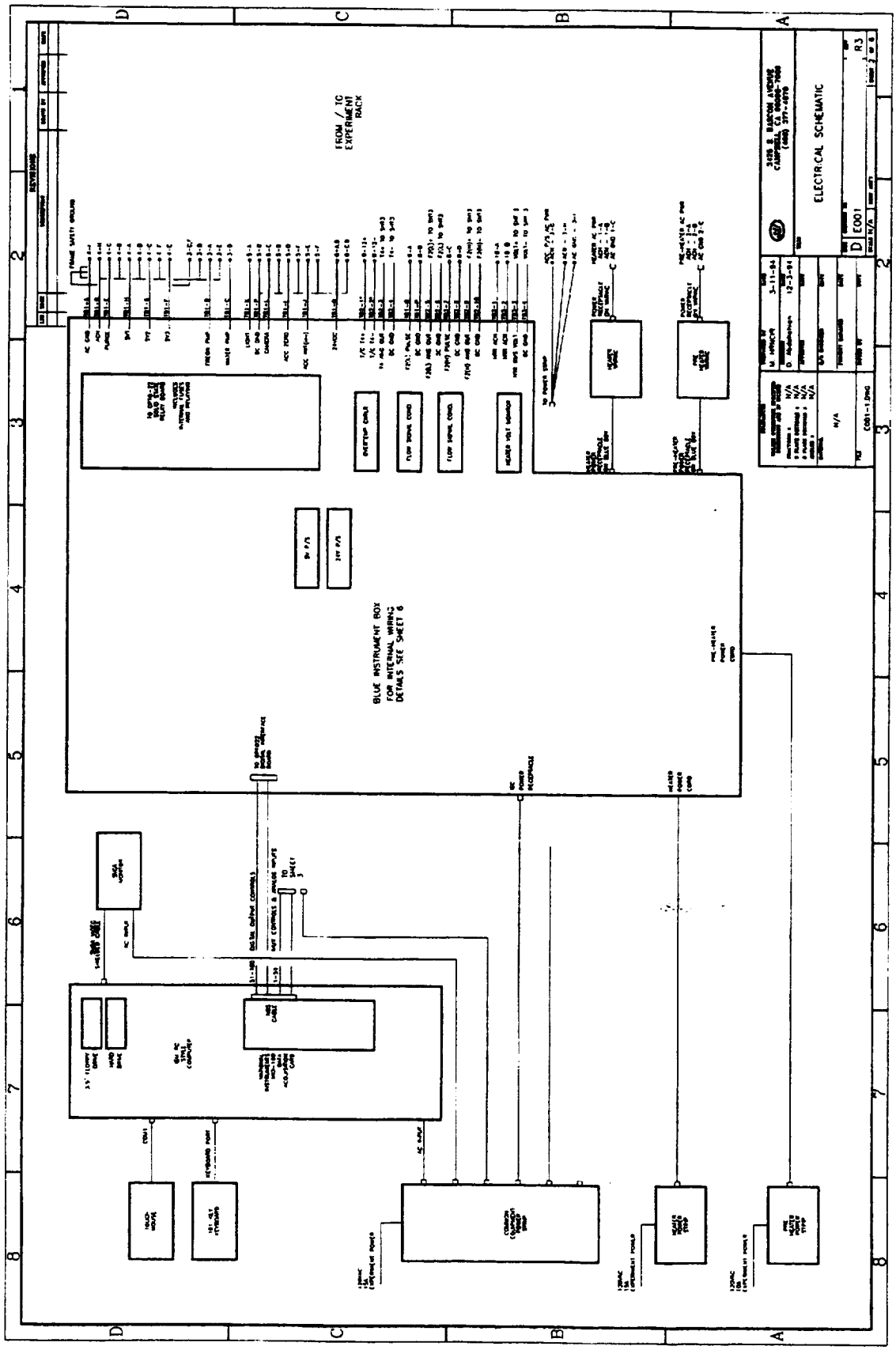

Figure C.2 - Schematic of Electrical Subsystem

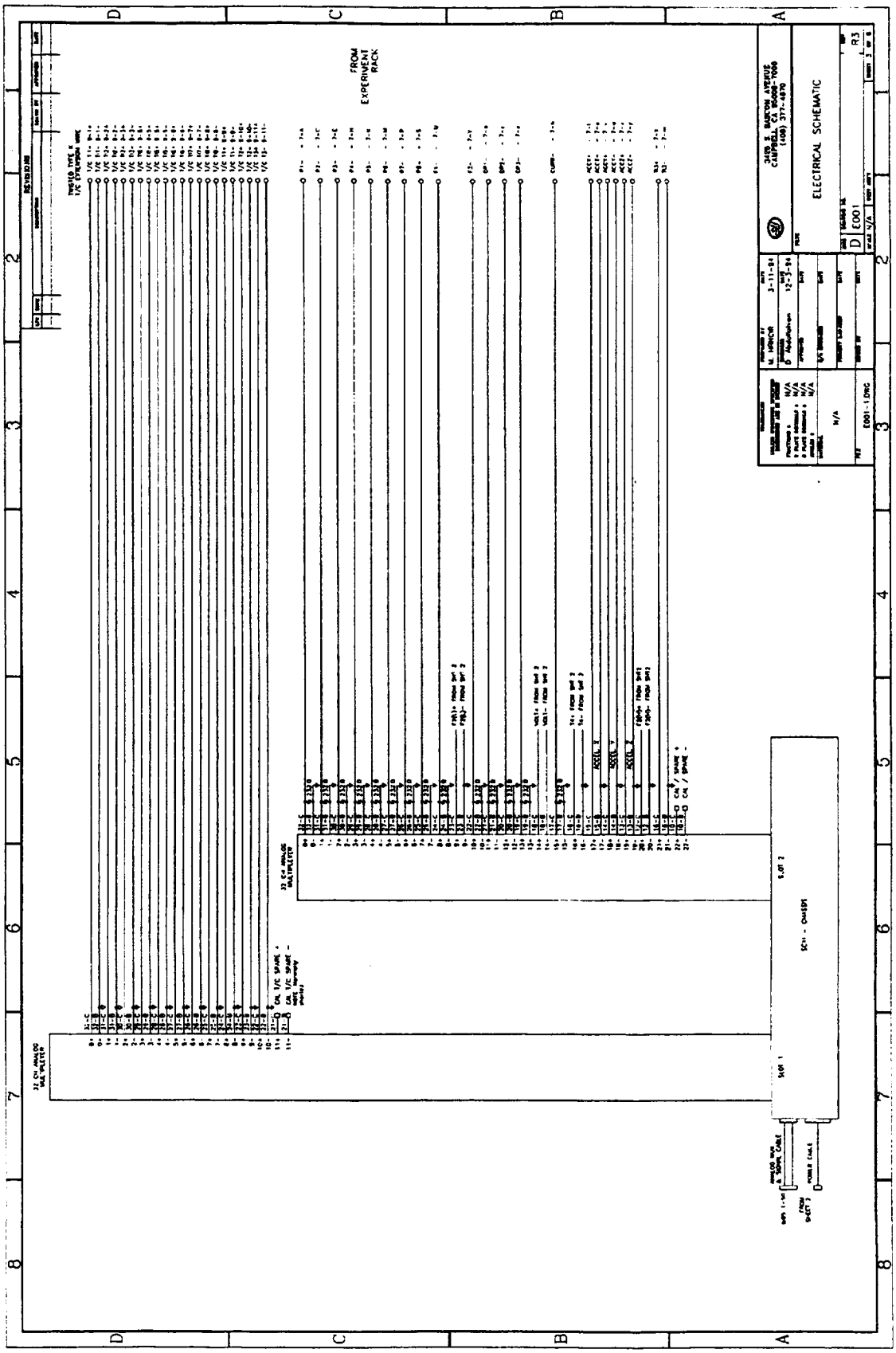

Figure C.3 - Schematic of Electrical Subsystem

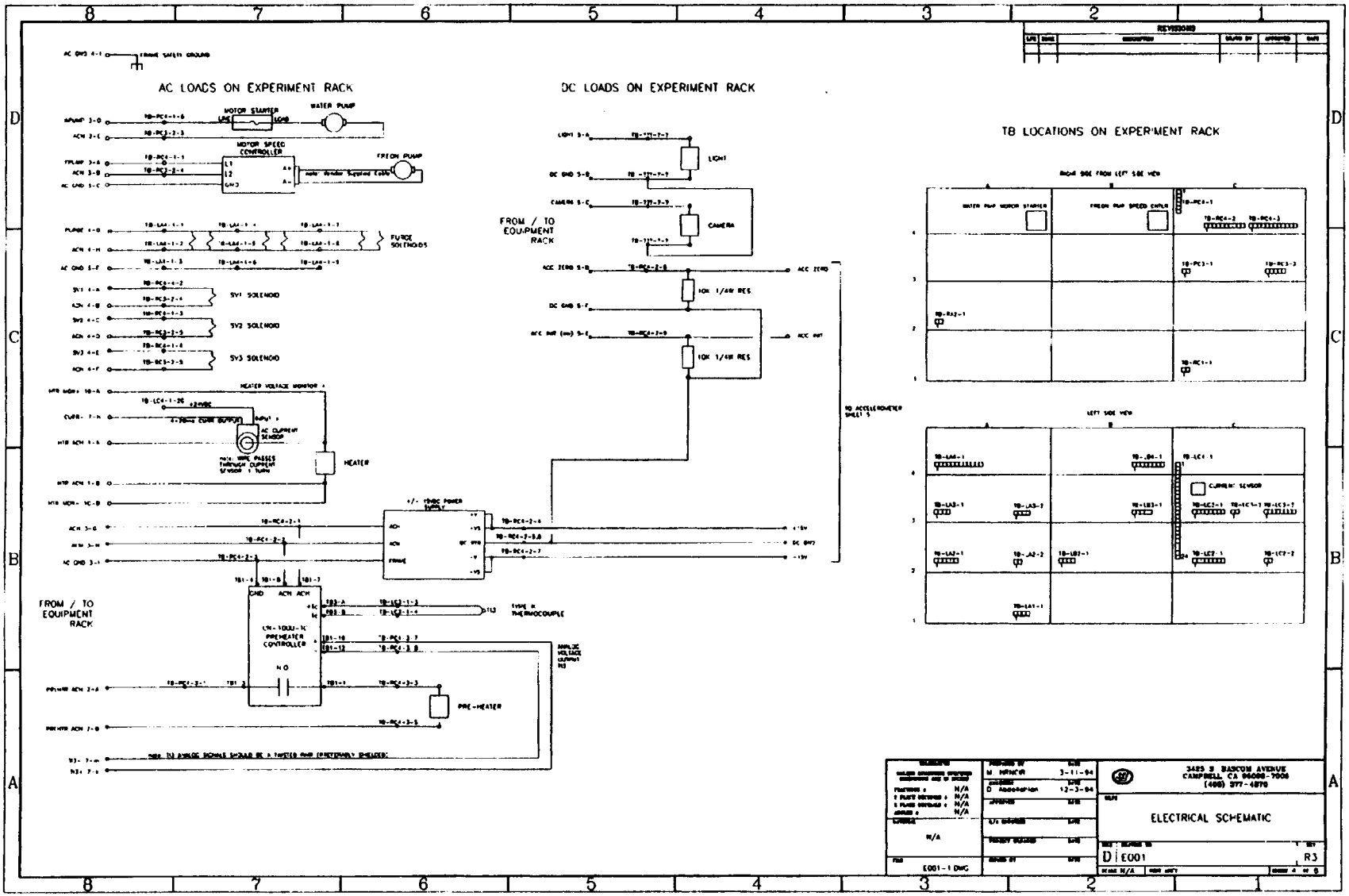

Figure C.4 - Schematic of Electrical Subsystem

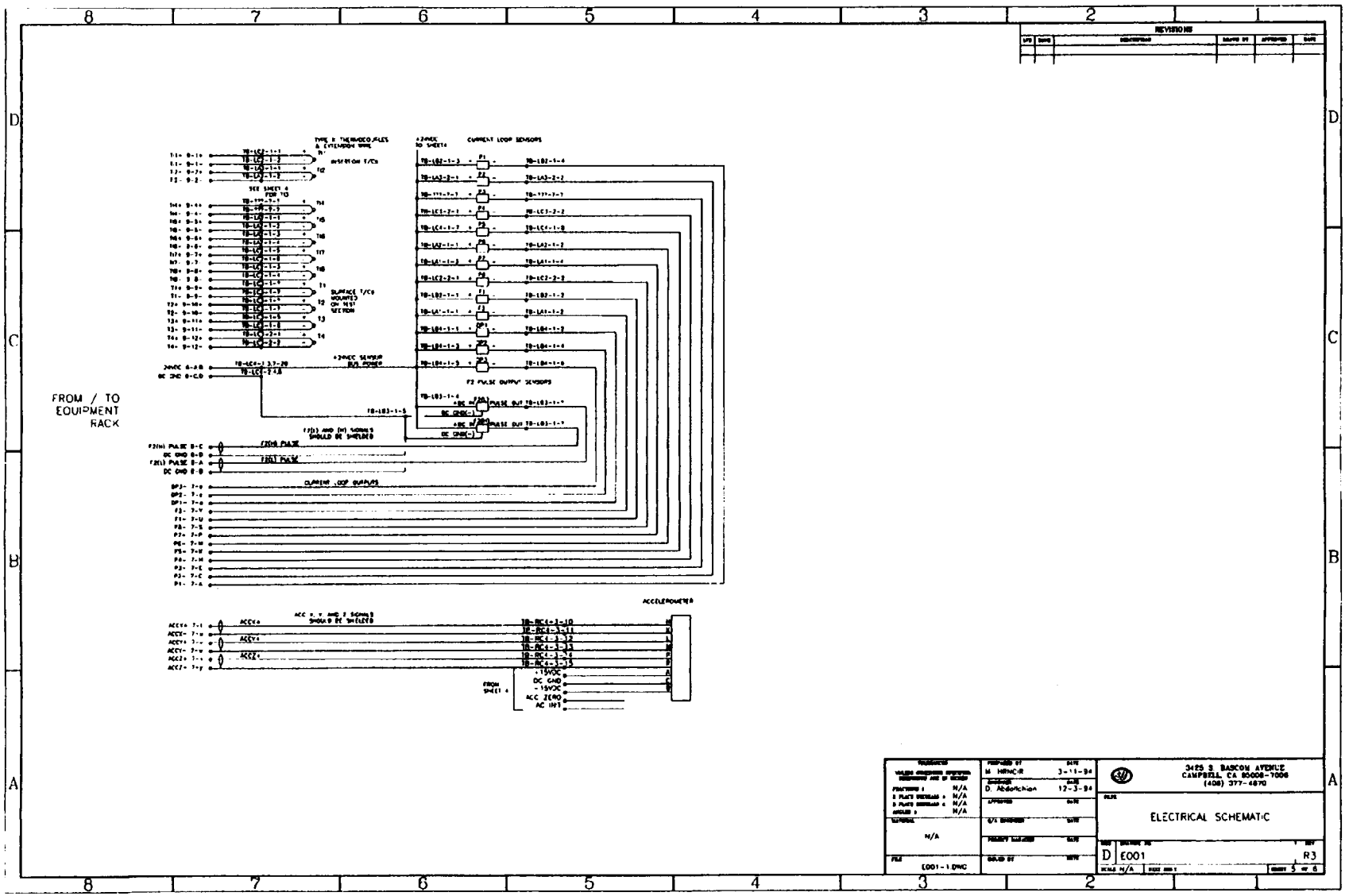

Figure C.5 - Schematic of Electrical Subsystem

Appendix D

IN-FLIGHT TEST PROCEDURE

Before First Parabola

1. Connect the pressurized air source to the accumulator.

2. Turn the main power strip on.
   115 VAC , 60 HZ

3. Turn on the manual switch to the water pump.

4. Set the heater and pre-heater variac settings to zero.

5. Turn the heater power strip on.

6. Verify the power for
   - computer
   - SCXI1100
   - Multiplexer board
   - heater and pre-heater variacs

7. Open LabVIEW on the computer
   - open NASA31 file
   - open NASA32.LLB
   - Open Shakedown Test#1b

8. Press the **"RUN"** button on the screen.

9. Set one **"INDEX"** to read **TI3**.

10. Switch **SOV1** and **SOV2** valves to low flow meter for CHF tests or high flow meter for instability tests.

11. Plug the corresponding (low or high flow meter) readout box to DAS.

12. Switch to corresponding (low or high) flow meter on the LabVIEW screen.

Before Each Parabola

1. Place a new labeled diskette in the computer.

2. Adjust the flow rate in the test section to the desired value using the **pump speed controller** and **RV5**.

3. Press **"PREHEATER"** on the computer screen and adjust the preheater variac. TI3 should be kept close to 100 °F.

4. Press the **"HEATER"** button on the computer screen.

5. Adjust the heater variac to read the desired power setting on the computer screen.

6. Flow rate may need to be re-adjusted after fluid heating.

7. Adjust **RV6** and/or the **accumulator air pressure** to set the pressure **P5** to 60 psia.

8. At the lower right side of the screen type the test identification number.

Just Before Entering the Parabola:

1. Just before entering the parabola press **"PURGE"** on the computer screen for 15 to 20 seconds.

2. Turn purge off before entering the parabola.

3. Press the **"RECORD"** button on the computer screen.

During Parabolas

1. Press the **"RESET"** button on the computer screen when system automatically shuts off.

2. Press the **"SHUT-OFF"** button on the screen if a leak is observed.

After Each Parabola

1. Copy the test data to a diskette.

2. Remove the diskette.

After the Last Parabola

1. Do not press the **"RESET"** button.
2. Press the "HEATER" and "PREHEATER" to turn the heaters off.
3. If the system did not shut off, press "FLOOD" on the computer screen and let the system cool for 3 to 5 minutes.
4. Press "STOP" on the computer screen.
5. Close the file and exit LabVIEW
6. Turn the power to the heater strip off.
7. Shut the cooling water pump off.

Turn the power to the main strip off.